On the spatial and temporal variability of ice arches associated with the formation of the North Water (NOW) Polynya

By

Heather Stark

A Thesis submitted to the Faculty of Graduate Studies of

the University of Manitoba

in partial fulfillment of the requirements of the degree of

MASTER OF SCIENCE

Department of Environment and Geography

University of Manitoba

Winnipeg

ABSTRACT

The formation and dissolution of the North Water Polynya (an area of open water surrounded by a sea-ice covered ocean) was examined to determine the spatial and temporal variability of the Smith Sound ice arch (a feature that prevents ice from covering the polynya). A passive microwave, sea ice concentration dataset was used to create an index classification algorithm that categorized the formation and dissolution of the North Water Polynya from 1979 to 2012. Multiple years were classified as atypical, with the polynya forming earlier, the ice arch not forming at Smith Sound, or the ice arch not forming at all. Secondly, we compare and contrast atmospheric factors that influenced the formation of the ice arch during a typical (2010-2011) and an atypical (2009-2010) formation year. A significant southerly wind event in 2009-2010 could have displaced the ice pack and prevented the consolidation of the ice arch. The importance of the changing ice pack in Nares Strait to the formation of the polynya is also discussed.

ACKNOWLEDGEMENTS

I would like to thank my supervisor, Dr. David Barber, and my graduate committee members Dr. CJ Mundy and Mr. Mike McKernan for their guidance, knowledge, and support throughout this research endeavor.

I would like to extend my thanks to everyone involved in the various field seasons I had the opportunity to participate in, especially the Captains and crew aboard the *CCGS Amundsen*. I would also like to especially thank Lauren Candlish, David Babb, and Kerri Warner for their endless support, counsel, and advice.

I would like to thank the following organizations for their financial contributions: the University of Manitoba, the ArcticNet program of the Network of Centres of Excellence, the Canada Research Chairs (CRC) program, the Natural Sciences and Engineering Research Council (NSERC), and the Northern Studies Training Program (NSTP).

To my family and friends, I thank you for your constant support and encouragement throughout this endeavor.

TABLE OF CONTENTS

LIST OF TABLES

LIST OF FIGURES

LIST OF COPYRIGHTED MATERIAL

CHAPTER ONE: INTRODUCTION

This thesis presents a detailed analysis of the formation and dissolution of the ice arch of the North Water Polynya. The ice arch is a critical feature that keeps ice from covering the polynya. Using a combination of satellite derived sea ice concentration data, atmospheric data, and satellite imagery, we determine the formation and dissolution of the North Water Polynya and the spatial and temporal variability associated with the ice arch at Smith Sound.

1.1 Rationale and context

In recent years there has been considerable investigation into the changing polar regions. The Arctic is experiencing accelerated change as it is incredibly sensitive to variability in climatological forcing [*Intergovernmental Panel on Climate Change (IPCC),* 2013]. In a region that was once dominated by thick multi-year sea ice, the Arctic is now dominated by first-year ice that is much thinner due to a shorter period of growth [*Kwok, 2007*; *Maslanik et al*., 2007]. The changes are affecting the ocean-sea ice-atmosphere interface, including geophysical processes of sea ice, such as growth [*Kwok et al.*, 2013] and drift [*Rampal et al.,* 2009]. Unique features of the ocean-sea ice-atmosphere interface are polynyas – consistent and persistent regions of reduced ice cover or open water in an area where sea ice is typically expected [*Smith et al.*, 1990].

Polynyas are sensitive regions because they experience physical (sea ice drift, upwelling of ocean currents, heat transfer) [see: *Maykut and Perovich,* 1987; *Smith et al.,* 1990; *Morales Maqueda et al.,* 2004], meteorological (cloud development, radiative forcing, albedo feedback) [see: *Andreas and Ackley,* 1982; *Arbetter et al.,* 2004], geochemical (carbon sequestration) [see: *Miller et al.,* 2002], and biological (primary productivity, nutrients) [see: *Tremblay et al.,* 2002; *Arrigo et al.,* 2012] characteristics and processes not seen in other areas. Moreover, polynyas are

heavily relied upon for commercial transportation and also by surrounding communities for social, economic, and hunting needs [*Schledermann*, 1980; *Henshaw,* 2003]. It is necessary to better understand the formation, maintenance, and dissolution of polynyas as the Arctic climate changes because potential variability could affect the unique characteristics and processes seen in these regions.

The largest polynya in the Arctic, the North Water polynya (NOW), is located in northern Baffin Bay just south of Nares Strait between Ellesmere Island and Greenland. The formation and dissolution of NOW is heavily dependent upon ocean-sea ice-atmosphere interactions, especially contributions of ice from the Arctic Ocean. When NOW is present, the regular supply of nutrients from ocean currents combined with open water helps overcome light and nutrient limitation of primary producers, which leads to one of the most biologically productive regions in the Canadian Arctic [*Stirling,* 1980; *Tremblay et al*., 2002]. Ice pack dynamics (including glacial and sea ice) of Nares Strait represent a source of hazards which impact shipping lanes in Baffin Bay [*Barber et al.,* 2014]. An investigation of the potential variability of NOW caused by a changing Arctic system is necessary to understand how changes will impact the physical, biological, meteorological, and geochemical processes of the region.

1.2 Thesis Objectives

The overall purpose of this thesis is to better understand the driving factors behind formation, maintenance, and dissolution of the North Water polynya. Specifically this work aims to investigate the spatial and temporal variability of the ice arches associated with the NOW polynya. To address this overarching objective, this thesis focuses on the following three research objectives:

1) To determine the variability in timing of the formation and dissolution of the North Water polynya.

2) To investigate the role of atmospheric forcing on recent variability of the Smith Sound ice arch consolidation.

3) To investigate the role of the timing of ice grounding relative to ice arch formation.

My thesis will be written sandwich style with the first manuscript seeking to meet objective 1, while the second paper will examine objectives 2 and 3.

1.3 Thesis Outline

This thesis is composed of 5 chapters. The first chapter introduces the rationale and objectives for this thesis. The second chapter provides an in-depth literature review comprised of three parts. In part I, growth, motion, and decay processes of sea ice are described. This includes discussion pertaining to the formation of polynyas and leads. In part II, a discussion on the history of passive remote sensing pertaining to the detection of sea ice is provided. Lastly, in part III the Baffin Bay Marine Complex is discussed, including the ocean-sea ice-atmosphere interface interactions that govern the formation and dissolution of NOW.

Chapter three addresses the first thesis objective and contains a manuscript written by *Stark et al*. [in review], entitled *Identifying changes in the formation and dissolution of the North Water Polynya, 1979-2012: an index classification approach*, which was submitted on 8 January 2016 to **Arctic** and is currently under review. This paper uses 34 years of satellite derived sea ice concentration to determine the formation and dissolution of the NOW polynya. In this paper we (1) develop a classification index, which uses a sea ice concentration threshold, to quantify timing (dates) of the NOW formation and dissolution; and (2) examine temporal trends of the derived NOW formation and dissolution dates.

Chapter four addresses the second and third thesis objectives and contains a second manuscript written by *Stark et al.* [in prep.], entitled *Investigating the factors influencing the formation of the North Water Polynya ice arch at Smith Sound*, which is in preparations to be

submitted to **Arctic.** This paper uses regional and *in situ* atmospheric data to investigate how atmospheric patterns in Nares Strait influence the formation of the ice arch at Smith Sound. This chapter examines (1) climatological trends of temperature and sea level pressure; (2) local atmospheric patterns during typical and atypical NOW Polynya formation years; and (3) large ice features exported through Nares Strait.

Conclusions and recommendations for future work on the subject of the formation and dissolution of the NOW Polynya are presented in chapter five. Implications of a changing Arctic system on the consolidation of the ice arch are also discussed.

Literature Cited

Andreas, E. L., and S. F. Ackley (1982), On the Differences in Ablation Seasons of Arctic and Antarctic Sea Ice, *J. Atmos. Sci.*, *39*(2), 440–447, doi:10.1175/1520-0469(1982)039<0440:OTDIAS>2.0.CO;2.

Arbetter, T. E., A. H. Lynch, and D. A. Bailey (2004), Relationship between synoptic forcing and polynya formation in the Cosmonaut Sea: 1. Polynya climatology, *J. Geophys. Res. Ocean.*, *109*(C04022), doi:10.1029/2003JC001837.

Arrigo, K. R., K. E. Lowry, and G. L. van Dijken (2012), Annual changes in sea ice and phytoplankton in polynyas of the Amundsen Sea, Antarctica, *Deep. Res. Part II Top. Stud. Oceanogr.*, *71-76*, 5–15, doi:10.1016/j.dsr2.2012.03.006.

Barber, D. G., G. McCullough, D. Babb, A. S. Komarov, L. M. Candlish, J. V. Lukovich, M. Asplin, S. Prinsenberg, I. Dmitrenko, and S. Rysgaard (2014), Climate change and ice hazards in the Beaufort Sea, *Elem. Sci. Anthr.*, *2*(000025), doi:10.12952/journal.elementa.000025.

IPCC (2013), Observations: Cryosphere, in: Climate Change 2013: The Physical Science Basis. Contribution of Working Group I to the Fifth Assessment Report of the Intergovernmental Panel on Climate Change edited by T.F. Stocker, D. Qin, G.- K. Plattner, M. Tignor, S.K. Allen, J. Boschung, A. Nauels, Y. Xia, V. Bex and P.M. Midgley. Cambridge University Press, Cambridge UK and New York, NY.

Henshaw, A. (2003), Polynyas and ice edge habitats in cultural context: Archaeological perspectives from southeast Baffin Island, *Arctic*, *56*(1), 1–13.

Kwok, R. (2007), Near zero replenishment of the Arctic multiyear sea ice cover at the end of 2005 summer, *Geophys. Res. Lett., 34*(5), 1–6, doi:10.1029/2006GL028737.

Kwok, R., G. Spreen, and S. Pang (2013), Arctic sea ice circulation and drift speed: Decadal trends and ocean currents, *J. Geophys. Res. Ocean.*, *118*, 2408–2425, doi:10.1002/jgrc.20191.

Maslanik, J. a., C. Fowler, J. Stroeve, S. Drobot, J. Zwally, D. Yi, and W. Emery (2007), A younger, thinner Arctic ice cover: Increased potential for rapid, extensive sea-ice loss, *Geophys. Res. Lett., 34*(24), L24501, doi:10.1029/2007GL032043.

Maykut, G. A., and D. K. Perovich (1987), The role of shortwave radiation in the summer decay of a sea ice cover, J. Geophys. Res., 92(C7), 7032–7044, doi:10.1029/JC092iC07p07032.

Miller, L. A. et al. (2002), Carbon distributions and fluxes in the North Water, 1998 and 1999, *Deep. Res. Part II Top. Stud. Oceanogr.*, *49*, 5151–5170, doi:10.1016/s0967-0645(02)00183-2.

Morales Maqueda, M. A., A. J. Willmott, and N. R. T. Biggs (2004), Polynya Dynamics: A

Review of Observations and Modeling, *Rev. Geophys., 42*(RG1004), doi:10.1029/2002RG000116.

Rampal, P., J. Weiss, and D. Marsan (2009), Positive trend in the mean speed and deformation rate of Arctic sea ice, 1979–2007, *J. Geophys. Res.*, *114*(C5013), doi:10.1029/2008JC005066.

Schledermann, P. (1980), Polynyas and Prehistoric Settlement Patterns, *Arctic*, *33*(2), 292–302.

Smith, S. D., R. D. Muench, and C. H. Pease (1990), Polynyas and leads: an overview of physical processes and environment, *J. Geophys. Res.*, *95*(C6), 9461–9479.

Stirling, I. (1980), The Biological Importance of Polynyas in the Canadian Arctic, *Arctic*, *33*(2), 303–315.

Tremblay, J. E., Y. Gratton, E. C. Carmack, C. D. Payne, and N. M. Price (2002), Impact of the large-scale Arctic circulation and the North Water Polynya on nutrient inventories in Baffin Bay, *J. Geophys. Res.,* 107(C8), doi: 10.1029/2000JC000595.

CHAPTER TWO: BACKGROUND AND LITERATURE REVIEW

This literature review is intended to provide the background knowledge upon which this thesis' research is based. Section 2.1 examines the formation of sea ice and how it responds to oceanic and atmospheric forcing. Section 2.2 discusses the use of microwave remote sensing to detect changes in polar regions, particularly in regions of polynyas. Section 2.3 reviews literature pertinent to the study area, the Baffin Bay Marine Complex, and the local ocean-sea ice-atmosphere interactions that drive the North Water Polynya.

2.1 Sea Ice Regime

2.1.1 Thermodynamic Growth

Thermodynamic growth of sea ice is governed by interactions between the ocean surface and the lower atmosphere. The transition from summer to fall in the Arctic initiates the onset of growth. The atmosphere, with a lower heat capacity than water, is more sensitive to cooling and the resulting temperature gradient between the cooler atmosphere and the warmer ocean produces a heat flux. During fall and winter, the heat flux is from the ocean to the atmosphere and vice versa during the spring and summer. The loss of heat to the atmosphere decreases the sea surface temperature and surface water density, resulting in the mixing of the upper oceanic layer down to the pycnocline, the first significant density gradient. This mixing is caused by a density gradient, as the more dense cold water sinks, initiating cyclic movement of the water parcels in the upper water column above the pycnocline [*Petrich and Eiken*, 2010]. As temperatures continue to decrease and reach -1.86°C, the freezing point of sea water, ice crystals begin to form in the upper column and will float to the surface due to their decreased density relative to surrounding water.

Once optimal atmospheric and oceanic conditions are met, ice growth occurs in two

different pathways: the nilas process or the pancake process. The nilas process occurs in calm conditions, when wind and wave energy are low, allowing the growth of small ice crystals in the upper ocean layer. These crystals are suspended in the surface water, referred to as frazil or grease ice, and will freeze together as conditions get colder, forming a thin sheet of continuous, transparent ice, known as nilas. Nilas is very flexible and will move with wave action.

When wind and wave energy are high, increased turbulence break the delicate structure of the ice crystals, densely packing the suspended crystals in the surface layer. The constant wave action compresses ice crystals together, forming small cakes of slushy ice crystals, known as pancakes. With continued turbulence, the pans of ice collide, creating raised edges consisting of suspended frazil. The pancakes continue to grow through collisions, increasing in diameter from centimetres to metres. The pans of ice can eventually freeze together through the rafting process, discussed in section 2.1.2 below, or through freezing together as nilas grows between pans, creating a continuous layer of ice [*Wadhams et al.,* 2000].

Once a continuous layer of ice has formed, the ocean-ice interface advances downwards, growing sea ice fastest perpendicular to the basal plane. As water molecules affix along the basal plane, salt ions and other impurities are rejected from the ice creating a thin layer of increased saline water. A larger heat flux between the cooler ocean and the warmer atmosphere results as the increase in salinity from the salt ions depresses the freezing point [*Dieckmann and Hellmer*, 2009]. This begins the transition from the granular ice crystal network to the columnar network, where ice will grow from the underside of the ice cover (known as congelation ice). The random orientation of the consolidated frazel crystals (granular ice) will dictate the speed of growth – an ice crystal orientated with the c-axis (basal plane) horizontally will grow faster than with the c-axis orientated a different way. Throughout the entire growth period, a temperature gradient

exists: temperatures are coldest at the sea ice-atmosphere interface and warmer at the ocean-sea ice interface. Ice growth will stop when the heat flux from the ocean to the atmosphere reaches equilibrium dictated by the insulative properties of the snow and ice cover [*Petrich and Eicken*, 2010].

During thermodynamic growth, pockets of water become trapped in the ice crystal framework. When these pockets eventually freeze, salt ions and other dissolved molecules and particulates remain trapped in the framework. The clusters of salt and ions are denser than the surrounding ice, eventually melting channels through the ice structure as gravity pulls brine from the newly forming ice [*Weeks and Ackley*, 1986]. Over time, a network of brine drainage channels develop, eventually releasing brine into the water due to the influences of three processes: a change in hydrostatic pressure, changes in pressure at the ocean-sea ice interface, and the pressure generated during the volume expansion of freezing water [*Dieckmann and Hellmer*, 2009].

The growth of ice can occur in two locations: affixed to land or in open ocean. Ice growth that occurs along coastlines is known as landfast ice as it is attached to the beach or shoreline. Landfast ice will form earlier and grow faster because a lower volume of water needs to be cooled to the freezing point. Moreover, the freezing point may be higher due to freshwater runoff from land [*Granskog et al.,* 2009]. Ice growth that occurs in open ocean is known as pack ice. It is mobile and will drift with winds and ocean currents.

2.1.2 Motion and Dynamic Growth

Atmospheric and oceanic forces drive sea ice motion and dynamic growth. The ability to move an ice floe is dependent upon ice rheology – every floe will react differently to stress based on how it thermodynamically formed, its internal strength, floe size, and ice thickness. There are

five forcing mechanisms that affect the movement/deformation of sea ice: air stress, water stress, Coriolis force, internal ice stress, and sea surface tilt [*Wadhams*, 2000]. The above forces acting on a sea ice floe results in the initiation of motion, as seen in the following equation:

$$M\,a = \tau_a + \tau_w + F_c + F_i + F_t \quad (1)$$

where sea ice floe mass (M) multiplied by the acceleration (a) equals the sum of air stress (τ_a), water stress (τ_w), Coriolis force (F_c), internal stress (F_i), and sea surface tilt (F_t) **[***Wadhams***,** 2000]. The most dominant forces acting on a sea ice floe are air stress, water stress, and Coriolis force. Air stress is generated through surface winds, which can often times be counteracted by water stress, i.e. ocean currents, as currents act as both an accelerative or decelerative force [*Thorndike and Colony*, 1982; *Leppäranta*, 2005]. Coriolis force is resultant of the Earth's rotation, deflecting objects of mass to the right at a 90° angle of the surface wind direction in the Northern Hemisphere. Multiple factors contribute to internal stresses of a sea ice floe, including: sea ice rheology, strength, and thickness. The sea ice pack may have multiple internal stresses, which could oppose motion, potentially negatively affecting sea ice drift speeds. Sea surface tilt forces arise due to horizontal inconsistencies in continental and oceanic bedrock, the Earth's rotation, and thermohaline circulation, leading to the piling up of water in some areas [*Wadhams*, 2000].

Surface winds and ocean currents play a role in the motion of sea ice, combining to move ice in and out of the Arctic Ocean. However, as ice is closer to land, the efficacy of wind induced ice motion is reduced and ocean currents will be the dominant source of energy for drift [*Thorndike and Colony*, 1982]. The energy transferred to sea ice results in divergence or convergence of ice floes. When ice floes diverge, they are pushed away from each other, directly exposing the ocean to the atmosphere, potentially allowing the thermodynamic energy transfer

through heat flux necessary for ice growth.

Ice floes converge when stress, from either winds or ocean currents, alters the trajectory of sea ice and drives floes together. The stability of ice plays a role in ice convergence; more stable ice floes, such as fast ice or multi-year floes, are more likely to have less stable ice floes, such as smaller pans or first year-ice, driven into them. Convergence results in the following dynamic growth processes: rafting or ridging. Rafting occurs when one floe overrides another, often times consolidating to form one piece of ice. Under specific conditions, finger rafting can also occur in which portions of two ice floes thrust alternatively over one another, creating the appearance of fingers [*Thorndike et al.,* 1975]. Finger rafting is most common in nilas, or young thin ice.

Ridging is the more common process of dynamic ice growth. Pressure generated by wind and/or wave action compresses floes together, breaking the flow along its edge, creating a wall of broken ice. The volume of ice submerged is called the keel, whereas the portion of ice above the surface is referred to as the sail [*Wadhams,* 2000]. Ridges can consolidate, permanently bonding the floes together, increasing overall thickness. A ridged ice floe is more susceptible to motion because there is a greater surface area both above and below the water to generate friction and initiate movement.

2.1.3 Decay

During the winter months, the atmosphere does not contribute a significant amount of solar radiation, creating a negative energy balance and therefore ice growth. However, in the summer months when the solar incidence angle is higher, the energy balance shifts from negative to positive. The Arctic experiences a positive energy balance as incident solar radiation increases, increasing the amount of energy available at the surface. The subsequent higher

atmospheric temperature results in the transfer of heat from the atmosphere to the ocean, initiating the onset of melt as sea ice temperatures increase.

As the surface temperature of sea ice increases, melt water gathers in pools on the ice surface, resulting in the formation of melt ponds. The pooling water lowers the surface albedo to 0.15-0.4, from its original albedo of 0.4-0.7 for bare sea ice [*Wadhams*, 2000]. Melt ponds will grow in size as they absorb solar radiation and can eventually melt through the sea ice, creating thaw holes. As melt continues, a floe will eventually consist of a series of melt ponds connected together via drainage channels that drain either through thaw holes or off the side of the ice floe. The underside of an ice floe also responds to melt, known as bottom melt. Beneath melt ponds ice is thinner, resulting in the absorption of incoming solar radiation by the ocean, creating an undulating topography of depressions on the underside of the ice, similar to the melting surface topography. Floes will begin to disintegrate as the drainage channels and thaw holes compromise floe structure, often times melting right through the sea ice creating weak points that are more susceptible to break when stress is applied.

The decay of sea ice re-introduces fresh water into the upper layer of the ocean, freshening the surface layer [*Aagaard and Woodgate*, 2001]. Following brine rejection during the growth of sea ice in the fall, the surface layer has increased salinity; however, as sea ice undergoes melt, the fresher melt water remains at the surface decreasing salinity and stratifying the upper water column. This cycle of low and high salinity at the surface contributes to the maintenance of the mixed layer of the Arctic Ocean [*Holland and Mysak*, 1996].

2.1.3.1 First-year and Multi-year ice

The cycle of growth and decay of ice is marked by the maximum sea ice extent in March and minimum sea ice extent in September. The classification of sea ice is dependent upon which

floes remain at the end of the summer melt season. Ice which melts out completely is categorized as first-year ice (FYI), whereas ice that has survived the melt season is old ice, second-year or multiyear ice (MYI). FYI, which can reach a mean thickness of 0.3-2 metres, is a combination of level ice and pressure ridges that are rough and angular. Since MYI has survived multiple melt seasons, ridges are constantly eroded creating the appearance of rolling hills, known as hummocks. During summer, MYI will contain numerous irregular shaped melt ponds along with a very intricate drainage channel network. Because MYI survives multiple melt seasons, brine trapped in drainage channels will drain out, leaving it less saline then FYI.

2.1.4 Polynyas and Leads

Polynyas and leads are unique characteristics of the marine icescape. Polynyas are regions in a sea ice environment that remain relatively free of ice on a persistent and recurrent basis in a region where sea ice should be expected based on climate mean temperatures [*Smith et al.,* 1990]. While polynyas occur in the same area and can be open for weeks-to-months at a time, leads are linear features that are highly variable, both in formation location and amount of time they remain open. The term 'polynya' originates from the Russian language, meaning natural ice hole, and was utilized in the 19th century by polar explorers describing navigable regions of open water found during the winter months. Prior to this, evidence presented by *Schledermann* [1980] and *Henshaw* [2003] suggests that circumpolar peoples relied on polynyas for subsistence, and potentially economic purposes, for at least 3000 years. Both polynyas and leads are important features of the polar icescape as they harbour biological diversity [*Stirling*, 1980; *Massom et al.,* 1998; *Arrigo and van Dijken*, 2003].

The classification of polynyas varies throughout the literature, with many derived from, but not limited to: mechanical forcing, convective forcing, and location relative to the continental

shelf. *Smith et al.* [1990] presented a process-based classification based on latent and sensible heat mechanisms, which is widely accepted today. Latent heat polynyas are driven by dynamic wind and/or ocean currents mechanically advecting ice from a region. These polynyas are maintained by the latent heat released to the atmosphere during the latent heat of fusion during continual ice formation and advection from a region [*Pease,* 1987; *Smith et al.,* 1990; *Lemke,* 2001]. Production of new ice is also a significant contributor to the formation of deep water through thermohaline circulation processes involving bring rejection [*Martin et al*., 2004]. Sensible heat polynyas form where upwelling currents transport oceanic heat to the surface, vertically mixing oceanic masses and preventing the growth of sea ice or initiating melt. While there are polynyas that exhibit one or the other forcing mechanism, the strongest and most persistent polynyas are formed and maintained by both latent and sensible heat mechanisms [*Morales Maqueda et al.,* 2004].

Polynyas form at both poles. Arctic polynyas are heavily influenced by the presence of landmass, which can create upwelling, restrict atmospheric winds and oceanic flow, and impede sea ice drift [*Smith and Rigby,* 1981]. The formation and maintenance of Arctic polynyas is governed by latent and/or sensible heat mechanisms. Antarctic polynyas are heavily influenced by glacial tongues, icebergs, and fast ice [*Massom et al.,* 1998] and are driven by latent-heat processes that are largely affected by the strong katabatic winds that move downslope off the inland ice sheet. The supercooled katabatic winds promote considerably higher sea ice growth rates than surrounding consolidated ice areas [*Cavalieri and Martin*, 1985; *Zwally et al.,* 1985; *Ushio et al.,* 1999].

Leads are similar to polynyas in that they are also regions lacking sea ice. Leads are intermittent linear cracks in sea ice as a result of pertinent ocean currents and/or surface winds.

They usually form near continental-shelf regions where strong upwelling currents and dominant surface winds disturb the landfast and pack ice interface [*Barber and Massom*, 2007]. Unlike polynyas that typically recur in the same area and reach a similar size from year to year, the location, size, and longevity of a lead is variable and heavily dependent on surface conditions [*Williams et al.,* 2007]. Initial formation of leads and polynyas can be from the same forcing mechanisms; however, the strength of the mechanism determines the formation of one versus the other.

The temperature of open water as a result of polynyas and leads is higher than that of the surrounding ice pack. This produces a significant heat flux from the ocean to the atmosphere, once the insulating properties of sea ice are lost, that is magnitudes higher than the pack ice heat flux to the atmosphere [*Kottmeier and Engelbart*, 1992; *Gallée*, 1997; *Minnet and Key*, 2007]. The overlaying atmosphere is greatly affected by this heat flux as the increased heat and moisture initiate the development of clouds [*Arbetter et al.,* 2004; *Key et al.,* 2004]. This heat flux also results in increased formation of thin ice, typical to polynyas, as the heat exchange from the ocean to the atmosphere is ideal for thermodynamic growth [*Cavalieri and Martin,* 1985]. The albedo feedback loop plays an integral role in sustaining the heat flux and maintaining and potentially increasing the polynya in size. The greater absorption of dark ocean compared to the reflective properties of sea ice and snow, melts surrounding ice increasing the size of the polynya during late spring [*Andreas and Ackley,* 1982; *Kottmeier and Engelbart,* 1992]. Polynyas are active for a variable amount of time – dependent upon the interaction between the open water and the atmosphere [*Yao and Tang,* 2003]. During the transition into summer, the ocean experiences a net gain of energy due to the increased amounts of solar radiation. At this time, the polynya will have reached its maximum extent and will begin to dissolve the surrounding ice as

the dark ocean surface absorbs more of the solar radiation, rapidly melting the bounding ice edges [*Hall and Rothrock,* 1987]. A schematic of the previously mentioned mechanisms and the mechanisms discussed in the following paragraph are shown in Figure 2.1.

Brine rejection is coupled with the high rates of ice production in polynyas. Due to the heat flux, the thermodynamic growth of sea ice occurs multiple times during the lifespan of a polynya, especially in coastal areas of the Arctic and Antarctic where winds continually advect ice from the region [*Lemke*, 2001; *Kern et al.,* 2007; *Williams et al.,* 2007]. As with typical brine rejection from the formation of frazil, an increase in salinity is observed at the surface, followed by a mixing of the surface layer. With continual frazil production, brine rejection occurs more frequently, increasing convection at the surface, eventually weakening the stable, dense layer and deepening the surface mixed layer [*Kato and Phillips*, 1969; *Moroni and Cenedese*, 2006; *Williams et al.,* 2007]. The relationship between frazil ice formation and brine rejection has not been fully examined. Basic observations from satellites and moorings indicate that frazil is present within the top 5-20 meters of the water column [*Drucker et al*., 2003]. However, quantifying fluxes of salt and freshwater during brine rejection processes when polynyas are active is difficult due to the challenges in making direct observations [*Muench et al.*, 1995; *Kirillov et al.*, 2013].

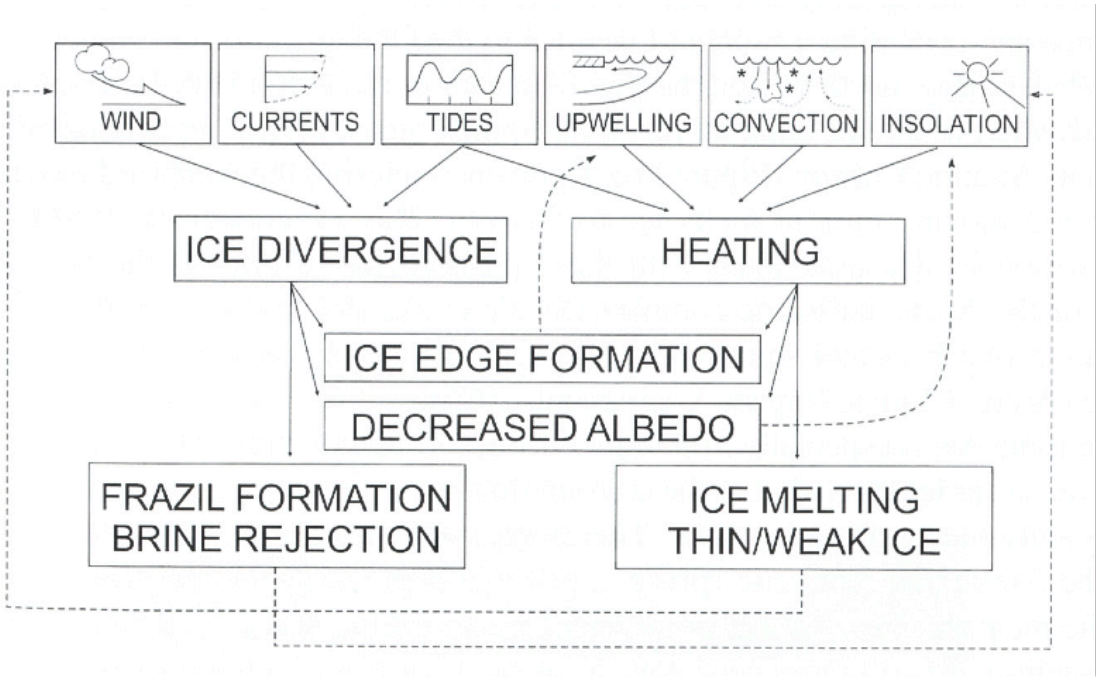

Figure 2.1: Schematic of the forcing mechanisms associated with the formation, maintenance, and dissolution of polynyas (used with permission from Williams et al., [2007]).

The size of polynyas varies based on location and formation and maintenance mechanisms. To define polynya geometry, *Williams et al.* [2007] have identified two categories: metric and operational. Metric polynyas are subdivided into two categories: open water polynyas or mixed ice-water region polynyas. Metric categories are more useful for remote sensing and modeling purposes due to their focus on open water and the production of sea ice [*Liu et al.,* 1997; *Morales Maqueda et al.,* 2004]. Open water polynyas allow for mechanistic examination of multiple influences on polynya behaviour, including heat fluxes, sea ice growth, atmospheric and oceanic forces, and biological impacts [*Stirling,* 1980*; Massom,* 1988]. Operational polynyas are subdivided into two categories: practical polynyas and full polynyas. Practical polynyas are unsafe for travel, and therefore are little studied, while full polynyas encompass both the open water and mixed ice regions [*Williams et al*., 2007].

Polynyas are often associated with high biologically productivity as they alleviate light limitation for primary productivity [*Smith,* 1995; *Smith and Gordon*, 1997; *Tremblay et al.*,

2002; *Arrigo and van Dijken*, 2003]. Winds and ocean currents that form and maintain polynyas can also help replenish surface nutrients, further augmenting primary production potential [*Arrigo and van Dijken*, 2003]. Not only do polynyas see stronger spring bloom of phytoplankton and zooplankton than surrounding areas, these regions are also rich and diverse at all levels of the ecosystem.

2.2 Remote Sensing of Sea Ice

Remote sensing is the method of acquiring information without direct contact. The monitoring of processes and systems interacting on or near the Earth's surface by way of satellite remote sensing offers a variety of products at various spatial and temporal scales. Satellite remote sensing caters to a large variety of applications, generating products from an assortment of wavelengths and illumination sources.

Remote sensing relies on the three interactions that are possible when incident energy interacts with a matter: reflection, absorption, and transmission. The interrelationship between incident energy (E_I) and the three possible interactions is seen in the following equation,

$$E_I(\lambda) = E_R(\lambda) + E_A(\lambda) + E_T(\lambda) \quad (2)$$

where E_R is reflected energy, E_A is absorbed energy, and E_T is transmitted energy [*Lillesand et al.,* 2008]. As indicated in Equation 2, the way in which energy interacts with a surface is based on wavelength.

The detection of Earth's processes and systems by remote sensing is based on radiation that is either reflected or emitted. The measurement of reflected energy relies on the reflectance of incident energy – energy from another source such as the sun or the sensor platform. The sensor will measure the energy reflected back from the matter. Active microwave products are generated from energy originating from the sensor platform, while optical imagery relies on the

reflection of natural visible light.

Emitted radiation is detected when an energy transfer induces a change in temperature, assuming that the matter is above 0 Kelvin (approximately -273°C) and induced changes are governed by the nature of the body itself, its emissivity. Remote sensing products that are generated from emitted radiation include thermal infrared and passive microwave.

The identification of an object is dependent upon emissivity – the physical properties of the matter. Physical properties, which include surface roughness and volumetric heterogeneity, will determine if a given wavelength, and its associated incidence angle, will be partitioned [*Parashar et al.,* 1977]. Sea ice has unique geophysical properties, including ice thickness, temperature gradients, brine inclusions, organic matter, and salts, making detection using large portions of the electromagnetic spectrum possible [*Tucker at al.,* 1992]. Sea ice has long been monitored for spatial variability and temporal change because there are strong electromagnetic differences between sea ice and open water [*Winbrenner et al.,* 1992; *Barber,* 2005]. In addition to long-term monitoring, modeling of sea ice has played in integral role in determining impacts of climate change [*Tang and Dunlap,* 2007*; Spreen et al.,* 2008; *Tivy et al.,* 2011*; Wang and Overland,* 2013].

2.2.1 Passive Microwave and Sea Ice

As mentioned briefly above, passive microwave radiometers do not supply their own illumination; instead they rely on energy emitted or reflected within their field of view. Passive microwave radiometers detect and measure the thermal emission of radiation from a surface in the electromagnetic range of 1 mm to 1 m wavelengths [*Massom*, 2009]. A range of calibrated brightness temperatures is created when the blackbody surface produces microwave radiation at the collected frequency and wavelength [*Comiso and Zwally*, 1989]. Frequencies range from 1 to

300 Ghz, with both wavelengths and frequencies varying based on field of study and application [*Carsey et al.,* 1992]. Cloud cover and precipitation do not affect microwave energy, as the longer wavelengths are less susceptible to atmospheric scattering. Moreover, passive microwave platforms do not rely on illumination from the sun, making them ideal for usage in the polar regions. Due to the large swath widths of most sensors, spatial resolution is reduced (12.5 km - 25 km); however, the polar regions benefit as there is daily coverage and thus the production of continuous datasets.

The first passive microwave radiometer was launched in 1972 aboard the Nimbus-5 Satellite: the Electronically Scanning Microwave Radiometer (ESMR). The use of passive microwave radiometers in polar regions is integral in monitoring sea ice concentration, type, extent, and drift [*Wadhams,* 2000]. Passive microwave data has been continuously collected since 1978 and is presently being collected by the Special Sensor Microwave Imager (SSM/I) which is onboard multiple Defense Meteorological Satellite Program satellites and the Advanced Microwave Scanning Radiometer EOS 2 (AMSR-E2). AMSR-E launched in 2002 but the instrument stopped rotating in 2011, which resulted in AMSR-E2 quickly replacing it in 2012.

Passive microwave radiometers operate at different frequencies and polarizations to optimize spatial resolution and reduce atmospheric interference, 89 GHz and 37 GHz respectively. To derive sea ice concentration and motion, SSM/I has 85GHz and 37GHz frequency channels are widely relied upon now as AMSR-E's 18GHz frequency no longer collects data [*Kwok*, 2008].

To derive sea ice concentration, two algorithms are commonly used: the NASA Team and the Bootstrap [*Cavalieri et al.*, 1990; 1999; *Comiso and Kwok*, 1996]. The NASA Team algorithm utilizes three polarization channels of SSM/I (19.4V, 19.4H, and 37V GHz) to

determine the ratio between polarizations and spectral gradients. The Bootstrap algorithm utilizes a combination of frequencies and polarizations to interpolate between clusters of ice types (seasonal ice: 19V and 37V GHz, perennial ice: 37V and 37H GHz). The NASA Team algorithm uses known ice concentration locations from summer and winter only as tiepoints (or reference points), while the Bootstrap algorithm uses tiepoints from all seasons to assist with ice concentration prediction. While these algorithms are fairly accurate, there are factors that introduce sources of error into the calculations. These include: thin ice, extremely cold surface temperatures, and regions that undergo melt and refreezing [*Grenfell et al.*, 1992; *Cavalieri et al*., 1995].

To make use of the higher resolution 85 GHz channel of SSM/I, *Kaleschke et al.,* [2001] developed an algorithm, ARTIST Sea Ice, to better improve the spatial prediction of ice concentration. The algorithm is able to eliminate larger portions of land interference compared to NASA's Bootstrap algorithm because of the increased spatial resolution of the 85 GHz channel. The atmospheric influences associated with 85 GHz were reduced by the inclusion of a weather filter that used known tiepoints of open ocean and sea ice. The algorithm has been successfully applied to coastal regions [*Kern,* 2008; *Spreen et al.,* 2008; *Smith et al*., 2011; *Cape et al.,* 2014] and is comparable to other active microwave sea ice algorithms used in coastal and marginal ice zones [*Heinrichs et al.,* 2006].

2.2.2 Measuring Sea Ice

The measurement of sea ice is limited by sensor platform specifications: field of view dictates spatial resolution and calibration dictates frequency and wavelength. The purpose/usage of the sensor and spatial resolution determine the revisit period – how long it takes the sensor to scan the same object twice (also known as the temporal resolution). Although sensors are limited

to certain specifications, utilizing satellite remote sensing in such remote areas supplements in situ measurements and strengthens models. The main foci of polar satellite remote sensing are: sea ice concentration, extent, area, volume, and thickness [*Lubin and Massom*, 2004].

Sea ice concentration (SIC) is the most basic spatial measurement of sea ice and is defined as the percentage of a given area covered by a continuous sheet of ice relative to the given area [*Lubin and Massom,* 2004]. SIC can be determined on a variety of spatial scales – from the entire Arctic Basin to Hudson Bay to Lancaster Sound. The smallest sea ice concentration value is dependent on the minimum mapping unit the sensor can detect.

The measurement of sea ice extent (SIE) is defined as the total area of sea ice above a defined concentration threshold. To determine SIE, each data cell is classified as 'ice covered' or 'not ice covered' using the threshold value. The areal extent of data cells classified as 'ice covered' is multiplied by 100% SIC. The SIC threshold value tends to vary based on scientific purpose as spatial features of polar regions have differing sea ice concentration trends. The National Snow and Ice Data Centre (NSIDC) defined the most widely used threshold: all values above the 15% SIC threshold are included in SIE measurements. However, other SIC thresholds determined for a specific region or phenomenon do exist. For example, marginal ice zones and polynyas are of particular interest. *Massom et al.* [1998], *Arrigo et al.* [2003], and *Smith et al.* [2011] used a variety of SIC thresholds (all of which are purpose dependent) to determine the variability of Antarctic and Arctic polynyas. Polynyas have differing SIC dynamics, which require the use of thresholds to determine all aspects of SIC, growth and decay, including when the polynya is active and when it is dissolving. Additionally, marginal ice zones and ice edges behave differently than pack ice – *Worby et al.* [2004] and *Heinrichs et al.* [2006] determined NSIDC's threshold of 15% is applicable for these regions.

Sea ice area (SIA) is similar to SIE as it calculates sea ice coverage; however, the classification of 'ice covered' and 'not ice covered' differs. Instead of assuming an entire grid cell is 'ice covered', SIA determines percentages of sea ice within a grid cell. The percentage of SIC (provided it is over the threshold value) within a grid cell is multiplied by the areal extent of that grid cell. The sum of the outputs from each grid cell is the total area of sea ice.

Sea ice thickness refers to distance from the top of an ice floe to the bottom portion submerged in the water. The thickness of sea ice is not uniform – thermodynamic properties vary as energy transfers from the ocean to the atmosphere during growth. Sea ice thickness measurements are often localized and crude estimates exist for the entire Arctic. Multiple studies have utilized NASA's ICESat program determine ice thickness. Studies by *Forsberg and Skourup* [2005], *Kwok et al.,* [2006; 2007], and *Zwally et al.* [2008] used the laser altimeter measurements from IceSat to determine ice freeboard. *Kwok and Cunningham* [2008] expanded upon this, using IceSat's snow depth measurements and constructed ice freeboard to determine distributions of Arctic MYI and FYI.

Sea ice volume (SIV) is described as the three-dimensional space that sea ice occupies. The calculation of SIV can only be determined if thickness measurements (or estimates) exist for sea ice features. SIV estimates are not often produced with remote sensing products and often a method to determine volume is derived from a variety of sources. *Erashin et al.* [2011] estimated SIV using the EGG code provided by Canadian Ice Service Operational Ice Charts. The multiplication of the percentage of ice concentration and stage of development was determined for each grid cell, which produced an estimate of ice volume.

2.2.3 Polynya Detection

A polynya contains both open water area and regions of reduced or thinner ice coverage; however, not all studies examine both open water and ice-covered regions. Instead, the measurement of polynyas varies based on underlying research themes.

Early polynya detection techniques focused on using optical sensors that differentiated between ice covered regions and open ocean. *Dey et al.* [1979] utilized Landsat's Multispectral Scanner to detect spectral differences between white ice and dark ocean, while *Smith and Rigby* [1981] utilized the infrared bands of NOAA-4 and -5 to detect emission differences between warm ocean and cold sea ice. More recently, *Stringer and Groves* [1991] mapped the location and extent of numerous Arctic polynyas using optical and thermal imagery, confirming that the higher spatial resolution of optical imagery could be used instead of the coarser passive microwave platforms available at the time. Due to the limitations of early optical platforms, i.e. infrequent revisit periods, diurnal cycles, and cloud cover, the early detection of polynyas was limited to determining the presence or absence of a polynya.

To make use of lower resolution passive microwave platforms, *Markus and Burns* [1995] developed the Polynya Signature Simulation Method (PSSM) to map small Antarctic polynyas. PSSM utilizes SSM/I brightness temperatures from 37- and 85-GHz frequencies to produce a dataset with minimal atmospheric influences and a higher spatial resolution, respectively. This method classifies on the sub-pixel scale, as most Antarctic polynyas are smaller than one SSM/I pixel, by simulating brightness temperatures of sea ice classes (sea ice, shelf ice, open water) and then coevolving with satellite antenna pattern to ensure accurate polynya classification. A series of validation points of nearby ice is required to validate the method. This presents a limitation to the applicability of the method in the land-bordered Arctic Ocean, as seen in the study by

Willmes et al. [2011] in the Laptev Sea. The Antarctic shelf contains all three categories – sea ice, shelf ice, and open water – allowing for the successful classification of multiple Antarctic polynyas [*Arrigo et al.,* 2003; *Kern,* 2008; *Arrigo et al.,* 2012].

As passive microwave platforms evolved and had higher resolutions, SIC and SIE were once again used to detect polynyas. SIC and SIE estimates derived from passive microwave algorithms often contain errors caused by heterogeneity of sea ice. Moreover, the contrast between open water and sea ice impart atmospheric interference on backscatter values, resulting in the over- and under-estimation of sea ice concentration. To reduce the amount of error, *Heinrichs et al.* [2006] determined that a 15% SIC threshold in marginal ice zones and polynyas is optimal when using passive microwave. The ARTIST Sea Ice algorithm by *Kaleschke et al.* [2001] used threshold values to ensure the atmospheric influences of the 85 GHz frequency were reduced. Other studies by *Smith et al.* [2011] and *Fu et al.* [2012] used threshold values in conjunction with previously developed passive microwave sea ice algorithms. Masking techniques introduced by *Bareiss and Görgen* [2005] assisted in categorization of sea ice trends and polynya dynamics by examining local climatology and polynya forcing mechanisms.

2.3 Baffin Bay Marine Complex

The Baffin Bay Marine Complex is situated in the eastern Canadian Arctic and is surrounded by one of the most heavily glaciated landscapes in the northern hemisphere. It is connected to the Arctic Ocean in the north via Nares Strait, Jones Sound, and Lancaster Sound and to the Labrador Sea/Atlantic Ocean in the south through Davis Strait. Baffin Bay experiences the growth and decay of sea ice on an annual basis. It also transports icebergs and ice islands from calving glaciers in the eastern Canadian Arctic Archipelago (CAA) and western Greenland. Due to the meeting of cold Arctic and warm Atlantic currents [*Muench,* 1971], Baffin

Bay is a complex marine system that supports a very diverse and large ecosystem with most of the biological productivity found in the north when the North Water Polynya (NOW) is active [*Tremblay et al.,* 2002; *Bailey et al.,* 2013].

2.3.1 Physical Oceanography

Baffin Bay contains waters from the Arctic Ocean, Atlantic Ocean [*Muench*, 1971] and, Pacific Ocean [*Jones et al.,* 2003]. Arctic water enters Baffin Bay via Nares Strait, a narrow passage between Ellesmere Island and Greenland (Figure 2.2). Atlantic water enters Baffin Bay via the West Greenland Current, which travels through Davis Strait and follows the coast of Greenland into northern Baffin Bay. The southward movement of cold water form the Arctic Basin is the dominant of the two currents [*Mundy and Barber*, 2001]. When the Arctic and Atlantic currents meet in northern Baffin Bay, the deeper warmer waters (associated with the West Greenland Current) vertically mix with the cooler surface waters (associated with the Arctic water), creating a cyclonic movement of the water mass [*Melling et al.,* 2001; *Tang et al.,* 2004]. Following the mixing of the two currents, the strong flow of the Arctic water current transports the water mass south along the east coast of Baffin Island, earning the name Baffin Island Current. The Baffin Island Current plays an important role in the circulation of Baffin Bay, transporting waters south through Davis Strait and eventually into the Labrador Sea [*Hamilton and Wu*, 2013].

The Arctic water is described as a fresh, cold water mass with a temperature less than 0°C and a salinity of 33.7 [*Tang et al.,* 2004]. The temperature minimum of this sub-zero water is approximately 100 m deep in northeastern Baffin Bay, eventually deepening to 300 m as the Baffin Island Current transports the water southwards [*Tang et al.,* 2004]. At 25 to 100 metres below the surface near Smith Sound and Devon Island, the strongest southward currents are

observed at 10-15 cm s^{-1}[*Melling et al.,* 2001].

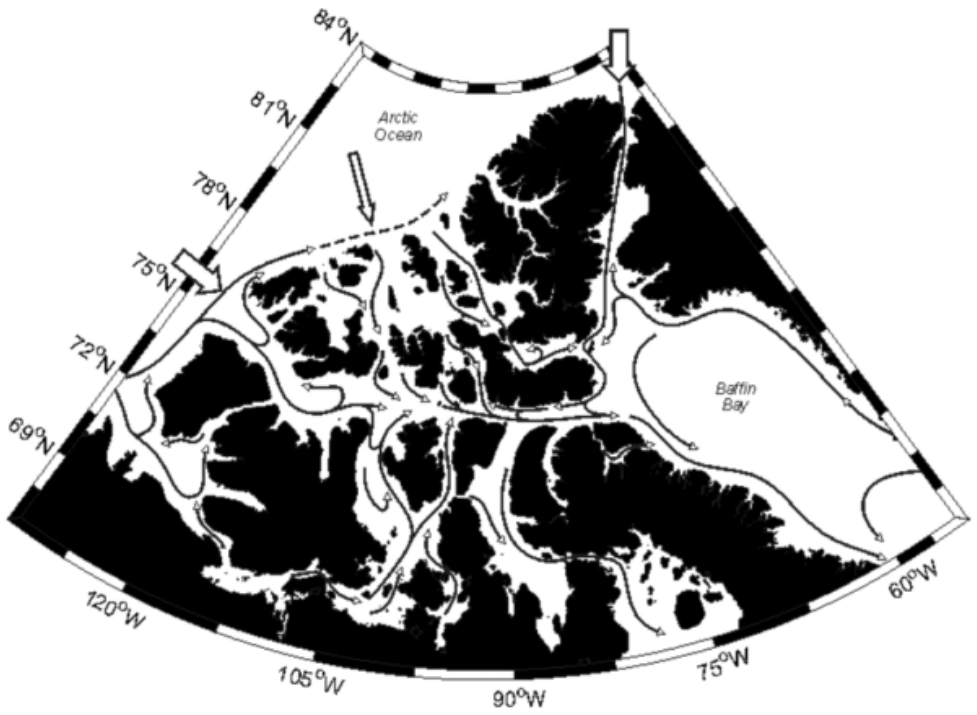

Figure 2.2: The dominant currents of the Canadian Arctic Archipelago. The main currents for Baffin Bay are on the right portion of the map. The Arctic water enters between Ellesmere Island and Greenland, the West Greenland Current follows the Greenland coast, and the Baffin Island Current flows southwards along Baffin Island ([McLaughlin et al., 2004] © 2006 by the President and Fellows of Harvard University).

The West Greenland Current is described as a warm, nutrient rich water mass, influenced by Atlantic waters transported via the Irminger Current and the East Greenland Current [*Lloyd et al.,* 2007]. The water mass has a temperature greater than 0°C and a salinity of 33.45 at the surface [*Bacle et al*., 2002; *Tang et al.,* 2004]. The water mass follows the 600 m isobath of the Greenland coast before moving westward into Baffin Bay at Lancaster Sound. As the current moves northward, it decreases in salinity as it mixes with the southward moving Arctic Basin current at 100 m depth [*Melling et al.,* 2001].

A three-layer structure of Baffin Bay is produced from the mixing currents: at the surface is a fresh, cold layer; at mid-depth is a warm salty layer; and, at depth is a cold slightly fresher

layer [*Tang et al.,* 2004]. The Arctic water makes up the fresh, cold layer at the surface; the warm salty layer at mid-depth is the result of the mixing of the Arctic water and the West Greenland Current; and cold slightly fresher Baffin Bay Deep Water is found below 1200 m in the centre of the bay [*Tang et al*., 2004].

The tidal cycle in northern Baffin Bay is one of the greatest ranges in the Canadian Arctic, with tidal amplitude reaching a maximum of 135 cm during a 12-hour cycle [*Dunphy et al.*, 2005]. Western Baffin Bay can have tides reach a maximum of 25 cm and eastern Baffin Bay tides can reach 36 cm during a semi-diurnal tidal cycle [*Greisman et al*., 1986]. The open water portion of the North Water Polynya is influenced by this large tide, often changing in size and shape, suggesting that the initial areal configuration is heavily influenced by tides [*Vincent and Marsden*, 2008].

There are multiple influences on the flux of freshwater, including but not limited to: sea ice, landfast and mobile, icebergs, atmospheric winds, and ocean currents [*Rabe et al.,* 2012]. Freshwater contributions into Baffin Bay mainly originate from runoff from the Canadian Arctic Archipelago and through Davis Strait. The volume of freshwater transport from northern channels into Baffin Bay is estimated to be 920-1460 $km^3 y^{-1}$ [*Tang et al.,* 2004], while Davis Strait transports 4100 $km^3 y^{-1}$ into the bay [*Cuny et al.,* 2005]. Freshwater inputs from melting icebergs and from precipitation do not significantly impact the freshwater volume [*Tang et al.,* 2004].

2.3.2 Atmospheric Influences

Baffin Bay is classified as a maritime climate when compared to the rest of the Canadian Arctic Archipelago [*Maxwell*, 1981]. Cyclonic activity originating from Davis Strait frequently tracks north, remaining in the region for some time before dissipating [*Maxwell,* 1981].

The precipitation distribution across Baffin Bay varies. Northern Baffin Bay experiences 150-200 mm of precipitation annually over open water, while 300 mm falls on Ellesmere and Devon Island, and Nares Strait receives less than 200 mm annually [*Maxwell*, 1981]. Very little of this precipitation occurs during winter months [*Dey,* 1980; *Barber et al.,* 2001]. Southern Baffin Bay sees more precipitation than the north, with 300-400 mm falling annually [*Maxwell*, 1981]. The North Water Polynya heavily influences the general meteorological setting of northern Baffin Bay. The open water area of the polynya initiates the development of cloud cover due to the contrast between warm open ocean and cold sea ice. The winter months experience 5-10 mm of annual precipitation as fog, while 15-20 mm of fog precipitate in the summer months [*Maxwell*, 1981].

During the winter months, temperatures range from -28°C to -20°C along the north-south gradient of Baffin Bay [*Maxwell,* 1989]. The winter temperature gradient is marked by cooler temperatures over the Canadian Arctic Archipelago, and warmer temperatures over central Baffin Bay and southwestern Greenland, often times with a 10-15°C gradient [*Maxwell,* 1989]. During summer, the entire region experiences +3°C to +5°C temperatures [*Maxwell*, 1989]. When the ice cover at the margins of the polynya dissolves in summer, the temperature gradient is much weaker as the open water of NOW is no longer dominating the local heat budget [*Baber et al.,* 2001].

The wind regime of Baffin Bay is influenced by a semi-static low-pressure system over southern Greenland [*Barber et al.,* 2001]. On occasion, downslope winds originating from Greenland and Ellesmere Island will influence Nares Strait [*Maxwell*, 1981]. A large portion of the surface winds observed is resultant of the strong northerly winds from the Arctic Ocean [*Samelson et al.,* 2006]. The surface winds observed in Nares Strait are confined by the

coastlines of Ellesmere Island and Greenland, accelerating and adjusting direction to follow the channel orientation [*Ito*, 1982].

2.3.3 Sea Ice Regime

The eastern Arctic Ocean has two main regions of ice export: Fram Strait and Nares Strait via the Lincoln Sea [*Kwok*, 2005]. Ice originating from the Lincoln Sea exports through Nares Strait when the strong oceanic flow regime of the Arctic current is coupled with strong north winds [*Samelson et al.,* 2006]. Ice originating from the Arctic Ocean and Beaufort Sea is exported into Baffin Bay via Lancaster Sound and other associated channels of the Canadian Arctic Archipelago. This flux is considerably less than the flux exported through Nares Strait [*Agnew et al.,* 2008].

There are multiple ice types found in Baffin Bay: first-, second-, and multi-year sea ice from the Arctic Ocean and icebergs and ice islands from the glaciers of the eastern CAA and western Greenland. Baffin Bay experiences partial sea ice coverage year round, except for August and September [*Tang et al.,* 2004]. Northern Baffin Bay ice coverage exhibits typical polynya behaviour as it has reduced sea ice concentration and thickness compared to adjacent regions. Ice concentration in this area is often only 95% ice-covered in winter, with floes less than 30 cm thick in 50% of the region [*Steffen,* 1986; *Smith et al.,* 1990].

With the constant flux of ice through Nares Strait, there is the potential for sea ice and icebergs to ground in the channel. An ice floe with a draught greater than water column depth will become lodged along the seabed floor [*Héquette et al*., 1995]. Scour marks along the seabed provide evidence of ice grounding events. Ice grounding events, along with scour marks, have been documented in Southern Baffin Bay and on the Canadian Beaufort Sea Continental Shelf [*Pereira et al.,* 1988]. Random grounding occurs in shallower waters and there have been

documented events of icebergs and ice islands becoming lodged in Nares Strait, disrupting ice motion [*Sadler*, 1976].

2.3.4 North Water Polynya

The North Water Polynya was first documented in 1616 by William Baffin, but did not receive its well-known name until the late 18th or early 19th Century [*Dunbar,* 1981]. Whalers frequently followed the ice edge up the western coast of Greenland into Melville Bay and eventually into the open water of Baffin Bay in hopes to reach the Greenlandic right whale grounds in Lancaster Sound [*Dunbar,* 1981]. The whalers coined the area the 'North Water' because the open water was located at the northern extent of Baffin Bay. Although the natives of Thule and Etah in Smith Sound and the Danes, who had settled in northern Greenland, knew of this region's phenomenon, it was the whalers who's name remained [*Dunbar,* 1969].

The North Water Polynya (NOW) is located between Ellesmere Island and Greenland, at the most northern extent of Baffin Bay where Nares Strait enters into Baffin Bay approximately between 75°N to 80°N (Figure 2.3). Its open water extent is on average 20,000 km^2, for a maximum extent of 80,000 km^2 [*Barber and Massom,* 2007]. The NOW region, similar to the rest of the Arctic, experiences the growth and decay of sea ice on an annual basis. However, the sea ice in the NOW only reaches a maximum of 90% ice concentration, with 50% less than 30 cm thick [Steffen, 1986]. Localized upwelling along the Greenlandic coast slows the growth of sea ice as the ocean-atmosphere flux is smaller here than near Ellesmere Island [*Bacle et al.,* 2002].

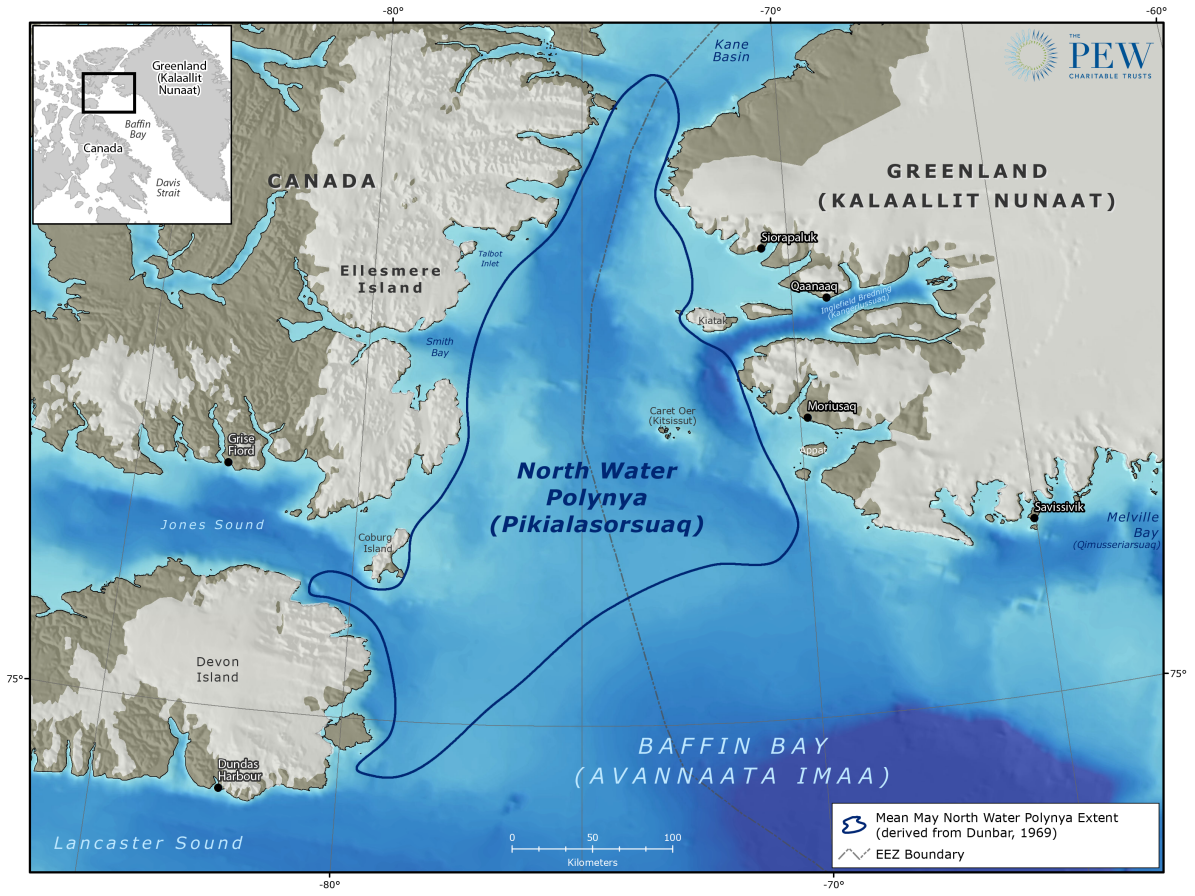

Figure 2.3: The location of the North Water Polynya. The blue line delineates the mean May extent derived from Dunbar, [1969] (used with permission from PEW Charitable Trusts).

Early studies described NOW as a latent and sensible heat polynya [*Dunbar and Dunbar*, 1972; *Dunbar*, 1981; *Ito*, 1982; *Steffan*, 1985; *Darby et al.*, 1994]. Currents from the Arctic Ocean coupled with strong northerly winds (latent heat) move ice through Nares Strait, creating a blockage of ice, known as an ice arch, at Smith Sound. Following the consolidation of the ice arch, the West Greenland Current introduced warm waters (associated with sensible heat) to northern Baffin Bay, slowing and/or preventing the growth of sea ice. However, investigations by *Bacle et al* [2002] determined that waters from the West Greenland Current were strongly constricted by the bathymetry of Baffin Bay and would not reach that far north. Instead, there are only localized heat flux contributions along the Greenlandic coast and NOW is formed and

maintained mainly by contributions of wind and ice from the Arctic Ocean [*Ingram et al.,* 2002]. The following will examine the formation, maintenance, and dissolution mechanisms of NOW.

The formation of NOW is dependent upon the consolidation of an ice arch in southern Nares Strait at the chokepoint of Smith Sound [*Dunbar*, 1973]. Continuous ice fluxes through Nares Strait begin to build-up in the narrow 46 km channel as the formation of land-fast ice along the Greenland and Ellesmere Island coasts slows and eventually stops the drift of ice [*Tang et al.,* 2004]. Atmospheric cooling begins to strengthen the ice arch, making it strong enough to withstand the pressure from ice behind [*Sodhi*, 1977]. Eventually a solid mass of ice extends from the eastern coast of Ellesmere Island to the northwest coast of Greenland, stopping the southerly drift of sea ice. The shape of the arch is variable from year to year, depending on how ice constricts and consolidates in the channel, but is always concave and resembles the typical arch shape.

Following the consolidation of the ice arch, latent heat mechanisms transport ice southward from the ice arch, initiating the formation of NOW. As ice is advected southwards, new ice will thermodynamically grow behind it. This cycle of ice growth and advection continues until the ocean-atmosphere energy balance reaches equilibrium. NOW will begin to expand in three directions: eastward along the Greenland coast, westward along the coast of Ellesmere Island, and southward into Baffin Bay; however, the southern extent is less defined because of the constant southward advection of ice from the north. The main mechanism for southward areal growth is persistently strong northerly winds [*Press and Blais,* 1993].

The dissolution of NOW can occur at any point following its formation with the degradation of the ice arch initiating dissolution. As temperatures increase in early summer, ice will begin to melt, impacting the stability of the arch. The ice arch will begin to melt first on the

Greenlandic side [*Yackel et al.,* 2001], where ice coverage is thinner due to upwelling [*Mundy and Barber,* 2001; *Bacle et al.,* 2002], followed by the thicker ice of Ellesmere Island. Initial investigations determined that wind speed and wind direction were the primary drivers of ice bridge degradation [*Ito and Muller*, 1977]. The strong winds and ocean currents from the Arctic Ocean easily displace the weaker ice and ice fragments will begin to break off. As the ice arch continues to melt, it will eventually lose strength and the region is returned to a state of flux. On average, the ice arch remains stable until June or July when the summer climate alters the ice environment and the region becomes an extension of Baffin Bay's marginal ice zone [*Barber et al.,* 2001].

NOW is of significant ecological importance as it is one of the most biologically productive polynyas in the Arctic [*Tremblay et al.,* 2002; *Bailey et al.,* 2013]. The open water portion of the polynya has increased light penetration and also nutrients, compared to the sea ice coverage surrounding it, which increases the photosynthetically available radiation for productivity. The presence of NOW polynya also controls regional heat, moisture, and gas fluxes as a result of the large contrast between an ice cover and open water [*Smith et al.,* 1990; *Miller et al.,* 2002; *Yao and Tang,* 2003; *Boisvert et al.,* 2012].

Literature Cited

Aagaard, K., and R. A. Woodgate (2001), Some Thoughts on the Freezing and Melting of Sea Ice and Their Effects on the Ocean, *Ocean Model., 3*, 127-135.

Agnew, T., A. Lambe, and D. Long (2008), Estimating sea ice area flux across the Canadian Arctic Archipelago using enhanced AMSR-E, *J. Geophys. Res.*, *113*(C10011), doi:10.1029/2007JC004582.

Andreas, E. L., and S. F. Ackley (1982), On the Differences in Ablation Seasons of Arctic and Antarctic Sea Ice, *J. Atmos. Sci.*, *39*(2), 440–447.

Arbetter, T. E., A. H. Lynch, and D. A. Bailey (2004), Relationship between synoptic forcing and polynya formation in the Cosmonaut Sea: 1. Polynya climatology, *J. Geophys. Res. Ocean.*, *109*(C4), C04022, doi:10.1029/2003JC001837.

Arrigo, K. R., and G. L. van Dijken (2003), Phytoplankton dynamics within 37 Antarctic coastal polynya systems, *J. Geophys. Res., 108*(C8), 3271, doi:10.1029/2002JC001739.

Arrigo, K. R., K. E. Lowry, and G. L. van Dijken (2012), Annual changes in sea ice and phytoplankton in polynyas of the Amundsen Sea, Antarctica, *Deep Sea Res. Part II Top. Stud. Oceanogr.*, 71-76, 5–15, doi:10.1016/j.dsr2.2012.03.006.

Bacle, J., E. Carmack, and R. Ingram (2002), Water column structure and circulation under the North Water during spring transition: April–July 1998, *Deep Sea Res. Part II Top. Stud. Oceanogr.*, *49*, 4907–4925.

Bailey, J. N.-L., R. W. Macdonald, H. Sanei, P. M. Outridge, S. C. Johannessen, K. Hochheim, D. Barber, and G. a. Stern (2013), Change at the margin of the North Water Polynya, Baffin Bay, inferred from organic matter records in dated sediment cores, *Mar. Geol.*, *341*, 1–13, doi:10.1016/j.margeo.2013.04.017.

Barber, D. G. (2005), Microwave Remote Sensing, Sea ice and Arctic Climate, *Phys. Canada*, *61*(5), 105–111.

Barber, D. G., J. M. Hanesiak, W. Chan, and J. Piwowar (2001), Sea-Ice and Meteorological Conditions in Northern Baffin Bay and the North Water Polynya between 1979 and 1996, *Atmosphere-Ocean*, *39*(3), 342–359.

Barber, D. G., and R. A. Massom (2007), The Role of Sea Ice in Arctic and Antarctic Polynyas, in *Polynyas: Windows to the World*, edited by W. O. Smith and D. G. Barber, pp. 1–54, Elsevier Science, Amsterdam.

Belchansky, G. I., D. C. Douglas, I. V. Alpatsky, and N. G. Platonov (2004), Spatial and temporal multiyear sea ice distributions in the Arctic: A neural network analysis of SSM/I data, 1988-2001, *J. Geophys. Res. C Ocean.*, *109*(10), 1988–2001, doi:10.1029/2004JC002388.

Boisvert, L. N., T. Markus, C. L. Parkinson, and T. Vihma (2012), Moisture fluxes derived from EOS aqua satellite data for the north water polynya over 2003–2009, *J. Geophys. Res.*, *117*(D06119), doi:10.1029/2011JD016949.

Cape, M. R., M. Vernet, M. Kahru, and G. Spreen (2014), Polynya dynamics drive primary production in the Larsen A and B embayments following ice shelf collapse, *J. Geophys. Res. Ocean.*, *119*, 572–594, doi:10.1002/2013JC009441.

Carsey F.D., Barry R.G., and Weeks R.F. (1992). Introduction. In: Carsey F.D., Microwave remote sensing of sea ice. *American Geophysical Union*, 1-7.

Cavalieri, D. J., and S. Martin (1985), A passive microwave study of polynyas along the Antarctic Wilkes Land coast, in Oceanology of the Antarctic Continental Shelf, edited by S. S. Jacobs, pp. 227–252, American Geophysical Union, Washington D.C.

Cavalieri, D. J., B. A. Burns, and R. G. Onstott (1990), Investigation of the effects of summer melt on the calculation of sea ice concentration using active and passive microwave data, *J. Geophys. Res.,* 95(C4), 5359, doi:10.1029/JC095iC04p05359.

Cavalieri, D. J., K. M. Stgermain, and C. T. Swift (1995), Reduction of weather effects in the calculation of sea ice concentration with the DMSP SSM/I, *J. Glaciol.,* 41(139), 455–464.

Cavalieri, D. J., C. L. Parkinson, P. Gloersen, J. C. Comiso, and H. J. Zwally (1999), Deriving long-term time series of sea ice cover from satellite passive- microwave multisensor data sets, *J. Geophys. Res.,* 104(C7), 15803, doi:10.1029/1999JC900081.

Comiso, J. C., and R. Kwok (1996), Surface and radiative characteristics of the summer Arctic sea ice cover from multisensor satellite observations, *J. Geophys. Res.,* 101(96), 28397–28416.

Cuny, J., P. B. Rhines, and R. Kwok (2005), Davis Strait volume, freshwater and heat fluxes, *Deep. Res. Part I Oceanogr. Res. Pap.*, *52*(3), 519–542, doi:10.1016/j.dsr.2004.10.006.

Dey, B. (1980), Applications of satellite thermal infrared images for monitoring north water during the periods of polar darkness, *J. Glaciol.*, *25*(93).

Dey, B., H. Moore, and A. F. Gregory (1979), Monitoring and mapping sea-ice breakup and freezeup of Arctic Canada from satellite imagery, *Arct. Alp. Res.*, *11*(2), 229–242, doi:10.1657/1938-4246-42.1.45.

Dieckmann, G. S., and H. H. Hellmer (2009), The Importance of Sea Ice: An Overview, in *Sea Ice*, edited by D. N. Thomas and G. S. Dieckmann, pp. 1–110, Wiley- Blackwell, Oxford.

Drucker, R., S. Martin, and R. Moritz (2003), Observations of ice thickness and frazil ice in the St. Lawrence Island polynya from satellite imagery, upward looking sonar, and salinity/temperature moorings, *J. Geophys. Res. Ocean.*, *108*(C5), doi:10.1029/2001JC001213.

Dumont, D., Y. Gratton, and T. E. Arbetter (2009), Modeling the Dynamics of the North Water Polynya Ice Bridge, *J. Phys. Oceanogr.*, *39*(6), 1448–1461, doi:10.1175/2008JPO3965.1.

Dunbar, M. (1969), The Geographical Position of the North Water, *Arctic*, *22*(4), 438–441.

Dunbar, M. (1973), Ice Regime and Ice Transport in Nares Strait, *Arctic*, *26*(4), 282–291.

Dunbar, M. J. (1981), Physical Causes and biological significance of polynyas and other open water in sea ice, in *Polynyas in the Canadian Arctic*, edited by I. Stirling and H. Cleator, pp. 29–43, Canadian Wildlife Service, Ottawa, ON.

Dunphy, M., F. Dupont, C. G. Hannah, and D. Greenberg (2005), Validation of a Modelling System for Tides in the Canadian Arctic Archipelago, *Can. Tech. Rep. Hydrogr. Ocean Sci. 243*, pp 76.

Forsberg, R., and H. Skourup (2005), Arctic Ocean gravity, geoid and sea-ice freeboard heights from ICESat and GRACE, *Geophys. Res. Lett.*, *32*(L21502), doi:10.1029/2005GL023711.

Fu, H. L., J. P. Zhao, and K. E. Frey (2012), Investigation of polynya dynamics in the northern Bering Sea using greyscale morphology image-processing techniques, *Int. J. Remote Sens.*, *33*(7), 2214–2232, doi:10.1080/01431161.2011.608088.

Gallée, H. (1997), Air-sea interactions over Terra Nova Bay during winter: Simulation with a coupled atmosphere-polynya model, *J. Geophys. Res. Atmos., 102*(D12), 13835-13849, doi:10.1029/96JD03098.

Gordon, A. L., and J. C. Comiso (1988), Polynyas in the Southern Ocean the global heat engine that couples the ocean and the atmosphere, *Sci. Am.*, *258*(6), 90–97.

Granskog, M. A., R. W. Macdonald, Z. Z. a. Kuzyk, S. Senneville, C.-J. Mundy, D. G. Barber, G. a. Stern, and F. Saucier (2009), Coastal conduit in southwestern Hudson Bay (Canada) in summer: Rapid transit of freshwater and significant loss of colored dissolved organic matter, J. Geophys. Res., 114(C8), C08012, doi:10.1029/2009JC005270.

Greisman, P., S. Grant, and A. Blaskovich (1986), Tidal propagation measurements in Baffin Bay, Lancaster Sound, and Nares Strait, *Canadian Contractor Report of Hydrography and Ocean Sciences No. 25,* pp558, Dartmouth, Nova Scotia.

Grenfell et al. (1992), Considerations for microwave remote sensing of thin sea ice, in *Microwave Remote Sensing of Sea Ice*, edited by F. D. Carsey, American Geophysical Union, Washington D.C.

Hamilton, J., and Y. Wu (2013), Synopsis and trends in the physical environment of Baffin Bay and Davis Strait, Canadian Technical Report of Hydrography and Ocean Sciences 282, Bedford Institute of Oceanography, Dartmouth, Nova Scotia.

Hall, R. T., and D. A. Rothrock (1987), Photogrammetric observations of the lateral melt of sea ice floes, J. Geophys. Res., 92(C7), 7045, doi:10.1029/JC092iC07p07045.

Heinrichs, J. F., D. J. Cavalieri, and T. Markus (2006), Assessment of the AMSR-E Sea Ice-Concentration Product at the Ice Edge Using RADARSAT-1 and MODIS Imagery, *IEEE Trans. Geosci. Remote Sens.,* 44(11), 3070–3080, doi:10.1109/TGRS.2006.880622.

Héquette, A., M. Desrosiers, and P. W. Barnes (1995), Sea ice scouring on the inner shelf of the southeastern Canadian Beaufort Sea, *Mar. Geol.*, *128*(3-4), 201–219, doi:10.1016/0025-3227(95)00095-G.

Henshaw, A. (2003), Polynyas and ice edge habitats in cultural context: Archaeological perspectives from southeast Baffin Island, *Arctic*, *56*(1), 1–13.

Hibler, W. D., J. K. Hutchings, and C. F. Ip (2006), Sea-ice arching and multiple flow states Arctic ice pack, *Ann. Glaciol.*, *44*(1), 339–344, doi:10.3189/172756406781811448.

Holland, D. M., and L. A. Mysak (1996), Simulation of the mixed-layer circulation in the Arctic Ocean, *J. Geophys. Res. Oceans, 101*(95), 1111–1128, doi:10.1029/95JC02819.

Ingram, R., J. Bacle, D. Barber, Y. Gratton, and H. Melling (2002), An overview of physical processes in the North Water, *Deep Sea Res. Part II Top. Stud. Oceanogr.*, *49*(22-23), 4893–4906, doi:10.1016/S0967-0645(02)00169-8.

Ito, H. (1982), Wind Through a channel: surface wind measurements in Smith Sound and Jones Sound in Northern Baffin Bay, *J. Appl. Meteorol.*, *21*(8), 1053–1062.

Ito, H., and F. Muller (1977), Horizontal movement of fast ice in the North Water area, *J. Glaciol.*, *19*(81), 547–554.

Jones, E. P., J. H. Swift, L. G. Anderson, M. Lipizer, G. Civitarese, K. K. Falkner, G. Kattner, and F. McLaughlin (2003), Tracing Pacific water in the North Atlantic Ocean, *J. Geophys. Res.*, *108*(C4), doi:10.1029/2001JC001141.

Kaleschke, L., C. Lüpkes, T. Vihma, J. Haarpaintner, A. Bochert, J. Hartmann, and G. Heygster (2001), SSM/I sea ice remote sensing for mesoscale ocean-atmosphere interaction analysis, *Can. J. Remote sensing, Vol. 27(5)*, *27*(5), 526–537, doi:10.1080/07038992.2001.10854892.

Kato, H., and O. M. Phillips (1969), On penetration of a turbulent layer into stratified fluid, J. Fluid Mech., 37, 643–655.

Key, E. L., P. J. Minnett, and R. a. Jones (2004), Cloud distributions over the coastal Arctic Ocean: surface-based and satellite observations, *Atmos. Res.*, *72*, 57–88, doi:10.1016/j.atmosres.2004.03.029.

Kern, S. (2009), Wintertime Antarctic coastal polynya area: 1992–2008, *Geophys. Res. Lett.*, 36(14), L14501, doi:10.1029/2009GL038062.

Kern, S. (2008), Polynya Area in the Kara Sea, Arctic, obtained with microwave radiometry for 1979–2003, *IEEE Geosci. Remote Sens. Lett.*, *5*(2), 171–175, doi:10.1109/LGRS.2008.916831.

Kirillov, S. A., I. A. Dmitrenko, J. A. Hölemann, H. Kassens, and E. Bloshkina (2013), The penetrative mixing in the Laptev Sea coastal polynya pycnocline layer, *Cont. Shelf Res.*, 63(March 2008), 34–42, doi:10.1016/j.csr.2013.04.040.

Kottmeier, C., and D. Engelbart (1992), Generation and atmospheric heat exchange of coastal polynyas in the Weddell Sea, *Boundary-Layer Meteorology*, 60(3), 207-234, doi:10.1007/BF00119376.

Kozo, T. L. (1991), The hybrid polynya at the northern end of Nares Strait, *Geophys. Res. Lett.*, *18*(11), 2059–2062.

Kwok, R. (2005), Variability of Nares Strait ice flux, *Geophys. Res. Lett.*, *32*(24), 1–4, doi:10.1029/2005GL024768.

Kwok, R. (2008), Summer sea ice motion from the 18 GHz channel of AMSR-E and the exchange of sea ice between the Pacific and Atlantic sectors, *Geophys. Res. Lett.*, *35*(3), L03504, doi:10.1029/2007GL032692.

Kwok, R., and G. F. Cunningham (2008), ICESat over Arctic sea ice: Estimation of snow depth and ice thickness, *J. Geophys. Res.*, *113*(C08010), doi:10.1029/2008JC004753.

Kwok, R., G. F. Cunningham, H. J. Zwally, and D. Yi (2006), ICESat over Arctic sea ice: Interpretation of altimetric and reflectivity profiles, *J. Geophys. Res.*, *111*(C06006), C06006, doi:10.1029/2005JC003175.

Kwok, R., L. Toudal Pedersen, P. Gudmandsen, and S. S. Pang (2010), Large sea ice outflow into the Nares Strait in 2007, *Geophys. Res. Lett.*, *37*(3), L03502, doi:10.1029/2009GL041872.

Kwok, R., G. F. Cunningham, H. J. Zwally, and D. Yi (2007), Ice, Cloud, and land Elevation Satellite (ICESat) over Arctic sea ice: Retrieval of freeboard, *J. Geophys. Res.*, *112*(C12013), doi:10.1029/2006JC003978.

Lemke, P. (2001), Open the Windows to Polar Oceans, Science, 292(5522), 1670– 1671.

Leppäranta, M. (2005), *The drift of sea ice*, Springer, Chichester, UK, pp 261.

Lillesand, T. M., R. W. Kiefer, and J. W. Chipman (2008), *Remote sensing and image interpretation,* 6th ed., Wiley, New York, NY.

Lloyd, J. M., A. Kuijpers, A. Long, M. Moros, and L. a Park (2007), Foraminiferal reconstruction of mid- to late-Holocene ocean circulation and climate variability in Disko Bugt, West Greenland, *The Holocene*, *17*(8), 1079–1091, doi:10.1177/0959683607082548.

Lubin, D., and R. A. Massom (2004), *Polar Remote Sensing: Volume 1 Atmosphere and Oceans*, Praxis Publishing Ltd., Chichester, UK.

Liu, A. K., S. Martin, and R. Kwok (1997), Tracking of Ice Edges and Ice Floes by Wavelet Analysis of SAR Images, J. Atmos. Ocean. Technol., 14, 1187–1199.

Marsden, R. F., J. Serdula, E. Key, and P. J. Minnett (2004), Are polynyas self-sustaining?, *Atmosphere-Ocean*, *42*(4), 251–265.

Martin, S., R. Drucker, R. Kwok, and B. Hold (2004), Estimation of the thin ice thickness and heat flux for the Chukchi Sea Alaskan coast polynya from Special Sensor Microwave/Imager data, 1990–2001, *J. Geophys. Res.*, *109*(C10012), doi:10.1029/2004JC002428.

Massom, R. A. (1988), The biological significance of open water within the sea ice covers of the polar regions, Endeavour, 12(1), 21–27.

Massom, R.A. (2009), Principal Uses of Remote Sensing in Sea Ice Field Research, in Field Techniques for Sea Ice Research edited by H. Eicken, R. Gradinger, M. Salganek, K. Shirasawa, D. Perovich and M. Leppäranta, pp. 405-466 University of Alaska Press, Fairbanks.

Massom, R. A., P. T. Harris, K. J. Michael, and M. J. Potter (1998), The distribution and formative processes of latent-heat polynyas in East Antarctica, *Ann. Glaciol., 27*, 420–426.

Maxwell, J. B. (1981), Climatic regions of the Canadian Arctic Islands, *Arctic*, *34*(3), 225–240.

McLaughlin, F. A., E. C. Carmack, R. G. Ingram, W. J. Williams, and C. Michel (2004), Oceanography of the Northwest Passage, in *The Sea*, vol. 14, edited by A. R. Robinson and K. Brink, pp. 1211–1242, Harvard University Press.

Melling, H., Y. Gratton, and G. Ingram (2001), Ocean circulation within the North Water polynya of Baffin Bay, *Atmosphere-Ocean*, *39*(3), 301–325, doi:10.1080/07055900.2001.9649683.

Miller, L. a. et al. (2002), Carbon distributions and fluxes in the North Water, 1998 and 1999, *Deep. Res. Part II Top. Stud. Oceanogr.*, *49*, 5151–5170, doi:10.1016/s0967-0645(02)00183-2.

Minnet, P. J., E. L. Key (2007), Meteorology and Atmosphere-Surface Coupling in and around Polynyas, in *Windows to the World,* edited by W. O. Smith and D. G. Barber, pp127–154, Elsevier Science, Amsterdam.

Morales Maqueda, M. A., A. J. Willmott, and N. R. T. Biggs (2004), Polynya Dynamics: A Review of Observations and Modeling, *Rev. Geophys., 42*(RG1004), doi:10.1029/2002RG000116.

Moroni, M., and A. Cenedese (2006), Nonlinear Processes in Geophysics Penetrative convection in stratified fluids : velocity and temperature measurements, Nonlinear Process. Geophys., 13(3), 353–363.

Muench, R. D. (1971), The physical oceanography of the northern Baffin Bay region, in *The Baffin Bay-North Water Project,* Project Scientific Report Number 1, pp1-150, Arctic Institute of North America, Montreal.

Muench, R. D., D. C. Smith, and C. A. Paulson (1995), Convection beneath freezing leads: New observations compared with numerical model results, *J. Geophys. Res. Ocean.*, *100*(C3), 4681–4692.

Münchow, A., H. Melling, and K. K. Falkner (2006), An Observational Estimate of Volume and Freshwater Flux Leaving the Arctic Ocean through Nares Strait, *J. Phys. Oceanogr.*, *36*(11), 2025–2041, doi:10.1175/JPO2962.1.

Mundy, C. J., and D. G. Barber (2001), On the relationship between spatial patterns of sea-ice type and the mechanisms which create and maintain the North Water (NOW) polynya, *Atmosphere-Ocean*, *39*(3), 327–341, doi:10.1080/07055900.2001.9649684.

Mysak, L. A., and F. Huang (1992), A latent- and sensible-heat polynya model for the North Water, Northern Baffin Bay, *J. Phys. Oceanogr.*, *22*, 596–608.

Parashar, S. K., R. M. Haralick, R. K. Moore, and a W. Biggs (1977), Radar Scatterometer Discrimination of Sea-Ice Types, *Ieee Trans. Geosci. Remote Sens.*, *15*(2), 83–87.

Pereira, C. P. G., C. M. T. Woodworth-lynas, and J. V. Barrie (1988), Iceberg scour investigations and sedimentology of the Southeast Baffin Island continental shelf, *Arctic*, *41*(3), 221–230.

Petrich, C., and H. Eicken (2010), Growth, structure and properties of sea ice, in Sea Ice, edited by D. N. Thomas and G. S. Dieckmann, pp. 23–77, Wiley-Blackwell, Hoboken, NJ.

Rabe, B., H. L. Johnson, A. Munchow, and H. Melling (2012), Geostropic ocean currents and freshwater fluxes across the Canadian polar shelf via Nares Strait, *J. Mar. Res.*, *70*(4), 603–640.

Richmond, O., and Gardner (1962), Limiting spans for arching of bulk materials in vertical channels, *Chem. Eng. Sci.*, *17*, 1071–1078.

Samelson, R. M., T. Agnew, H. Melling, and a Münchow (2006), Evidence for atmospheric control of sea-ice motion through Nares Strait, *Geophys. Res. Lett.*, *33*(2), 2–5, doi:10.1029/2005GL025016.

Schledermann, P. (1980), Polynyas and Prehistoric Settlement Patterns, *Arctic*, *33*(2), 292–302.

Smith W.O. Jr. (1995), Primary productivity and new production in the Northeast Water (Greenland) Polynya during summer 1992., *J. Geophys. Res.*, *100*(C3), 4357–4370, doi:10.1029/94jc02764.

Smith, W. O., and L. I. Gordon (1997), Hyperproductivity of the Ross Sea (Antarctica) polynya during austral spring, *Geophys. Res. Lett.*, *24*(3), 233–236, doi:10.1029/96GL03926.

Smith, M., and B. Rigby (1981), Distribution of polynyas in the Canadian Arctic, in *Polynyas in the Canadian Arctic*, edited by I. Stirling and H. Cleator, pp. 7–28, Canadian Wildlife Service, Ottawa, ON.

Smith, S. D., R. D. Muench, and C. H. Pease (1990), Polynyas and Leads: An Overview of Physical Processes and Environment, *J. Geophys. Res.*, *95*(C6), 9461–9479, doi:10.1029/JC095iC06p09461.

Smith, M. B., J.-P. Labat, A. D. Fraser, R. A. Massom, and P. Koubbi (2011), A GIS approach to estimating interannual variability of sea ice concentration in the Dumont d'Urville Sea near Terre Adélie from 2003 to 2009, *Polar Sci.,* 5(2), 104–117, doi:10.1016/j.polar.2011.04.007.

Sodhi, D.S. (1977), Ice arching and the drift of pack ice through restricted channels, Report 77-18, Cold Regions Research and Engineering Laboratory, Hanover, New Hampshire.

Spreen, G., L. Kaleschke, and G. Heygster (2008), Sea ice remote sensing using AMSR- E 89-GHz channels, *J. Geophys. Res.*, *113*(C2), C02S03, doi:10.1029/2005JC003384.

Steffen, K. (1986), Ice Conditions of an Arctic Polynya: North Water in Winter, *J. Glaciol.*, *32*(112), 383–390.

Stirling, I. (1980), The Biological Importance of Polynyas in the Canadian Arctic, *Arctic, 33*(2), 303–315.

Tang, C. C. L., and E. Dunlap (2007), Modeling Annual Variation of sea-ice cover in Baffin Bay, *Int. J. Offshore Polar Eng.*, *17*(3), 176–181.

Tang, C. C. L., C. K. Ross, T. Yao, B. Petrie, B. M. DeTracey, and E. Dunlap (2004), The circulation, water masses and sea-ice of Baffin Bay, *Prog. Oceanogr.*, *63*(4), 183–228, doi:10.1016/j.pocean.2004.09.005.

Thorndike, A. S., D. A. Rothrock, G. A. Maykut, and R. Colony (1975), The Thickness Distribution of Sea Ice, *J. Geophys. Res.*, *80*(33), 4501–4513, doi:10.1029/JC080i033p04501.

Thorndike, A. S., and R. Colony (1982), Sea ice motion in response to geostrophic winds, *J. Geophys. Res., 87*(C8), 5845–5852.

Tivy, A., S. E. L. Howell, B. Alt, S. McCourt, R. Chagnon, G. Crocker, T. Carrieres, and J. J. Yackel (2011), Trends and variability in summer sea ice cover in the Canadian Arctic based on the Canadian Ice Service Digital Archive, 1960–2008 and 1968–2008, *J. Geophys. Res.*, *116*(C3), doi:10.1029/2009JC005855.

Tremblay, J. E., Y. Gratton, E. C. Carmack, C. D. Payne, and N. M. Price (2002), Impact of the large-scale Arctic circulation and the North Water Polynya on nutrient inventories in Baffin Bay, *J. Geophys. Res.*, *107*(C8), doi:10.1029/2000JC000595.

Tucker, W., D. K. Perovich, A. J. Gow, W. F. Weeks, and M. R. Drinkwater (1992), Physical properties of sea ice relevant to remote sensing, in *Microwave Remote Sensing of Sea Ice*, pp. 9–27, American Geophysical Union, Washington, D.C.

Ushio, S., T. Takizawa, K. I. Ohshima, and T. Kawamura (1999), Ice production and deep-water entrainment in shelf break polynya off Enderby Land, Antarctica, *J. Geophys. Res.*, *104*(C12), 29771–29780, doi:10.1029/1999JC900249.

Vincent, R. F. (2013), The 2009 North Water anomaly, *Remote Sens. Lett.*, *4*(11), 1057–1066, doi:10.1080/2150704X.2013.837227.

Vincent, R. F., and R. F. Marsden (2001), An analysis of the dissolution of ice in Nares Strait using AVHRR Imagery, *Atmosphere-Ocean*, *39*(3), 209–222, doi:10.1080/07055900.2001.9649677.

Vincent, R. F., and R. F. Marsden (2008), A Study of Tidal Influences in the North Water Polynya using Short Time Span Satellite Imagery, *Arctic*, *61*(4), 373–380.

Wadhams, P. (2000), Ice in the Ocean, Gordon and Breach Science Publishers, London UK, pp 351.

Wang, M., and J. E. Overland (2012), A sea ice free summer Arctic within 30 years: An update from CMIP5 models, *Geophys. Res. Lett.*, *39*(L07502), doi:10.1029/2012GL052868.

Wilson, K. J., D. G. Barber, and D. J. King (2001), Validation and Production of RADARSAT-1 Derived Ice-Motion Maps in the North Water (NOW) Polynya, January–December 1998, *Atmosphere-Ocean*, *39*(3), 257–278, doi:10.1080/07055900.2001.9649680.

Williams, W. J., E. C. Carmack, and R. G. Ingram (2007), Physical oceanography of polynyas, in Polynyas: Windows to the World, edited by W. O. Smith and D. G. Barber, pp. 55–85, Elsevier Science, Amsterdam.

Willmes, S., S. Adams, D. Schröder, and G. Heinemann (2011), Spatio-temporal variability of polynya dynamics and ice production in the Laptev sea between the winters of 1979/80 and 2007/08, *Polar Res.*, *30*, doi:10.3402/polar.v30i0.5971.

Winebrenner, D., et al. (1992), Microwave sea ice signature modeling, in *Microwave Remote Sensing of Sea Ice*, edited by F. D. Carsey, American Geophysical Union, Washington

D.C.

Worby, A. P., and J. C. Comiso (2004), Studies of the Antarctic sea ice edge and ice extent from satellite and ship observations, *Remote Sens. Environ.,* 92(1), 98– 111, doi:10.1016/j.rse.2004.05.007.

Yackel, J. J., D. G. Barber, and T. N. Papakyriakou (2001), On the Estimation of Spring Melt in the North Water Polynya using RADARSAT-1, *Atmosphere-Ocean*, *39*(3), 195–208.

Yao, T., and C. L. Tang (2003), The formation and maintenance of the North Water Polynya, *Atmosphere-Ocean*, *41*(3), 187–201, doi:10.3137/ao.410301.

Zwally, H. J., J. C. Comiso, and A. L. Gordon (1985), Antarctic Offshore Leads and Polynyas and Oceanographic Effects, in *Oceanology of the Antarctic Continental Shelf*, edited by S. S. Jacobs, pp. 203-226, American Geophysical Union, Washington, D. C..

Zwally, H. J., D. Yi, R. Kwok, and Y. Zhao (2008), ICESat measurements of sea ice freeboard and estimates of sea ice thickness in the Weddell Sea, *J. Geophys. Res. Ocean.*, *113*(C02S15), doi:10.1029/2007JC004284.

CHAPTER THREE: IDENTIFYING CHANGES IN THE FORMATION AND DISSOLUTION OF THE NORTH WATER POLYNYA, 1979-2012: AN INDEX CLASSIFICATION APPROACH

This paper has been prepared and was submitted on 8 January 2016 for peer review in *Arctic*. The work represents a core chapter of my thesis that was conceived, analyzed, and reported by me as the senior author.

Stark, H.F., L. Candlish, and D.G. Barber (in review), Identifying changes in the formation and dissolution of the North Water Polynya, 1972-2012: An index classification approach, *Arctic*. Manuscript ID Number 16-105.

Abstract

A 34-year passive microwave sea ice concentration dataset was used to examine the variability of the Smith Sound ice arch associated with formation and dissolution of the North Water Polynya (NOW) from 1979-2012. An index classification algorithm was generated to determine the presence or absence of the Smith Sound ice arch using an 80% sea ice concentration threshold. The algorithm focused on two points of interest: Kane Basin, which had a known sea ice concentration during winter, and northern Baffin Bay, which was situated in the open water of the polynya. Results show that several years were characterized by anomalous behaviour, including the polynya forming earlier (2003 and 2006), the ice arch not forming in Smith Sound (1983, 1990, 2009), and the ice arch not forming at all (1993, 1995, 2007, 2010). The algorithm results indicated a shift in the timing of polynya formation and dissolution, with both occurring earlier. Formation of the polynya occurred 18 days earlier by the end of the study period, while dissolution occurred 17 days earlier, on average. These shifts are speculated to be a response to large scale climate changes currently ongoing in the Arctic. The implications of the

timing of formation and dissolution are important when considering the physical, biological, , meteorological, and geochemical implications of changing ice conditions in the NOW polynya.

3.1 Introduction

The Arctic environment is rapidly changing; a regime dominated by thick multiyear sea ice has now shifted to a regime of thinner first-year ice [*Maslanik et al.,* 2011; *Comiso,* 2012; *Parkinson and Comiso,* 2013]. Multiyear ice has lost approximately 42% of its surface area coverage and thinned 0.6 m since 2005, concurrent with increased spatial extent and volume of first-year ice [*Kwok et al.,* 2009]. This shift is affecting all aspects of the Arctic marine icescape, including the formation and dissolution of polynyas, impacting local oceanographic and biological processes [*Arrigo and van Dijken*, 2004; *Tamura and Ohshima*, 2011; *Arrigo et al*., 2012; *Bauch et al.*, 2012; *Ciappa et al.*, 2012; *Nihashi and Ohshima*, 2015]. Polynyas are unique regions of the marine icescape defined by persistent open water or very thin ice, where sea ice is typically expected due to local climatological temperature. Local atmospheric and oceanic conditions contribute to the prevention and/or reduction in the thermodynamic growth of sea ice [*Smith et al.*, 1990; *Agnew and Shokr*, 1998; *Barber and Massom*, 2007].

The North Water Polynya (NOW), one of the most biologically productive regions in the Arctic [*Stirling*, 1977, 1980], is located at the northern extent of Baffin Bay between Ellesmere Island and Greenland (Figure 3.1a). Early studies described NOW as both a latent and sensible heat polynya, as winds (associated with latent heat) drive ice from the region, while the upwelling of Atlantic water from the West Greenland Current (associated with sensible heat) melt newly forming ice [*Dunbar and Dunbar*, 1972; *Dunbar*, 1981; *Ito*, 1982; *Steffan*, 1985; *Darby et al.*, 1994]. *Ingram et al.* [2002] confirmed that while there are localized heat flux contributions along the Greenlandic coast, the polynya is formed and maintained mainly by

contributions of wind and ice from the Arctic Ocean.

Nares Strait is a major thoroughfare for the drift of sea ice from the Arctic Ocean, exporting approximately 40,000 km^2, or 120 km^3, of ice annually [*Kwok*, 2005; 2010]. The ice flux moving through Nares Strait has been affected by changes in ice type, as well as ice thickness [*Kwok*, 2005]. This large but highly variable flux of first and multi-year sea ice influences the formation of NOW, which is heavily dependent on the consolidation of ice in the narrow channel upstream of the polynya formation. Smith Sound, measuring 30 km across, acts as a constriction-point for sea ice, slowing down the flux and leading to the formation of an ice arch from blockage in the narrow sound. The ice arch stabilizes during the winter months, strengthening as lower temperatures support ice consolidation. Ice arch formation allows for northerly winds and ocean currents to advect the newly forming sea ice downstream of the arch, subsequently opening the polynya [*Yao and Tang,* 2003].

The mechanics of ice arching were first related to granular materials moving through a fixed channel. The formation of arches is dependent upon the width of a channel, internal friction, and cohesion [*Richmond and Gardner*, 1962]. The thermodynamic growth properties of sea ice introduce additional flow states, creating multiple combinations of cohesive strength (internal bonding of particles) and frictional strength (resistance to movement) to determine the overall shear strength (strength of the material against failure) of sea ice [*Hibler et al.*, 2006]. *Sodhi* [1977] was one of the first to apply models of soil arching to that of sea ice, concluding that ice needed to be of a certain cohesive strength to ensure that the stress applied would not cause arch failure. *Dumont et al.* [2009] applied an elastic-viscous-plastic elliptical rheology model to describe ice arch dynamics in Nares Strait. To form the ice arch sea ice has to be thick enough to dynamically consolidate and there must be consistent strong northerly winds. These

parameters are required to create an arch that is able to withstand the pressure from the building of sea ice behind the arch. The longevity of the arch is directly related to the cohesion of the sea ice, which is dominated by local thermodynamic forces [*Dumont et al.,* 2009].

Recent studies have documented several years of atypical NOW formation and dissolution. In 2007, the ice arch did not consolidate at Smith Sound, resulting in a passageway for sea ice to drift southward from the Arctic Ocean. Nares Strait remained a thoroughfare for ice flux for the entire year, exporting approximately 87,000 km^2 (254 km^3) of ice, which was more than double the export compared to adjacent years [*Kwok et al.*, 2010]. Similarly, an ice arch did not consolidate in Smith Sound in 2009; however, an arch at the mouth of the Lincoln Sea held back the flux of ice until mid-July [*Vincent*, 2013].

The dissolution of NOW occurs during the summer months when warming temperatures trigger melt onset [*Ito*, 1985], which is followed by the break up of the ice arch and the southward drifting of ice into northern Baffin Bay. The exact date of dissolution is dependent upon the strength of the ice arch and the atmospheric conditions during summer [*Yackel et al.*, 2001].

Changes in the dominant ice pack of Nares Strait may have important implications for the usage of northern waterways. The formation of the polynya, associated ice arches, and the fluxes of ice through Nares Strait represent a source of ice hazards (glacial and sea ice) which impact shipping lanes in Baffin Bay [*Barber et al.,* 2014].

As the icescape in the Arctic changes, the long-term impacts of variability on the ice arch and accompanying NOW polynya formation are unknown. The reduced ice cover associated with polynyas allows light penetration to extend longer than in regions where ice is still thick, increasing productivity. Because NOW is one of the most biologically productive marine regions

in the Arctic [*Stirling*, 1977; 1980] it is imperative to examine variability in the ice arch in response to a changing climate and ice conditions in order to determine potential impacts for biological productivity in the future. The presence or absence of the NOW polynya also can control regional heat, moisture, and gas fluxes as a result of the large contrast between an ice cover and open water [*Smith et al.,* 1990; *Miller et al.,* 2002; *Yao and Tang,* 2003; *Boisvert et al.,* 2012]. The regional impact of the polynya requires us to have an understanding of the formation and dissolution dates and their trends over the last several decades.

The overarching objective of this study is to examine the long-term variability of the formation and dissolution of the North Water Polynya. In particular, we explore the following questions:

1. Can we develop a classification index or algorithm to quantify NOW formation and dissolution using satellite based sea ice concentration data?
2. If so, what are the formation and dissolution dates of NOW?
3. Are there temporal trends of these NOW formation and dissolution dates?

3.2 Methods

To accomplish the objectives outlined above, we present an analysis of a sea ice concentration (SIC) dataset from 1979 to 2012. This analysis generated an index that classifies the formation and dissolution of NOW using the ice arch in Smith Sound, and coincident open water immediately south in the NOW polynya, as a proxy.

3.2.1 Passive Microwave Sea Ice Dataset

The primary SIC dataset was obtained from the National Snow and Ice Data Center (NSIDC) for 1979 to 2012 via ftp server (ftp://sidads.colorado.edu/pub/DATASETS/nsidc0051_gsfc_nasateam_seaice/). This SIC dataset was generated from converted brightness

temperatures from a coordinated series of passive microwave data: Scanning Microwave Radiometer (Nimbus-7), Special Sensor Microwave/Imagers (DMSP-F8, -F11, -F13), and Special Microwave Imager/Sounder (DMSP-17). A variety of frequencies were used, including 19.3, 22.2, 37.0 GHz for SSM/I and SSMIS and 6.6, 10.7, 18.0, 21.0, and 37.0 GHz for SMMR, resulting in a gridded spatial resolution of 25 km. The dataset has a temporal resolution of every other day for SMMR (1979 to 1987) and every day for SSM/I-SSMIS (1987 to present) [*Cavelieri et al*., 1996]. The data were processed using the Bootstrap Algorithm by the NSIDC and have a one-year processing lag [*Cavelieri et al.*, 1996].

The original data values were scaled SIC values using a fractional coverage to the scale of 1-250. The data were divided by 2.5 to convert them to a scale of 0-100% ice coverage. From hereon in, the NSIDC sea ice concentration dataset will be referred to as the SSM/I dataset.

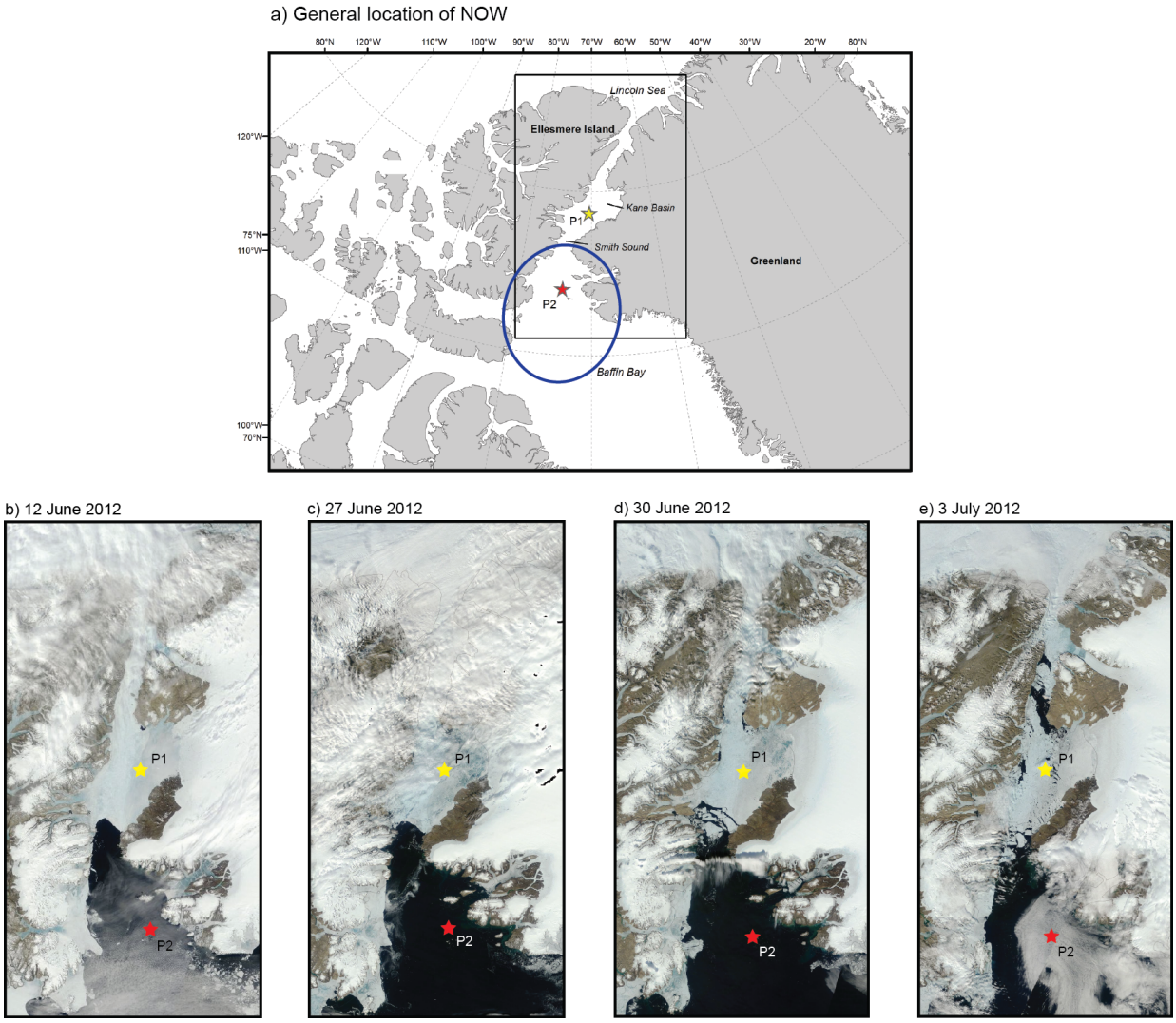

Figure 3.1: Location of P1 and P2 in central Kane Basin and northern Baffin Bay, respectively (a). The blue line in (a) delineates the region NOW typically forms. MODIS imagery displaying the dissolution of the Smith Sound ice arch in 2012. SIC values of P1 were determined by SSMI/I: b) 90% on 12 June 2012; c) 74% on 27 June 2012; d) 68% on 30 June 2012; and e) 65% on 3 July 2012. Arch failure occurred between 27 June (c) and 30 June (d) (Source: NASA Worldview).

To ensure the accuracy of SSM/I for the NOW region, a higher-resolution AMSR-E sea ice concentration dataset was used to validate the lower-resolution SSM/I SIC dataset (Figure 3.1). This was done to ensure the coarser 25 km spatial resolution of the SSM/I dataset could be used to correctly identify ice from open water as required by the index. The AMSR-E dataset was obtained from the University of Bremen as part of the GMES Polar View and the Arctic

Regional Ocean Observing System [*Spreen et al.*, 2008]. The daily sea ice concentration dataset has a spatial resolution of 6.25 km and is available from 2003 to 2011 [*Spreen et al.,* 2008]. SIC values were extracted for two locations in the NOW region, Kane Basin and northern Baffin Bay, for both SSM/I and AMSR-E. The SSM/I dataset were highly correlated to the AMSR-E dataset at both locations from 2003 to 2011. The Spearman's correlations for AMSR-E and SSM/I sea ice concentration values were 0.988 for Kane Basin and 0.972 for northern Baffin Bay with a p-value <0.01, indicating significant correlation. Therefore, the coarser resolution SSM/I data can be used to precisely define SIC and identify long-term trends in the NOW region.

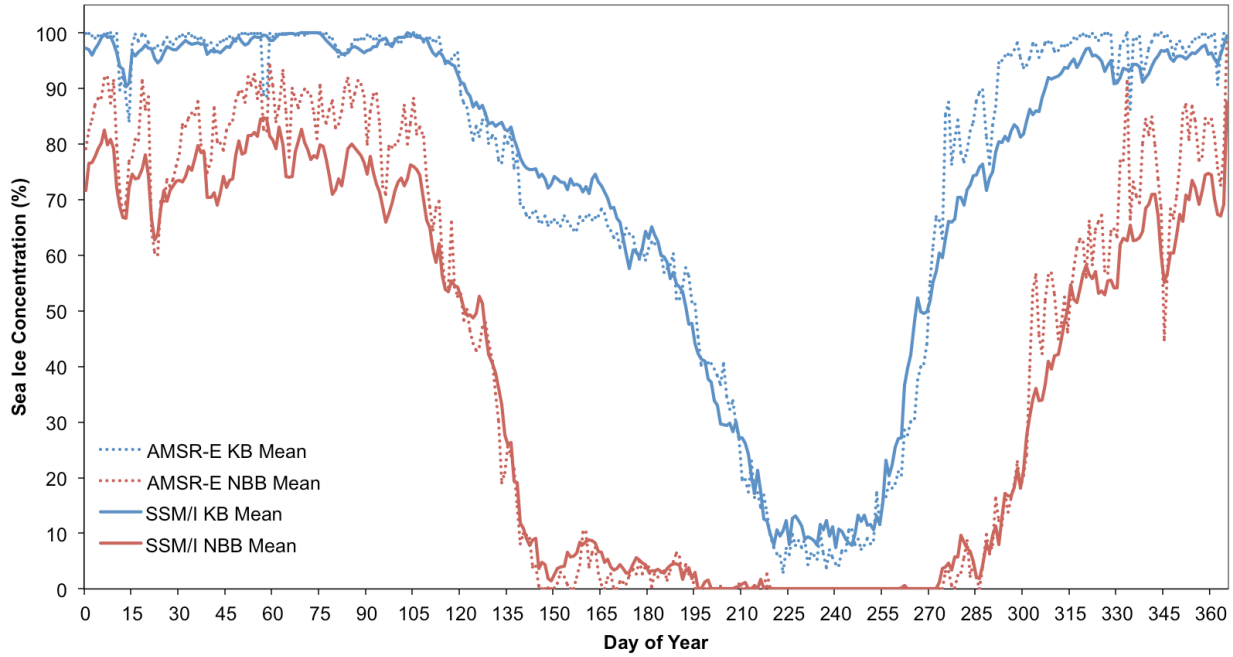

Figure 3.2: Sea ice concentration values extracted for AMSR-E and SSM/I. An average sea ice concentration value for each day was determined by averaging data from 2003-2001 for both AMSR-E and SSM/I.

3.2.2 Creating an Index Classification Algorithm

Passive microwave datasets have been particularly effective for long term monitoring in polar regions [see: *Markus and Burns*, 1994; 1995; *Belchansky et al.*, 2004; *Hwang and Barber*, 2006; *Kern et al.*, 2007; *Kern,* 2008; 2009]. Studies by *Worby et al.* [2004] and *Heinrichs et al.*

[2006] have used remote sensing datasets to examine seasonal ice flux in coastal regions. To determine if a passive microwave dataset would be suitable for the NOW region, an index classification algorithm was developed. This algorithm assisted in categorizing the variability of NOW based on the presence or absence of an ice arch in Smith Sound. The algorithm was generated in a five step process that trained the algorithm to classify NOW as formed or dissolved. The first step involved creating a series of quantifications to classify the dynamics of NOW. NOW was formed when a high-to-low sea ice concentration gradient existed between Kane Basin and northern Baffin Bay and dissolved when there was no high-to-low gradient.

The second step of the generation process was the identification of two points of interest: central Kane Basin and northern Baffin Bay. Canadian ice charts (http://iceweb1.cis.ec.gc.ca/Archive/page1.xhtml;jsessionid=E4BA77F534AF302F3C291FBD79223E76?lang=en) indicated these two locations showed consistent sea ice conditions when NOW was present. Kane Basin typically had a SIC of 80-100% during the winter and spring, whereas northern Baffin Bay exhibited typical polynya behaviour with reduced or thinner ice cover. These two points defined the ice concentration gradient needed to classify NOW as formed or dissolved.

Due to the narrow confines of Nares Strait and the coarse spatial resolution of the SSM/I dataset, care had to be taken when selecting the exact pixel locations to avoid selecting areas containing land. Although the SSM/I dataset contains a filter to reduce land interference, a more rigorous criterion of 25 km from land was used when selecting pixels to ensure no land contamination. The selected points were also closest to the northern and southern segments of the ice arch. The points of interest have the following latitude and longitude: central Kane Basin (P1) at 79.4469°N and 70.1679°W and northern Baffin Bay (P2) at 76.9860°N and 74.056°W

(Figure 3.1a). A time series of ice concentration values were extracted for 1979 to 2012 for both points.

The third step involved the consultation of ice charts. Canadian Ice Service (CIS) weekly ice charts from 1982 to 2012 (via http://iceweb1.cis.ec.gc.ca/Archive/page1.xhtml;jsessionid=E4BA77F5 34AF302F3C291FBD79223E76?lang=en) were consulted to determine a SIC threshold for P1 and P2. *Howell et al.* [2009] indicate that weekly ice charts are sufficient for identifying openings in the Canadian Arctic Archipelago due to slow ice motion in this region. Moreover, ice charts provide accurate forecasting of sea ice drift for the Canadian archipelago and polynyas [*Dey and Feldman*, 1990; *Agnew and Howell,* 2003].

Studies by *Massom et al.* [1998], *Arrigo and van Dijken* [2003], and *Smith et al.* [2011] have used thresholds to classify the dynamics of polynyas. Within this study a threshold was used to classify NOW as formed or dissolved based on the loss of the ice arch. An average SIC value was determined through an iterative process when two sequential ice charts were compared and a window of time identified arch loss. MODIS imagery of P1 in Kane Basin shows the transition from a stable ice arch to arch failure (Figure 3.1b-e). SIC of 90% on 12 June 2012 (Figure 3.1b), 74% on 27 June 2012 (Figure 3.1c), 68% on 30 June 2012 (Figure 3.1d), and 65% on 3 July 2012 (Figure 3.1e), showing arch failure occurred between 68 to 74% ice concentration.

In the fourth step of the generation process, the dates derived from the ice charts were compared to SIC values at P1 from the SSM/I dataset. Multiple comparisons were made between MODIS, ice charts, and SSM/I, producing an average ice concentration value of 78%. There was variation in SIC in Kane Basin before arch failure. In the last step of the generation process, a

sensitivity analysis was conducted to ensure accuracy. A range of ice concentration values, such as 70, 75, 80, and 85%, were tested to determine the threshold value. The analysis indicated that a value of 80% ice concentration was suitable to determine ice arch presence or absence. From this preliminary analysis 80% ice concentration values or above were considered consolidated and NOW was defined as 'formed', while any value below was considered unconsolidated ice and NOW was 'dissolved'.

3.3 Results and Discussion

3.3.1 Determining Ice Arch Formation

The goal of the index classification algorithm was to generate a universal method that would classify the dynamics of multiple polynya types using a passive microwave dataset. The algorithm can classify a polynya as open or not open when two points of interest are identified, one in an area of the typical bridge formation and one in the open water of the polynya. To determine if NOW was formed or dissolved, the ice concentrations of P1 and P2 had to meet certain criteria. The 80% threshold value in Kane Basin (P1) derived from the CIS ice charts was used as the main technique. The steps of the algorithm are outlined in Figure 3.3. There were three output scenarios:

1. NOW formed, with high ice concentrations (≥80%) in Kane Basin (P1) and low ice concentrations (<80%) in Baffin Bay (P2);
2. NOW did not form with a high concentration (≥80%) of sea ice in both Kane Basin (P1) and northern Baffin Bay (P2); and
3. NOW did not form with a low concentration (<80%) of sea ice in Kane Basin (P1).

Every polynya cycle between 1979 and 2012 was classified using this algorithm. In addition, fall freeze-up was manually determined by noting the day of year sea ice concentration began to

increase at P1.

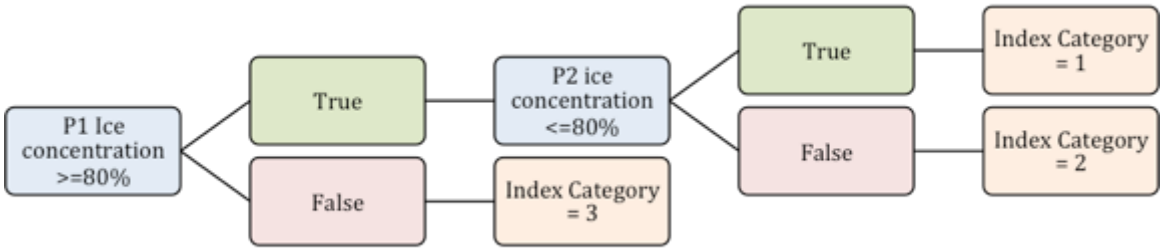

Figure 3.3: Classification index algorithm for NOW.

It is important to note that the algorithm uses the presence of the arch as a proxy for the polynya. When ice concentrations at P1 and P2 indicate a flux of sea ice (i.e. both high SIC or both low SIC or P1 low SIC and P2 high SIC) the algorithm does not detect a polynya. The consolidation of the ice arch is the driving mechanism in the formation of NOW; if it does not consolidate, Nares Strait becomes a thoroughfare for ice export from the Lincoln Sea.

3.3.2 NOW Formation and Dissolution

The formation and dissolution dates calculated by the index classification algorithm (Figure 3.3) fall within two categories: typical and atypical years. Typical years are when the arch consolidated in Smith Sound, the polynya opened anytime in April, and the onset of summer dissolved the arch in June. On average, in a typical formation year NOW formed on 13 April (day of year 103) and dissolution followed on 29 June (day of year 180), for an open period of 77 days. Atypical years happened when one of the following scenarios occurred: the arch did not form at Smith Sound (blue markers, Figure 3.4); the arch did not form at all (red markers, Figure 3.4); or NOW opened earlier in the year (green markers, Figure 3.4). For reference purposes, the exact formation and dissolution dates are attached in Table 3.1.

Of the 34 years of this study, nine years were marked as atypical formation years: two

years of early formation (2003 and 2006), four years without ice arch consolidation (1993, 1995, 2007, 2010), and three years without ice arch consolidation in Smith Sound (1983, 1990, 2009). From 2003-2012, NOW experienced five of these abnormal years, with the remaining 4 occurring between 1979-2002. The frequency of anomalies during the 2003-2012 time period suggests more recent changes in the polynya within the decades of the two thousands relative to the earlier period.

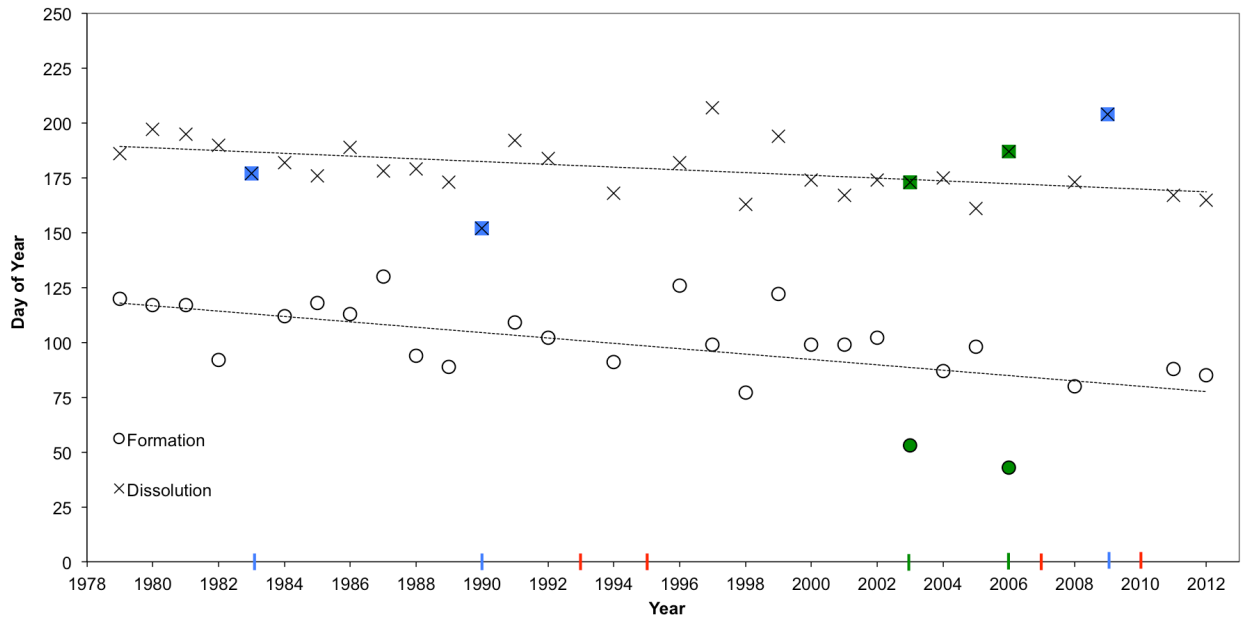

Figure 3.4: Formation and dissolution of NOW determined by the index classification algorithm. Red markers indicate years with no ice arch, blue markers indicate no ice arch in Smith Sound, and green makers indicate early formation years. The years of no ice arch in Smith Sound have dissolution days because the SIC at P1 was <80%, indicating there was an arch elsewhere in Nares Strait.

In addition to the atypical formation years, six years were identified as anomalous in the context of NOW polynya duration; 1985, 1987, 1996, 1997, 2003, and 2006 fell outside one standard deviation of ±19.7 days (red circles; Figure 3.5). It is important to note that these anomalies were not the same years the ice arch and polynya did not form; however, two years, 2003 and 2006, were associated with earlier polynya formation.

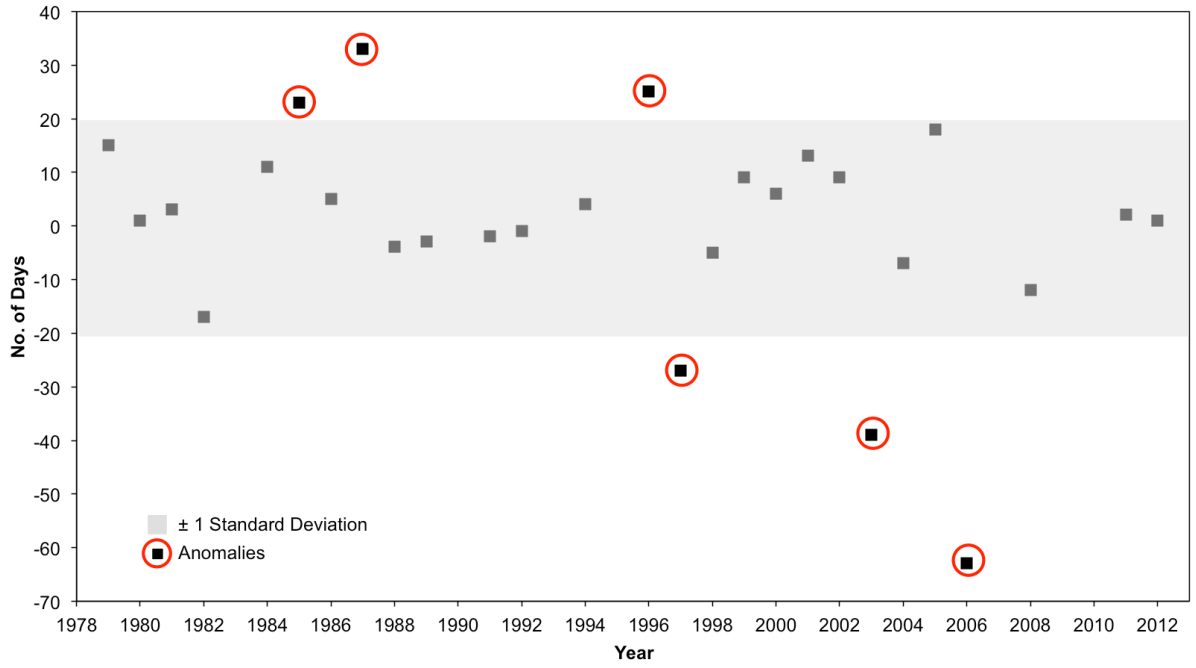

Figure 3.5: Deviations from the mean for the number of days NOW is classified as open. Anomalous years outside ± one standard deviation are circled in red: 1985, 1987, 1996, 1997, 2003, and 2006.

During years when the Smith Sound ice arch was absent, there was no formation date. There was a dissolution date because SIC at P1 was <80%, indicating that an arch formed at a location other than Smith Sound which prevented the southward drift of ice. When SIC at P1 increased, the arch was failing, and thus the polynya was dissolving. However, we do not have confidence in the respective dissolution days of 1983, 1990, and 2009 because the ice arch location was not in Smith South and ice dynamics further north in Nares Strait were unknown.

Table 3.1: Formation DOY, dissolution DOY, number of days NOW is open, and fall freeze-up DOY using the index classification algorithm.

Year	Formation DOY	Dissolution DOY	No. Days Polynya Open	Fall Freeze-up DOY	Comments
1979	120	186	66	290	
1980	117	197	80	277	
1981	117	195	78	271	
1982	92	190	98	266	
1983		177		259	Ice arch formed further north than normal, cannot determine formation date. Determined dissolution date by noting increase in ice flux at P2
1984	112	182	70	280	
1985	118	176	58	248	
1986	113	189	76	275	
1987	130	178	48	284	
1988	94	179	85	302	
1989	89	173	84	267	
1990		152		275	Ice arch formed further north than normal, cannot determine formation date. Determined dissolution date by noting increase in ice flux at P2
1991	109	192	83	265	
1992	102	184	82	287	
1993				274	Ice arch did not consolidate
1994	91	168	77	282	
1995				284	Ice arch did not consolidate
1996	126	182	56	260	
1997	99	207	108	259	
1998	77	163	86	273	
1999	122	194	72	286	
2000	99	174	75	282	
2001	99	167	68	285	
2002	102	174	72	295	
2003	53	173	120	308	
2004	87	175	88	293	
2005	98	161	63	285	
2006	43	187	144	308	
2007				280	Ice arch did not consolidate
2008	80	173	93	280	
2009		204		300	Ice arch consolidated at Lincoln Sound, cannot determine formation date based on location of P2. Determined dissolution date by noting increase in ice flux at P2
2010				288	Ice arch did not consolidate
2011	88	167	79	286	
2012	85	165	80	287	

Results show that both polynya formation and dissolution occurred earlier in recent years, with the largest variations seen during formation. The trend lines for formation and dissolution have a slope of -1.22 d yr^{-1} (F_{df} = 1; r^2 = 0.348; *p-value* <0.01) and -0.63 d yr^{-1} (F_{df} = 1; r^2 = 0.235; p-value <0.01), respectively (Figure 3.4). The dissolution dates of 1983, 1990, and 2009 were excluded from the dissolution analysis because the arch formed in a different location. Earlier formation may be attributed to one or more of the following changes: a shift in the dominant wind regime, a change in the ice pack of Nares Strait, or a change in ocean thermodynamics. Earlier dissolution could be a consequence of the response to a changing Arctic ice pack as thinner sea ice will melt faster in warming Arctic temperatures [*Screen and Simmonds,* 2010], dissolving the arch, and thus the polynya, faster.

Although formation and dissolution dates occur earlier in the year, the time period in which NOW remains open (dissolution date minus formation date) had no statistically significant trends (Figure 3.6). On average, NOW remains open for 81 days and can be open for as little as 48 days (1987) or a maximum of 144 days (2006).

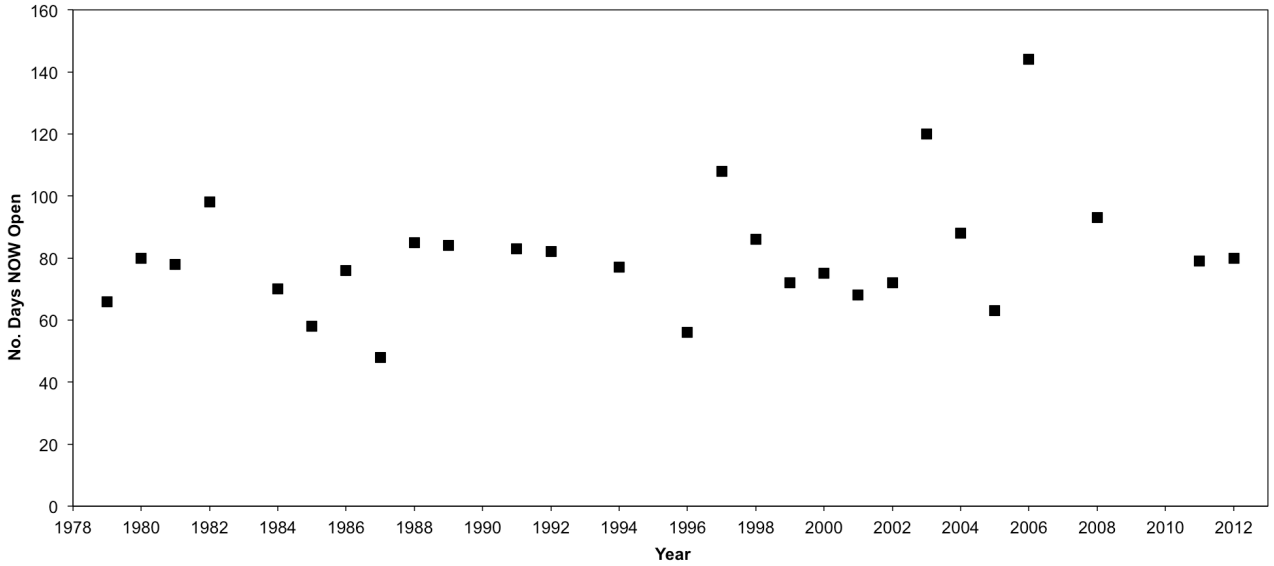

Figure 3.6: Number of days per year NOW was classified as open (dissolution date minus formation date).

Also of interest are fall freeze-up dates following NOW polynya dissolution. The regression analysis of the fall freeze-up dates shows a significant result at a p-value of <0.05 (Figure 3.7). In recent years, fall freeze-up has delayed, as indicated by the slope of the trend line, 0.66 d yr^{-1}. Our results do not conincide with the 1 to 2 days per decade later fall freeze-up *Stroeve et al.* [2014] documented in the Canadian Artic Archipelago and Baffin Bay. Increased sea surface temperautres would impact the thermodynamic growth of sea ice and potentially affect the consolidation of the ice arch; however, further investigation of the sea surface temperature and ice dyanmics in the NOW region are recommended to better understand fall freeze-up trends.

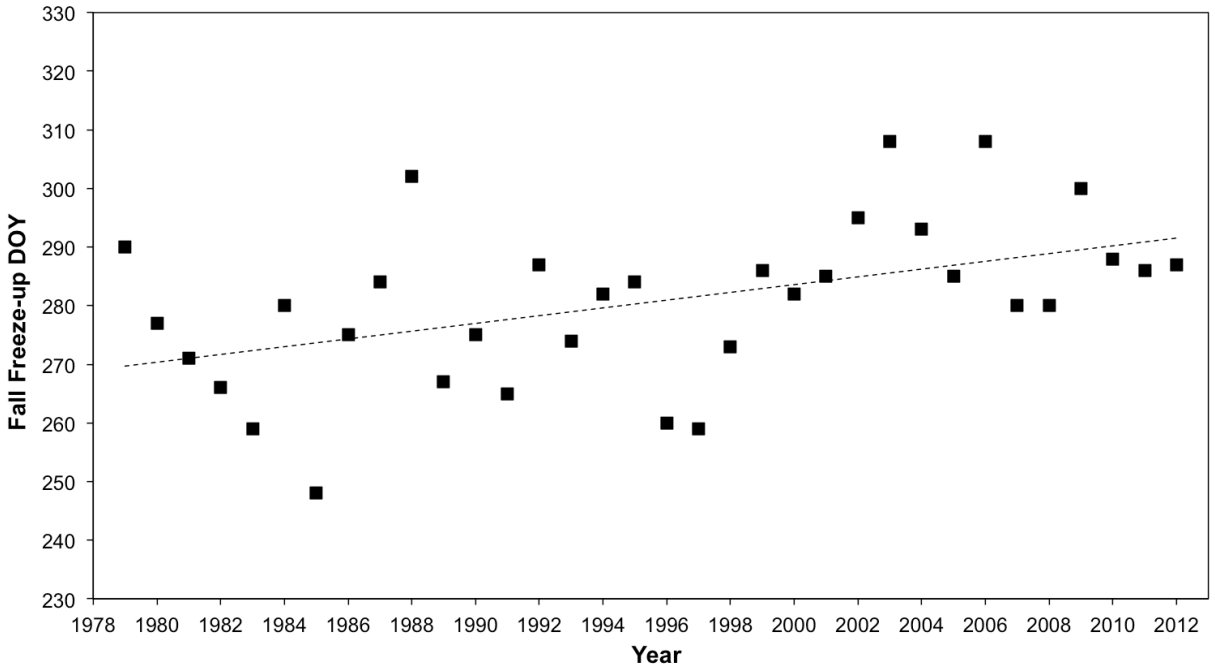

Figure 3.7: Day of year (DOY) of fall freeze-up in the NOW region using the increase in SIC at P1 as the indicator.

The anomalies and atypical years give no indication that the behaviour of NOW is periodic. Instead, the trends indicate that the variability of NOW (formation, dissolution, fall freeze-up,

SIC) has increased over the last two decades.

Between the four metrics of formation, dissolution, open period, and fall freeze-up, there was a correlation between fall freeze-up and formation. The Pearson product-moment test produced a correlation of -0.516, significant at a p-value <0.01 interval. The negative correlation suggests that there is a correspondence between later fall freeze-up and an earlier formation and vice versa. There is also a correlation between formation and dissolution. The relation produced a nonparametric (Spearman's rank order) correlation of 0.538, also significant at a p-value of <0.01. However, causality cannot be determined from these relationships. This correspondence may be an artifact of ice conditions, sea ice drift, ice interactions, atmospheric, and/or oceanic contributions.

3.3.3 Intra-annual Trends

To better understand the seasonality of NOW, the index classification outputs (categories 1, 2, and 3) were further divided into 4 distinct seasons: winter, formation, dissolution, and fall freeze-up. To showcase the variability of NOW, formation and dissolution onset were compared between 4 years (1 typical, 3 atypical): typical formation year (Figure 3.8a), ice arch did not consolidate at Smith Sound (Figure 3.8b), no ice arch consolidation (Figure 3.8c), and early formation year (Figure 3.8d).

In the typical year of 1982 (index classification algorithm category 1) (Figure 3.8a), formation occurred on 2 April (day of year 92), and dissolution occurred on 9 July (day of year 190). When the arch does not form at Smith Sound, the year is indexed as an atypical year (index classification algorithm categories 2 or 3). In 1990 (Figure 3.8b) the arch formed further north in Nares Strait as confirmed by a low ice concentration value at P1 and P2. Although formation cannot be determined because the arch formed further north of P1, an increase in SIC at P2

indicated a sea ice flux due to dissolution which occurred on 1 June (day of year 152). In 1995 (Figure 3.8c), there was no ice arch in Nares Strait or Smith Sound, remaining a thoroughfare for sea ice drift. The behaviour was captured by the algorithm output associated with category 3 – low ice concentrations at P1 and P2. During the early formation year of 2006 (Figure 3.8d), the polynya formed on 11 February (day of year 43) and did not dissolve until 6 July (day of year 187).

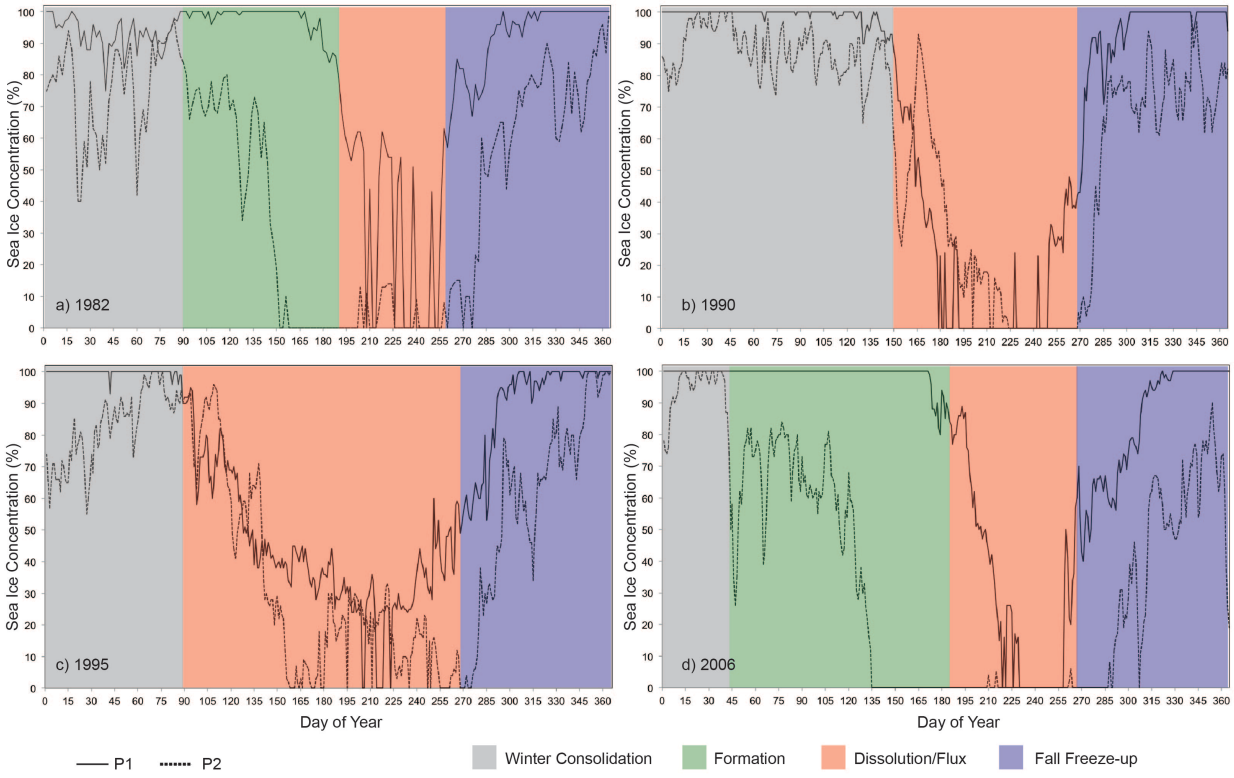

Figure 3.8: Comparisons of typical and atypical formation years: a) typical formation year where formation occurred on 2 April (day of year 92), dissolution occurred on 9 July (day of year 190), and fall freeze-up commenced on 23 September (day of year 266); b) ice arch did not form at Smith Sound, instead forming further north in Nares Strait where dissolution occurred on 1 June (day of year 152) and fall freeze-up commenced on 2 October (day of year 275); c) ice arch did not consolidate resulting in no polynya and fall freeze-up commenced on 11 October (day of year 284); and d) early formation year where formation occurred on 11 February (day of year 43), dissolution occurred on 6 July (day of year 187), and fall freeze-up occurred on 8 November (day of year 308).

The length of each season is a direct result of the local conditions in a given year. No two years of polynya formation and dissolution were the same, confirming that NOW is influenced by multiple factors. The presence of atypical years, especially when the ice arch did not form at Smith Sound, shows how the ice arch responds to changes in the dominant ice pack in Nares Strait [*Kwok et al.,* 2005, *Kwok et al.,* 2010] and decreases in the overall Arctic ice extent [*Cavellieri and Parkinson,* 2012].

3.3.4 Inter-annual Trends

Also of interest was the variation within the overall trends of earlier formation and dissolution. Table 3.2 displays the variance of NOW's formation, dissolution, time open, and fall freeze-up over three time periods (1979-1989, 1990-1999, 2000-2012). Variation in formation has doubled from the first time period to the most recent, with the greatest changes occurring between 1990-1999 and 2000-2012. The spread of the dissolution dates also increased over time, variability in 2000-2012 was almost 5 times greater than 1979-1989. The most variation occurred during 2000-2012 (Table 3.2), when the largest changes in the Arctic ice pack were observed [*Nghiem et al.,* 2007; *Parkinson and Comiso*, 2013]. Variation in freeze-up date has decreased over time, potentially indicating the stabilization of thermodynamic ice growth in the region.

Table 3.2: The variance for each of the time periods was calculated for the formation and dissolution of the polynya along with the time the polynya was open and the date of the fall freeze up. The variance was calculated as the average of the squared differences from the mean.

	Formation	Dissolution	Time Open	Fall Freeze-up
1979-1989	188.4	65.36	207.12	220.67
1990-1999	293.24	329.39	246.62	108.72
2000-2012	405.6	327.27	642.18	93.44

The sea ice concentrations at P1 and P2 over the entire study period, 1979 to 2012,

provide insight in the large-scale changes in the ice pack of Nares Strait (Figure 3.9). It is important to note that the trends at P1 and P2 differ in part because of their geographical locations, but also because of the influences of polynya formation and dissolution.

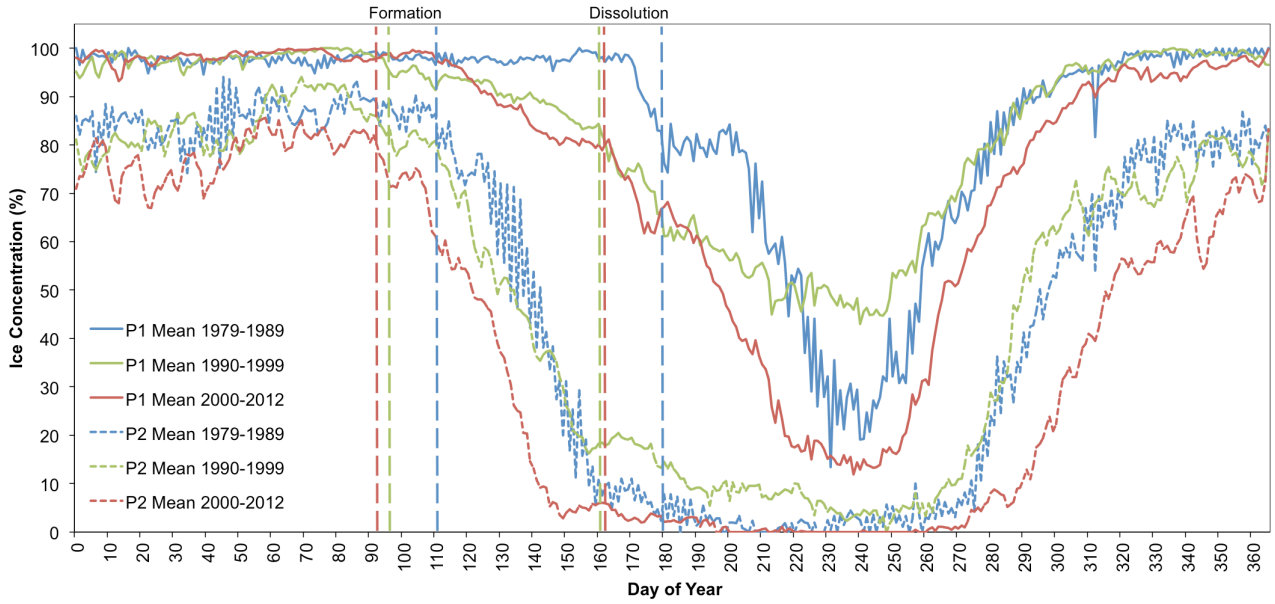

Figure 3.9: Mean SIC values for indicated intervals, as well as formation and dissolution of the polynya, in the NOW region.

Sea ice concentration in the NOW region over the three examined time periods (1979-1989, 1990-1999, 2000-2012) shows a decrease during the annual sea ice cycle, with implications on both the formation and dissolution of the polynya. The formation date of NOW increased by approximately 18 days, 0.53 days/year, over the entire time period. From 1979-1989 the average formation date was 20 April (day of year 110; blue formation line; Figure 3.9), while from 1990-1999 it was 6 April (day of year 96; green formation line; Figure 3.9), and from 2000-2012 it was 2 April (day of year 92; red formation line; Figure 3.9). The period from 1990-1999 experienced the greatest change, which could be linked to the rapidly changing sea ice thickness trends observed for the entire Arctic sea ice cover [*Kwok and Rothrock*, 2009].

Mean sea ice concentration values during winter, defined as the period before arch consolidation, at P2 might indicate trends in thermodynamic ice growth. During 1979-1989 and 1990-1999 at P2, SIC were approximately 80-90% during the winter. The last time period, 2000-2012, had lower SIC during winter, between 70-80%. A reduced ice cover in this region is expected as winds and ocean currents advect ice from the region; however, decadal decreases in SIC during the winter could indicate changes at the ocean-sea ice-atmosphere interface. A change in oceanic temperatures affects in the alteration of the energy flux necessary for sea ice growth, warmer water slows down the growth of sea ice. Additionally, atmospheric influences could also be affecting wintertime ice concentrations as increased wind speeds or a change in dominant wind regime could prevent or slow the growth of sea ice.

Mean decadal SIC values indicate dissolution is also occurring earlier in the year, the dissolution date at P1 occurred approximately 18 days earlier in 1990-1999 than 1979-1989, 10 June and 28 June (day of year 161 and 179; green and blue dissolution lines; Figure 3.9), respectively. From 1990-1999 to 2000-2012, the dissolution date shifted one day later (11 June, day of year 162; red dissolution line; Figure 3.9). For the whole study period the dissolution date has shifted 17 days earlier, or 0.5 days/year. A potential cause for an earlier dissolution is the faster melt of thinner ice. However, the dissolution of the arch is determined by many factors, including atmospheric temperature, and thus no definitive cause can be concluded.

Mean SIC values after the dissolution of the arch indicate changes in the sea ice flux moving through Nares Strait. During 1979-1989, P1 reached a minimum of 15% SIC around 18 August (day of year 230). The trend during 1990-1999 differed considerably; ice concentrations did not drop below 50% the entire summer. We speculate the ice pack anomalies of this time period were driven by the high positive index of the Arctic Oscillation causing the increased

export of sea ice through Nares Strait [*Rigor et al.,* 2002]. During 2000-2012, a minimum SIC of 20% was observed 10 days earlier (8 August) than during the period from 1979-1989 (18 August). An earlier minimum sea ice concentration is likely as a result of melt onset occurring earlier; melt onset was documented to occur 1 to 4 days per decade earlier [*Stroeve et al.,* 2014].

SIC patterns at P2 are different because the region already experiences reduced ice cover when the polynya is formed. A lower concentration of sea ice requires less time to fully melt. During 1979-1989, sea ice concentrations were approximately 10% during summer, whereas decades after, concentrations dropped below 10% and even reached zero in 2000-2012. The trends in the latter two decades coincide with large summer extent losses observed by *Maslanik et al.* [2011].

Reaching the minimum sea ice concentration earlier, at both P1 and P2, can be a result of the transitioning sea ice regime – first-year ice melts at the faster rate than second- or multi-year ice [see *Rigor and Wallace*, 2004]. When the ice melts earlier, the ocean is exposed to the warmer summer atmosphere for a longer time, approximately 20 days over 30 years as determined by *Markus et al.* [2009], which can increase ocean temperatures. The thermodynamic growth of sea ice is dependent upon the temperature gradient generated between the ocean and the atmosphere. Increased oceanic temperatures from a longer exposure to warmer atmospheric temperatures will result in the delay of ice formation; freezing is an exothermic process, thermodynamic energy from the ocean is lost to the surrounds, thus the more thermodynamic energy the ocean has absorbed the longer the freezing process will take. An increased open water period of NOW can not only affect sea ice thermodynamics and dynamics, but also biological productivity and transportation logistics. A longer open water period can increase

biological productivity as there is more phytosynthetic radiation available for a longer period of time.

3.4 Conclusion

A 34-year sea ice concentration dataset was used to examine the long-term variability of the Smith Sound ice arch associated with the formation and dissolution of the North Water Polynya. The first objective was to create an algorithm to quantify NOW formation and dissolution. The index classification algorithm was developed to compare two locations depicting high and low ice concentrations characteristic of the ice arch, and thus polynya formation. This algorithm can be used for other polynyas using two points of interest: one point in the ice surrounding the polynya and the other in the reduced ice concentration of the polynya. Moreover, this algorithm can be incorporated into models to examine the long-term formation and dissolution trends of polynyas.

The second objective was to determine the formation and dissolution dates of NOW. The algorithm results demonstrate a shift in the timing of both the formation and dissolution of the North Water Polynya, with both occurring earlier in the year. On average, NOW remained open for 81 days; however, there is considerable variation in this as it was open for 48 days in 1987 and 144 days in 2006.

The third objective of this study was to examine the temporal trends and anomalies of the NOW formation and dissolution dates. The index classification algorithm identified several years in which the polynya acted abnormally using NOW's ice arch as proxy; the algorithm classified 9 years as atypical. During the years 1993, 1995, 2007, and 2010 the arch did not consolidate; while during 1983, 1990, and 2009 the arch consolidated further north in Nares Strait rather than in Smith Sound; and in 2003 and 2006 NOW formed earlier.

The decadal values identified an 18-day shift in the formation and a 17-day shift in the dissolution of the polynya. Causes of this shift, and also of the increased variability of NOW, are difficult to conclude as numerous factors influence NOW. Therefore it is not possible to suggest a single cause for the variability. We can only conclude that the changing Arctic system is negatively impacting the NOW polynya. Further investigations into the mechanisms responsible for ice arch consolidation are needed in order to provide an explanation of the variability observed. Future studies could further this investigation by comparing the variability in formation and dissolution of NOW to trends in biological productivity of the region.

Acknowledgements: We gratefully acknowledge the contributions of the Canada Excellence Research Chair (CERC) and Canada Research Chair (CRC) programs. Support was also provided by the Natural Sciences and Engineering Research (NSERC) Council, the Canada Foundation for Innovation, and the University of Manitoba. Special thanks for J. Lukovich at the University of Manitoba for her helpful feedback. Thanks to W. Chan at the University of Manitoba and G. Gunn at IISD for assisting with the sea ice concentration datasets. This work is a contribution to the ArcticNet Networks of Centres of Excellence and the Arctic Science Partnership (ASP).

Literature Cited

Agnew, T., and S. Howell (2003), The use of operational ice charts for evaluating passive microwave ice concentration data, *Atmosphere-Ocean*, *41*(4), 317–331, doi:10.3137/ao.410405.

Arrigo, K. R., and G. L. van Dijken (2004), Annual cycles of sea ice and phytoplankton in Cape Bathurst polynya, southeastern Beaufort Sea, Canadian Arctic, *Geophys. Res. Lett.*, *31*(8), L08304, doi:10.1029/2003GL018978.

Arrigo, K. R., K. E. Lowry, and G. L. van Dijken (2012), Annual changes in sea ice and phytoplankton in polynyas of the Amundsen Sea, Antarctica, *Deep. Res. Part II Top. Stud. Oceanogr.*, *71-76*, 5–15, doi:10.1016/j.dsr2.2012.03.006.

Barber, D. G., J. M. Hanesiak, W. Chan, and J. Piwowar (2001), Sea-Ice and Meteorological Conditions in Northern Baffin Bay and the North Water Polynya between 1979 and 1996, *Atmosphere-Ocean*, *39*(3), 342–359.

Barber, D. G., and R. A. Massom (2007), The Role of Sea Ice in Arctic and Antarctic Polynyas, in *Polynyas: Windows to the World*, edited by W. O. Smith and D. G. Barber, pp. 1–54, Elsevier Science, Amsterdam.

Barber, D.G., G. McCullough, D. Babb, A.S. Komarov, L.M. Candlish, J.V. Lukovich, M. Asplin, S. Prinsenberg, I. Dmitrenko and S. Rysgaard (2014), Climate change and ice hazards in the Beaufort Sea, Elem. Sci. Anth. 2:000025 doi:10.12952/journal.elementa.000025.

Bauch, D., J. A. Hölemann, I. A. Dmitrenko, M. A. Janout, A. Nikulina, S. A. Kirillov, T. Krumpen, H. Kassens, and L. Timokhov (2012), Impact of Siberian coastal polynyas on shelf-derived Arctic Ocean halocline waters, *J. Geophys. Res. Ocean.*, *117*, C00G12, doi:10.1029/2011JC007282.

Belchansky, G. I., D. C. Douglas, I. V. Alpatsky, and N. G. Platonov (2004), Spatial and temporal multiyear sea ice distributions in the Arctic: A neural network analysis of SSM/I data, 1988-2001, *J. Geophys. Res.*, *109*, C10017, doi:10.1029/2004JC002388.

Boisvert, L. N., T. Markus, C. L. Parkinson, and T. Vihma (2012), Moisture fluxes derived from EOS aqua satellite data for the north water polynya over 2003–2009, *J. Geophys. Res.*, *117*(D06119), doi:10.1029/2011JD016949.

Cavalieri, D. J., and C. L. Parkinson (2012), Arctic sea ice variability and trends, 1979-2006, *Cryosph.*, *6*, 881–889, doi:10.5194/tc-6-881-2012.

Cavalieri, D., C. Parkinson, P. Gloersen, and H. J. Zwally (1996), updated yearly, Sea Ice Concentrations from Nimbus-7 SMMR and DMSP SSM/I-SSMIS Passive Microwave Data (1979-2012), in *NASA National Snow and Ice Data Center Distributed Active Archive*, Boulder, Colo.

Ciappa, A., L. Pietranera, and G. Budillon (2012), Observations of the Terra Nova Bay (Antarctica) polynya by MODIS ice surface temperature imagery from 2005 to 2010, *Remote Sens. Environ.*, *119*, 158–172, doi:10.1016/j.rse.2011.12.017.

Comiso, J. C. (2012), Large Decadal Decline of the Arctic Multiyear Ice Cover, *J. Clim.*, *25*, 1176–1193, doi:10.1175/JCLI-D-11-00113.1.

Darby, M. S., A. J. Willmott, and L. a. Mysak (1994), A nonlinear steady-state model of the NOW Polynya, Baffin Bay, *J. Phys. Oceanogr.*, *24*, 1011–1020.

Dey, B., and U. Feldman (1990), Observations of winter polynyas and Frfactures using NOAA AVHRR TIR images and Nimbus-7 SMMR sea ice concentration charts, *Remote Sens. Environ.*, *30*, 141–149.

Dumont, D., Y. Gratton, and T. E. Arbetter (2009), Modeling the dynamics of the North Water Polynya ice bridge, *J. Phys. Oceanogr.*, *39*(6), 1448–1461, doi:10.1175/2008JPO3965.1.

Dunbar, M., and M. J. Dunbar (1972), The History of the North Water, *Proc. R. Soc. Edinburgh - B*, *72*(21), 231–241.

Dunbar, M. J. (1981), Physical causes and biological significance of polynyas and other open water in sea-ice, in *Polynyas in the Canadian Arctic*, Occasional Paper 45, pp. 28-43, Canadian Wildlife Service, Ottawa, Ont.

Heinrichs, J. F., D. J. Cavalieri, and T. Markus (2006), Assessment of the AMSR-E sea ice concentration product at the ice edge using RADARS AT-1 and MODIS imagery, *IEEE Trans. Geosci. Remote Sens.*, *44*(11), 3070–3079, doi:10.1109/TGRS.2006.880622.

Hibler, W. D., J. K. Hutchings, and C. F. Ip (2006), Sea-ice arching and multiple flow states Arctic ice pack, *Ann. Glaciol.*, *44*, 339–344, doi:10.3189/172756406781811448.

Howell, S. E. L., C. R. Duguay, and T. Markus (2009), Sea ice conditions and melt season duration variability within the Canadian Arctic Archipelago: 1979–2008, *Geophys. Res. Lett.*, *36*, L10502, doi:10.1029/2009GL037681.

Hwang, B. J., and D. G. Barber (2006), Pixel-scale evaluation of SSM/I sea-ice algorithms in the marginal ice zone during early fall freeze-up, *Hydrol. Process.*, *20*, 1909–1927, doi:10.1002/hyp.5958.

Ito, H. (1985), Decay of the sea ice in the North Water area: Observation of ice cover in Landsat imagery, *J. Geophys. Res.*, *90*(D5), 8102–8110.

Kern, S. (2008), Polynya Area in the Kara Sea, Arctic, obtained with microwave radiometry for 1979–2003, *IEEE Geosci. Remote Sens. Lett.*, *5*(2), 171–175, doi:10.1109/LGRS.2008.916831.

Kern, S. (2009), Wintertime Antarctic coastal polynya area: 1992–2008, *Geophys. Res. Lett.*, *36*(L14501), doi:10.1029/2009GL038062.

Kern, S., G. Spreen, L. Kaleschke, S. De La Rosa, and G. Heygster (2007), Polynya Signature Simulation Method polynya area in comparison to AMSR-E 89 GHz sea ice concentrations in the Ross Sea and off the Adelie Coast, Antarctica, for 2002-05: first results, *Ann. Glaciol.*, *46*, 409-418.

Kozo, T. L. (1991), The hybrid polynya at the northern end of Nares Strait, *Geophys. Res. Lett.*, *18*(11), 2059–2062.

Kwok, R. (2005), Variability of Nares Strait ice flux, *Geophys. Res. Lett.*, *32*(L24502), doi:10.1029/2005GL024768.

Kwok, R., G. F. Cunningham, M. Wensnahan, I. Rigor, H. J. Zwally, and D. Yi (2009), Thinning and volume loss of the Arctic Ocean sea ice cover: 2003–2008, *J. Geophys. Res.*, *114*(C07005), doi:10.1029/2009JC005312.

Kwok, R., L. Toudal Pedersen, P. Gudmandsen, and S. S. Pang (2010), Large sea ice outflow into the Nares Strait in 2007, *Geophys. Res. Lett.*, *37*(L03502), doi:10.1029/2009GL041872.

Kwok, R., and D. a. Rothrock (2009), Decline in Arctic sea ice thickness from submarine and ICESat records: 1958-2008, *Geophys. Res. Lett.*, *36*(L15501), doi:10.1029/2009GL039035.

Markus, T., and B. A. Burns (1994), Wind events compared with polynya area estimages derived from SSM/I Data, *EARSeL Adv. Remote Sens.*, *3*(2-XII), 90–99.

Markus, T., and B. A. Burns (1995), A method to estimate subpixel-scale coastal polynyas with satellite passive microwave data, *J. Geophys. Res.*, *100*(C3), 4473–4487.

Markus, T., J. C. Stroeve, and J. Miller (2009), Recent changes in Arctic sea ice melt onset, freezeup, and melt season length, *J. Geophys. Res.*, *114*(C12), doi:10.1029/2009JC005436.

Maslanik, J., J. Stroeve, C. Fowler, and W. Emery (2011), Distribution and trends in Arctic sea ice age through spring 2011, *Geophys. Res. Lett.*, *38*(L13502), doi:10.1029/2011GL047735.

Massom, R. A., P. T. Harris, K. J. Michael, and M. J. Potter (1998), The distribution and formative processes of latent-heat polynyas in East Antarctica, *Ann. Glaciol.*, *27*, 420–426.

Melling, H., Y. Gratton, and G. Ingram (2001), Ocean circulation within the North Water polynya of Baffin Bay, *Atmosphere-Ocean*, *39*(3), 301–325, doi:10.1080/07055900.2001.9649683.

Miller, L. a. et al. (2002), Carbon distributions and fluxes in the North Water, 1998 and 1999, *Deep. Res. Part II Top. Stud. Oceanogr.*, *49*, 5151–5170, doi:10.1016/s0967-0645(02)00183-2.

Nghiem, S. V, I. G. Rigor, D. K. Perovich, P. Clemente-Colón, J. W. Weatherly, and G. Neumann (2007), Rapid reduction of Arctic perennial sea ice, *Geophys. Res. Lett.*, *34*(L19504), doi:10.1029/2007GL031138.

Nihashi, S., and K. I. Ohshima (2014), Circumpolar mapping of Antarctic coastal polynyas and landfast sea ice: relationship and variability, *J. Clim.*, *28*, 3650–3671, doi:10.1175/JCLI-D-14-00369.1.

Parkinson, C. L., and J. C. Comiso (2013), On the 2012 record low Arctic sea ice cover: Combined impact of preconditioning and an August storm, *Geophys. Res. Lett.*, *40*, 1356–1361, doi:10.1002/grl.50349.

Richmond, O., and G. C. Gardner (1962), Limiting spans for arching of bulk materials in veritcal channels, *Chem. Eng. Sci.*, *17*, 1071–1078.

Rigor, I. G., and J. M. Wallace (2004), Variations in the age of Arctic sea-ice and summer sea-ice extent, *Geophys. Res. Lett.*, *31*(L09401), doi:10.1029/2004GL019492.

Rigor, I. G., J. M. Wallace, and R. L. Colony (2002), Response of sea ice to the Arctic Oscillation, *J. Clim.*, *15*(18), 2648–2663, doi:10.1175/1520-0442(2002)015<2648:ROSITT>2.0.CO;2.

Screen, J. a, and I. Simmonds (2010), The central role of diminishing sea ice in recent Arctic temperature amplification, *Nature*, *464*, 1334–1337, doi:10.1038/nature09051.

Smith, M. B., J. P. Labat, A. D. Fraser, R. a. Massom, and P. Koubbi (2011), A GIS approach to estimating interannual variability of sea ice concentration in the Dumont d'Urville Sea near Terre Adelie from 2003 to 2009, *Polar Sci.*, *5*, 104–117, doi:10.1016/j.polar.2011.04.007.

Smith, S. D., R. D. Muench, and C. H. Pease (1990), Polynyas and Leads ' An Overview of Physical Processes and Environment, *J. Geophys. Res.*, *95*(C6), 9461–9479.

Sodhi, D. S. (1977), Ice arching and the drift of pack ice through restricted channels, *Rep. 77-18*, Cold Reg. Res. and Eng. Lab., Hanover, N. H.

Spreen, G., L. Kaleschke, and G.Heygster (2008), Sea ice remote sensing using AMSR-E 89 GHz channels *J. Geophys. Res.*, *113*, C02S03, doi:10.1029/2005JC003384.

Stirling, I. (1980), The Biological Importance of Polynyas in the Canadian Arctic, *Arctic*, *33*(2), 303–315.

Stirling, I. (1997), The importance of polynyas, ice edges, and leads to marine mammals and birds, *J. Mar. Syst.*, *10*(10), 9–21.

Stroeve, J. C., T. Markus, L. Boisvert, J. Miller, and A. Barret (2014), Changes in Arctic ice melt season and implications for sea ice loss, *Geophys. Res. Lett.*, *41*, 1216–1225, doi:10.1002/2013GL058951.

Tamura, T., and K. I. Ohshima (2011), Mapping of sea ice production in the Arctic coastal polynyas, *J. Geophys. Res.*, *116*(C07030), doi:10.1029/2010JC006586.

Vincent, R. F. (2013), The 2009 North Water anomaly, *Remote Sens. Lett.*, *4*(11), 1057–1066, doi:10.1080/2150704X.2013.837227.

Worby, a. P., and J. C. Comiso (2004), Studies of the Antarctic sea ice edge and ice extent from satellite and ship observations, *Remote Sens. Environ.*, *92*, 98–111, doi:10.1016/j.rse.2004.05.007.

Yackel, J. J., D. G. Barber, and T. N. Papakyriakou (2001), On the estimation of spring melt in the North Water Polynya using RADARSAT-1, *Atmosphere-Ocean*, *39*(3), 195–208.

Yao, T., and C. L. Tang (2003), The formation and maintenance of the North Water Polynya, *Atmosphere-Ocean*, *41*(3), 187–201, doi:10.3137/ao.410301.

CHAPTER FOUR: INVESTIGATING THE ATMOSOHERIC FACTORS INFLUENCING THE CONSOLIDATION OF THE NORTH WATER POLYNYA ICE ARCH AT SMITH SOUND

This paper is in preparation for submission to *Arctic*. This work represents a core chapter of my thesis that was conceived, analyzed, and reported by me as the senior author.

Stark, H. F., D. G. Babb, and D. G. Barber (in prep), Investigating the atmospheric factors influencing the formation of the north water polynya ice arch at Smith Sound, *Arctic.*

Abstract

A combination of NCEP re-analysis-2 and *in situ* observations of monthly sea level pressure (MSLP), winds, and atmospheric temperature were used to compare and contrast the atmospheric factors that influence the formation of the North Water Polynya (NOW) ice arch in Smith Sound during a typical year where the ice arch consolidated (2010-2011) and an atypical year where the ice arch did not consolidate (2009-2010). Climatological MSLP from 1979-2015 for Nares Strait confirmed the previously documented high-to-low pressure gradient from the Arctic Ocean to Baffin Bay during the months of December, January, and February. Anomalies for both 2009-2010 and 2010-2011 did not indicate any significant deviations from normal MSLP. The examination of atmospheric temperatures from the Hans Island weather station in Nares Strait indicated that 1 November to 25 January was 3.41°C colder in 2009-2010 than 2010-2011, flipping on 25 January to 2010-2011 being 6.8°C colder than 2009-2010 until the end of May, which resulted in the ice pack of 2010-2011 consolidating despite ice being thinner. Wind observations also from the Hans Island weather station show the wind direction to be northerly with relatively equal percentages from September to May in 2009-2010 (56%) and 2010-2011 (61%), with the difference between the two ice seasons offset by southerly winds at 25% in 2010-2011 and 33% in 2009-2010, which we speculate to be a large factor behindthe

lack of ice arch formation in 2009-2010. A significant wind event in January 2010 with wind speeds exceeding 10 m s^{-1} 66% of the time could have displaced the southerly drift of ice, preventing the consolidation of the ice arch as the dominant northerly winds easily moved the displaced ice pack through Smith Sound. As the Arctic ice pack is shifting, we present discussion on the ice pack of Nares Strait and how this change could influence the consolidation of the ice arch.

4.1 Introduction

Ice is exported from the Arctic Ocean through multiple channels and straits, specifically the Bering Strait, the interisland straits of the Canadian Arctic Archipelago (CAA), Nares Strait, and Fram Strait [*Aagaard and Carmack,* 1989]. The largest amount of ice is exported annually through Fram Strait, 706 x 10^3 km^2 yr^{-1} [*Kwok,* 2009], with the three remaining pathways exporting considerably less ice. For comparison, *Kwok* [2005] found that on average between 1996 and 2002 33 x 10^3 km^2 was exported annually through Nares Strait. Ice export through Nares Strait is limited by the seasonal formation of an ice arch between Greenland and Ellesmere Island in Smith Sound that impedes ice drift and leads to the formation of the North Water Polynya (NOW) [*Dunbar,* 1973; *Smith et al.,* 1990]

NOW can be described as a predominately latent heat polynya that forms as a result of northerly winds and ocean currents advecting ice southward from the ice arch [*Bacle et al.,* 2002; *Ingram et al.,* 2002]. Early studies linked the West Greenland Current to the maintenance of NOW [*Dunbar and Dunbar*, 1972; *Ito*, 1982; *Steffan*, 1985], but *Bacle et al.* [2002] determined that the West Greenland Current was restricted by the bathymetry of Baffin Bay and only localized upwelling along the coast of Greenland near Smith Sound impacts thermodynamic growth rates of sea ice. Due in part to NOW's large areal extent, approximately 80,000 km^2

[*Barber and Massom*, 2007], NOW is one of the most biologically productive regions in the Arctic [*Stirling,* 1977; 1980], impacting regional heat, moisture, and gas budgets, as the region provides a large contrast between the open ocean and surrounding ice covered environment [*Smith et al.,* 1990; *Miller et al.,* 2002; *Yao and Tang,* 2003; *Boisvert et al.,* 2012].

The formation of the ice arch in Smith Sound during winter is heavily influenced by the local atmospheric and oceanic patterns [*Dumont et al.,* 2009]. Due to the steep topography of Ellesmere Island and Greenland on each side of Nares Strait, winds follow the north-south orientation of the Strait [*Ito,* 1982; *Ingram et al.,* 2002] with northerly winds, of up to 10 m s^{-1}, occurring most often during winter [*Samelson and Barbour,* 2008]. Northerly winds are driven by a sea level pressure (SLP) gradient across Nares Strait that forms between a high pressure system over the Canadian Arctic and North Pole, and a low pressure system towards Southern Greenland and Baffin Bay [*Samelson et al.,* 2006]. Cyclonic activity within Baffin Bay originates from Davis Strait and typically moves northward to Nares Strait [*Maxwell,* 1981]. As for oceanic forcing, the dominant ocean current through Nares Strait is the southerly outflow from the Arctic Ocean, with a speed of 10-15 cm s^{-1} on the west side of the channel and 3-5 cm s^{-1} at 25 to 100 m depth [*Melling et al.*, 2001]. Although the ocean current is strong, it is the wind stress and atmospheric cooling that control the ice flux through Nares Strait [*Samelson et al.,* 2006]. Furthermore, *Dumont et al.,* [2009] found that surface winds and ice thickness within the Strait are directly related to the cohesion within the ice pack that leads to arch formation.

The ice pack within Nares Strait is comprised of a combination of first and multiyear sea ice [*Kwok,* 2005] with icebergs and ice islands from the glaciers and ice shelves on Ellesmere Island and Greenland embedded within the ice pack [*Newell,* 1993]. First year ice grows seasonally within Nares Strait, with a large portion being landfast throughout winter [*Mundy and*

Barber, 2001]. *Haas et al.* [2006] found first year sea ice in the nearby Lincoln Sea varied in thickness from 0.9 to 2.2 m. Multiyear ice entering Nares Strait comes from the dynamic area north of Ellesmere Island and Greenland where the thickest sea ice in the world is dynamically created [*Bourke and Garret,* 1987] and observed to have a modal thickness between 4.67 and 5.18 m [*Haas et al.,* 2006]. The type of ice within this area and therefore the type of ice that eventually enters Nares Strait, varies according to large scale atmospheric patterns (e.g. the Arctic Oscillation (AO)) which alter the drift patterns and transport pathways of Arctic sea ice [*Rigor et al.,* 2002]. Following pan arctic trends towards a younger and thinner ice pack [e.g. *Maslanik,* 2011; *Comiso,* 2012], similar trends have been observed in Nares Strait [*Belchansky et al.,* 2004] and will undoubtedly influence the formation of the ice arch [after *Dumont et al.,* 2009] as the formation of ice arches is heavily dependent upon ice shear strength and wind velocity [*Hibler et al.,* 2006; *Kubat et al.,* 2006]. As for icebergs and ice islands, there has been an observed increase in the discharge of icebergs from Greenland since the early 2000's [*Rignot and Kanagartnam,* 2006]. *Van Wychen et al.,* [2013] observed no significant trend to glacial discharge from Ellesmere Island though they did find glacial discharge to be highly episodic, which may influence the interannual variability of the presence of glacial ice in Nares Strait. These large ice features have been observed to impede ice drift in Robeson Channel [*Sadler,* 1976] and foster cohesion within the ice pack, which contributes to the development of an ice arch [*Kubat et al.,* 2006].

The ice arch across Smith Sound is a seasonal feature that typically forms during winter, persists through spring and dissolves during summer [*Dunbar,* 1973]. *Stark et al.,* [in review] found that between 1979 and 2012 the formation and dissolution of the ice arch tended to occur earlier in the year, in different locations and within the last decade has not formed at all during

some years [*Vincent,* 2013] which lead to greater ice export through Nares Strait in 2007 [*Kwok et al.,* 2010]. Pan-arctic trends towards a younger, thinner, and ultimately weaker ice pack that is inherently more mobile is changing the way that ice arches form. These changes have been cited as factors contributing to increased ice export through Nares Strait [*Kwok et al.,* 2010], the Bering Strait [*Babb et al.,* 2014], and the interisland straits of the CAA [*Howell et al.,* 2013]. The long-term impacts of a changing icescape on the consolidation of the ice arch in Nares Strait are relatively unknown. Investigating the influences that drive the formation of NOW are necessary to understand because of the unique and sensitive physical, geochemical, meteorological, and biological processes that rely upon the formation of NOW [see: *Miller et al.,* 2002; *Tremblay et al.,* 2002; *Kwok et al.,* 2010; *Vincent,* 2013]. Within this work we look at how changes in the atmospheric forcing over this region and the ice pack within Nares Strait have contributed to these observed changes in the Smith Sound ice arch.

4.2 Methods

Building on the historic analysis of the formation and dissolution of the Smith Sound ice arch presented by *Stark et al.* [in review], we use a combination of *in situ* and re-analysis datasets to compare and contrast atmospheric forcing throughout the sea ice season (September to May) during a year when the ice arch formed (2010-2011) and did not form (2009-2010). Given that ice arch formation is historically typical of this area we refer to 2010-2011 as the typical year and 2009-2010 as the atypical year.

Daily fields of sea level pressure (SLP) were acquired from the National Oceanic and Atmospheric Administration's (NOAA) National Centre for Environmental Prediction's (NCEP) re-analysis-2 dataset [*Kalnay et al.,* 1996; *Kanamitsu et al.,* 2002]. Climatological (1979-2015) fields of monthly mean sea level pressure (MSLP) were calculated and used to determine SLP

anomalies during our two periods of interest.

In situ observations of variables in the NOW region are available since 2009 from an automated weather station deployed on Hans Island. The weather station provides half-hourly *in situ* observations of air temperature, humidity, surface winds, sea level pressure, and solar radiation and transmits that data via the iridium network to an online data portal (http://dalriada.sams.ac.uk/aws_hans/) where it is available for download. Within this study we compare and contrast observations of surface air temperature, wind speed, and wind direction during the typical and atypical sea ice seasons.

Monthly scenes from the Advanced Synthetic Aperture Radar (ASAR) spaceborne sensor are used to highlight ice arch formation during the typical year (2010-2011) and the lack of an ice arch during the atypical year (2009-2010). ASAR imagery also provides a sense of when the ice arch formed and is used to focus our comparison of atmospheric forcing between the two years.

4.3 Results

A case study of a typical and an atypical formation year was used to determine how the regional and local atmospheric influences impact consolidation of the ice arch. During the atypical winter of 2009-2010, the ice arch at Smith Sound did not consolidate, NOW did not form, and Nares Strait was a thoroughfare for sea ice export (yellow arrows; Figure 4.1a-e). Conversely, during the typical winter of 2010-2011 an ice arch consolidated in the typical concave shape at the narrowest point between Greenland and Ellesmere Island (i.e. *Dumont et al.,* 2006) between 01 January (Figure 4.1f) and 01 February (red circle; Figure 4.1g). Upstream from the ice arch the ice pack remained stationary, as evident from the stationarity of specific features. Downstream the southward export of a large ice parcel that was not included in the ice

arch is evident during February (yellow arrow; Figure 4.1g), while new ice growth is evident during March, April, and May (green circle; Figure 4.1 h, i, and j). In fact it appears that during April (orange line; Figure 4.1i) a large parcel of new ice that grew *in situ* became locked in and moved the ice edge further south to a new, less concave orientation. South of this new first-year ice edge there is evidence of a vast expanse of open water in the NOW region on 05 May 2011 (blue rectangle; Figure 4.1j). During both years we note a clear divide between the landfast ice cover within Kane Basin (LF in Figures 4.1a and g) and the mobile ice stream that runs through the central channel of Nares Strait.

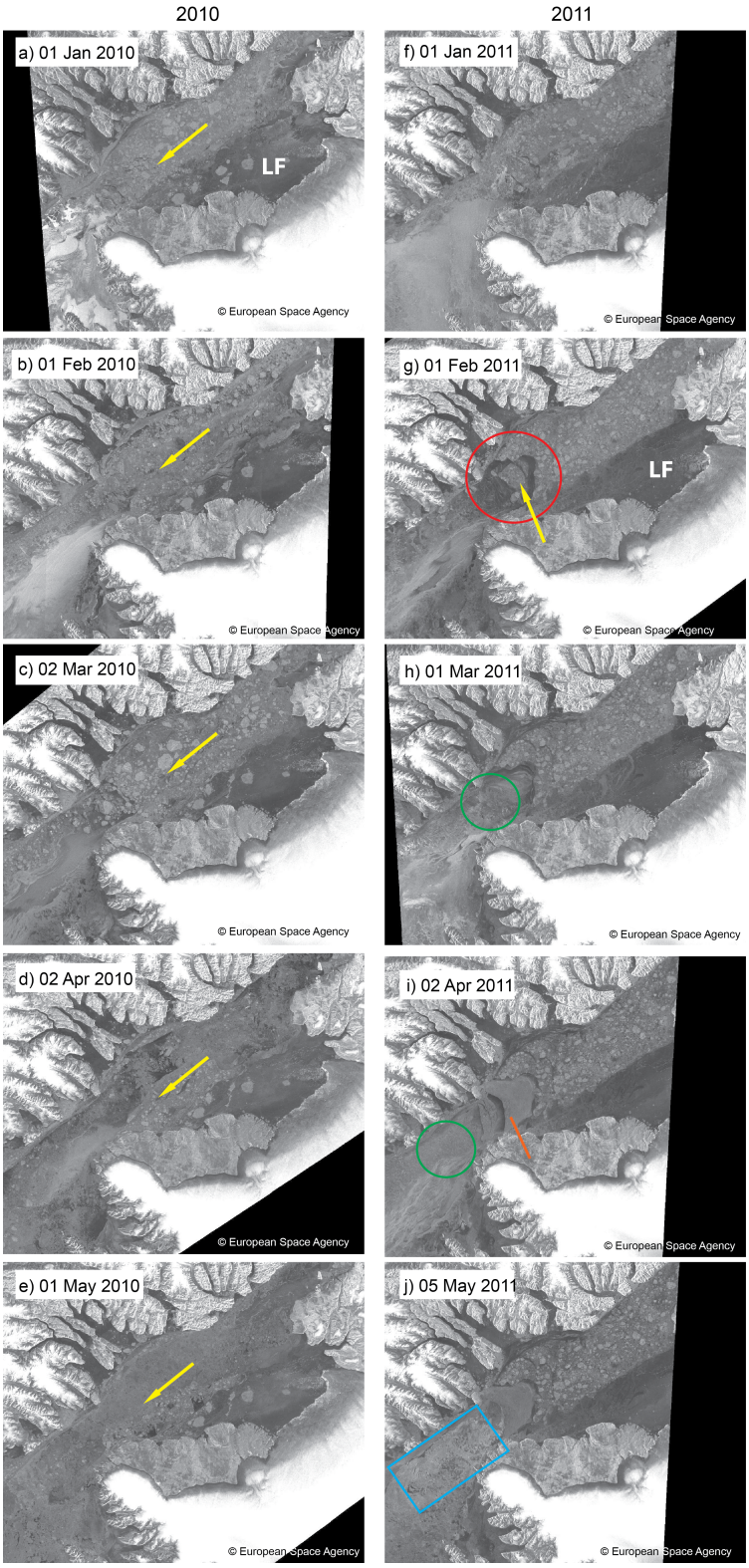

Figure 4.4: ASAR imagery of Smith Sound during January to May in 2010 (a-e) and 2011 (f-j). The top right corner is north (images courtesy of the European Space Agency).

4.3.1 MSLP

In order to compare MSLP over the NOW region during the typical and atypical years we first determine the climatological (1979-2015) patterns of MSLP during the ice season (Figure 4.2). During winter (January, February, and March) (Figure 4.2 e, f, and g) there is a steep SLP gradient over the NOW area; characterized by a high-pressure system situated over the CAA and a low-pressure system on the southern shores of Greenland. During the spring transition (Figure 4.2 h and i), SLP is relatively homogeneous in this region. The high-low gradient returns to the region in September (Figure 4.2a), gaining strength during the fall and early winter months before eventually returning to the maximum SLP gradient in January.

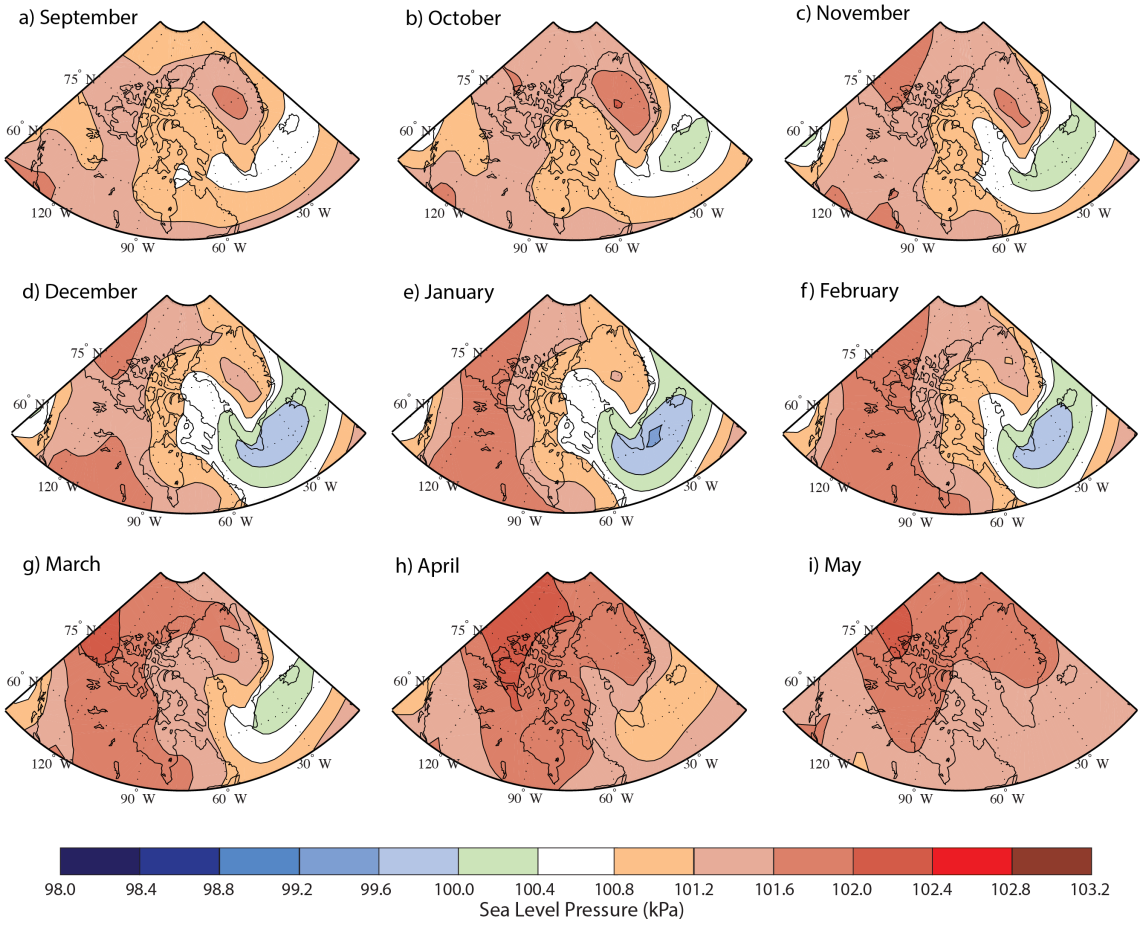

Figure 4.2: Climatological (1979-2015) MSLP over our study region.

During the 2010-2011 ice season September and October (Figure 4.3a-b) were characterized by negative anomalies in the southern portion of the study region and a slight positive anomaly in the northern CAA in September. A high-to-low pressure gradient in November (Figure 4.3c) from the above average MSLP in central and southern Greenland to the below average MSLP in the CAA increased the SLP gradient during across Baffin Bay. Strong positive anomalies over southern Greenland and the CAA in December (Figure 4.3d) created a large SLP gradient with the negative anomalies in western Canada, seen along the periphery. This gradient lingered into January (Figure 4.3e), however it was much weaker. February and April (Figures 4.3 f and h) were characterized by negative anomalies over the study region, with a stronger negative anomaly seen over southern Greenland in April.

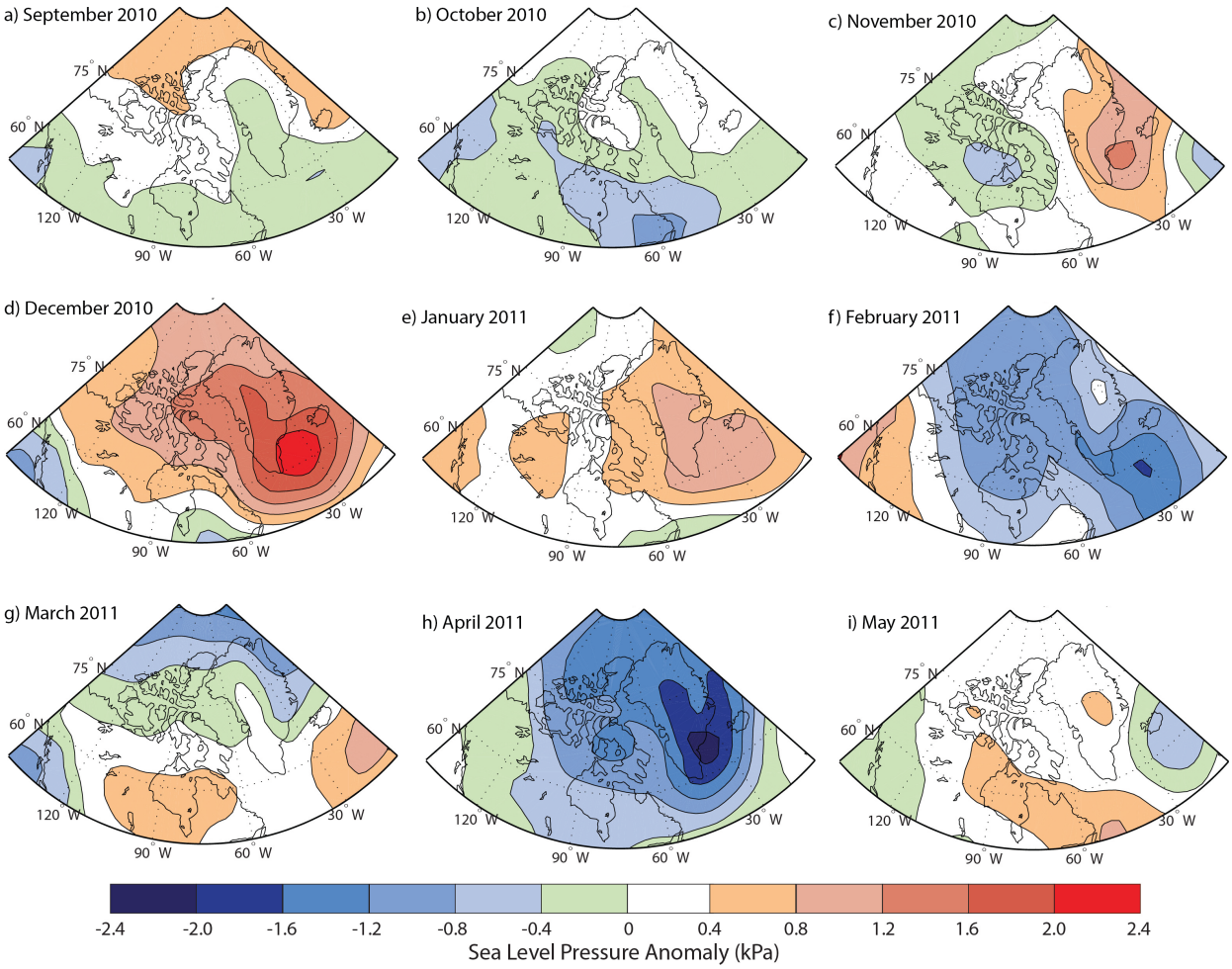

Figure 4.3: MSLP anomalies during the 2010-2011 ice season as compared to the 1979-2015 climatology.

MSLP from September 2009 to May 2010 (Figure 4.4) was characterized by a negative anomaly in September (Figure 4.4a) and then a positive anomaly in October (Figure 4.4b) over the CAA and Greenland. Negative anomalies over the periphery of Baffin Bay, the CAA, and Greenland decreased the SLP gradient over this region in December (Figure 4.4d). The opposite occurred in January – a positive anomaly over Greenland and the CAA increased the SLP gradient with the negative anomaly southeast of Greenland (Figure 4.4e). A much stronger SLP gradient characterizes February (Figure 4.4f) with the positive anomaly centred over Greenland and extending westward to Ellesmere Island and the negative anomaly in the west and south of

the study region. March (Figure 4.4g) is still characterized by a positive anomaly over Greenland, although much weaker, and a negative anomaly covers a much larger region of the western Canada and part of the CAA.

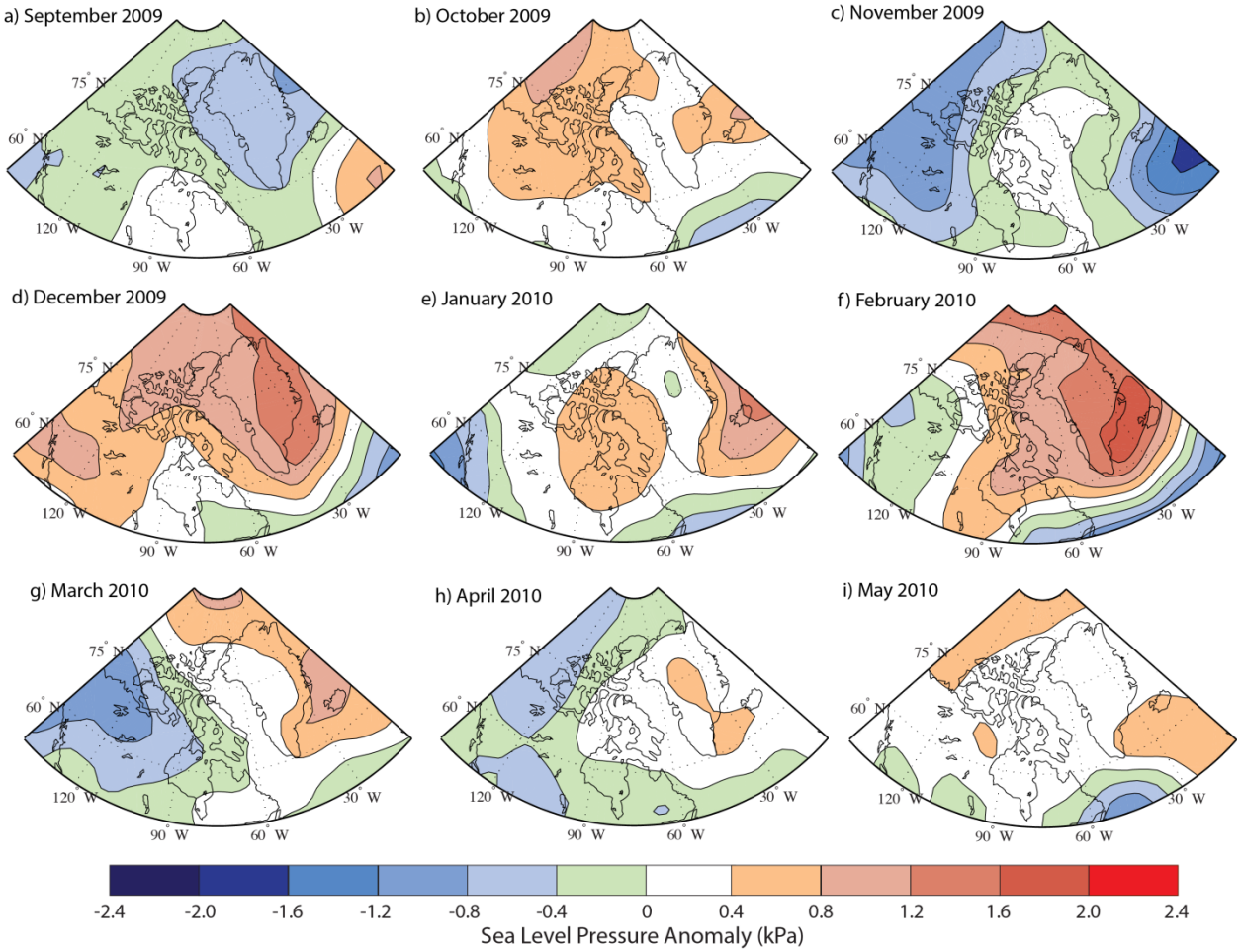

Figure 4.4: MSLP anomalies during the 2009-2010 ice season as compared to the 1979-2015 climatology.

4.3.2 Wind speed and direction

Following *Dumont et al.* [2009], we find that the predominant wind direction during both sea ice seasons was from the north (Figure 4.5), though we note a very strong bimodal distribution with a secondary peak in southerly winds. Easterly and westerly winds occur very rarely within Nares Strait as a result of the steep topography that parallels the channel (e.g.

Ingram et al., 2002). In 2010-2011, 61% of observations originated between 330° and 15°; while in 2009-2010, 56% originated from the same direction. The difference between these two years was predominantly offset by more frequent southerly winds (120°-210°) during 2009-2010 (33%) than 2010-2011 (25%; Figure 4.5).

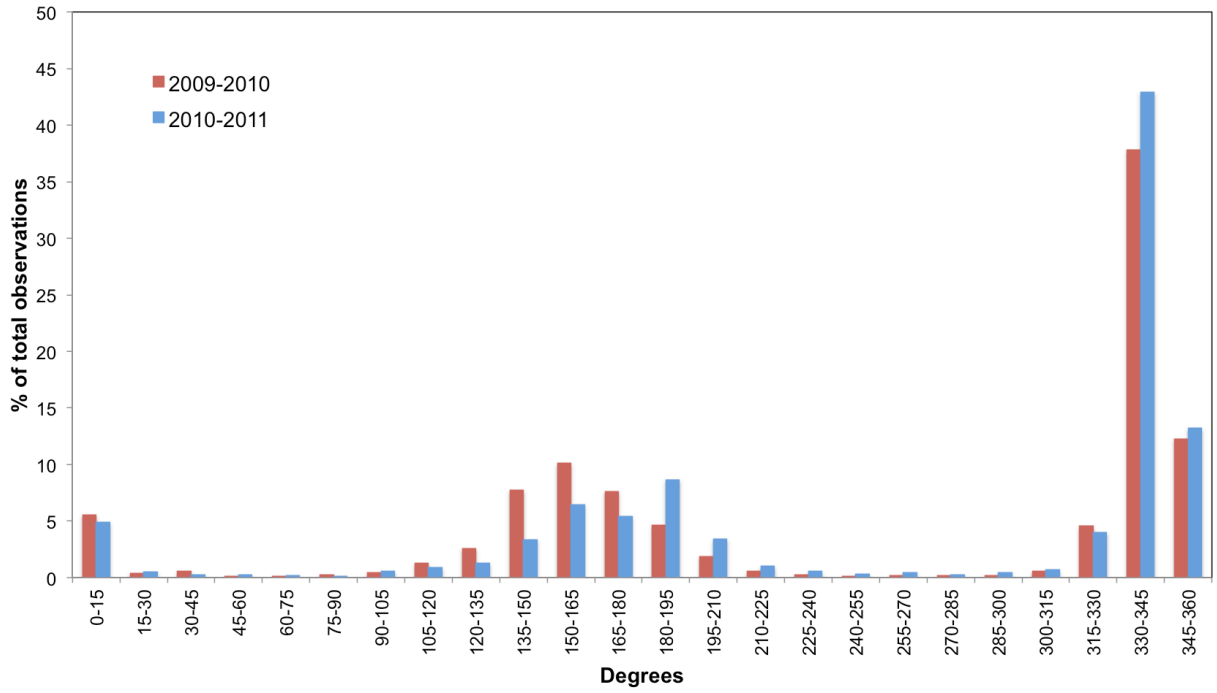

Figure 4.5: Frequency of wind direction observations recorded half-hourly at Hans Island in 2009-2010 (red) and 2010-2011 (blue).

Looking at wind direction and wind speed throughout the 2009-2010 and 2010-2011 sea ice seasons we find that wind patterns during the two years were very similar, especially during October, December, February, and May (Figure 4.6 b, d, f, and i, respectively). During these months northerly winds accounted for at least 20% of monthly observations and exceeded 10 m s^{-1} at least half the time, while southerly winds occurred infrequently and were considerably slower, often less than 10 m s^{-1}. During both ice seasons October, December, and May (Figure 4.6 b/g, d/i, and n/r, respectively) exhibit typical dominant northerly wind patterns with stronger wind speeds, reaching a maximum of 25-30 m s^{-1} in December 2009 (Figure 4.6d).

During February 2011, we observed a large block drifting south after the ice arch formed (Figure 4.2g) which was likely forced by the persistent and strong northerly winds recorded during February (Figure 4.6o). Northerly winds through March, April, and May 2011 (Figure 4.6 p-r) would have assisted in opening NOW and led to the new ice growth we observed in the ASAR images (Figure 4.2h-j). A combination of low northerly wind speeds and southerly winds during March 2011 (Figure 4.6 p) potentially reduced ice export from the NOW region for long enough that new ice was able to remain intact and grow strong enough to form a new ice arch to the south of the existing ice arch (Figure 4.1i).

The two ice seasons differ substantially during November, January, and March (Figure 4.6) when southerly winds were more frequent during one of the years. In November 2009 (Figure 4.6c) southerly winds occurred 53% of the time, compared to 20% in November 2010 (Figure 4.6h); however, both northerly and southerly wind speeds were <15 m s^{-1} the entire month. Southerly winds in January 2010 (Figure 4.6e) occurred 46% of the time, compared to 25% in January 2011 (Figure 4.6j). It was during January 2010 that southerly winds were >30 m s^{-1} (maroon in Figure 4.6e), making January 2010 as one of three months in 2009-2010 (December 2009 and March 2010 also recorded winds >30 m s^{-1}) to record such fast wind speeds. In March 2011 southerly winds occurred 43% of the time (Figure 4.6p) and only 12% originated from the south in March 2010 (Figure 4.6l). March 2011 was the only month during the 2010-2011 ice season to exhibit an almost equal frequency of northerly and southerly winds, while November 2009 and April 2010 exhibited the same proportions during the 2009-2010 ice season.

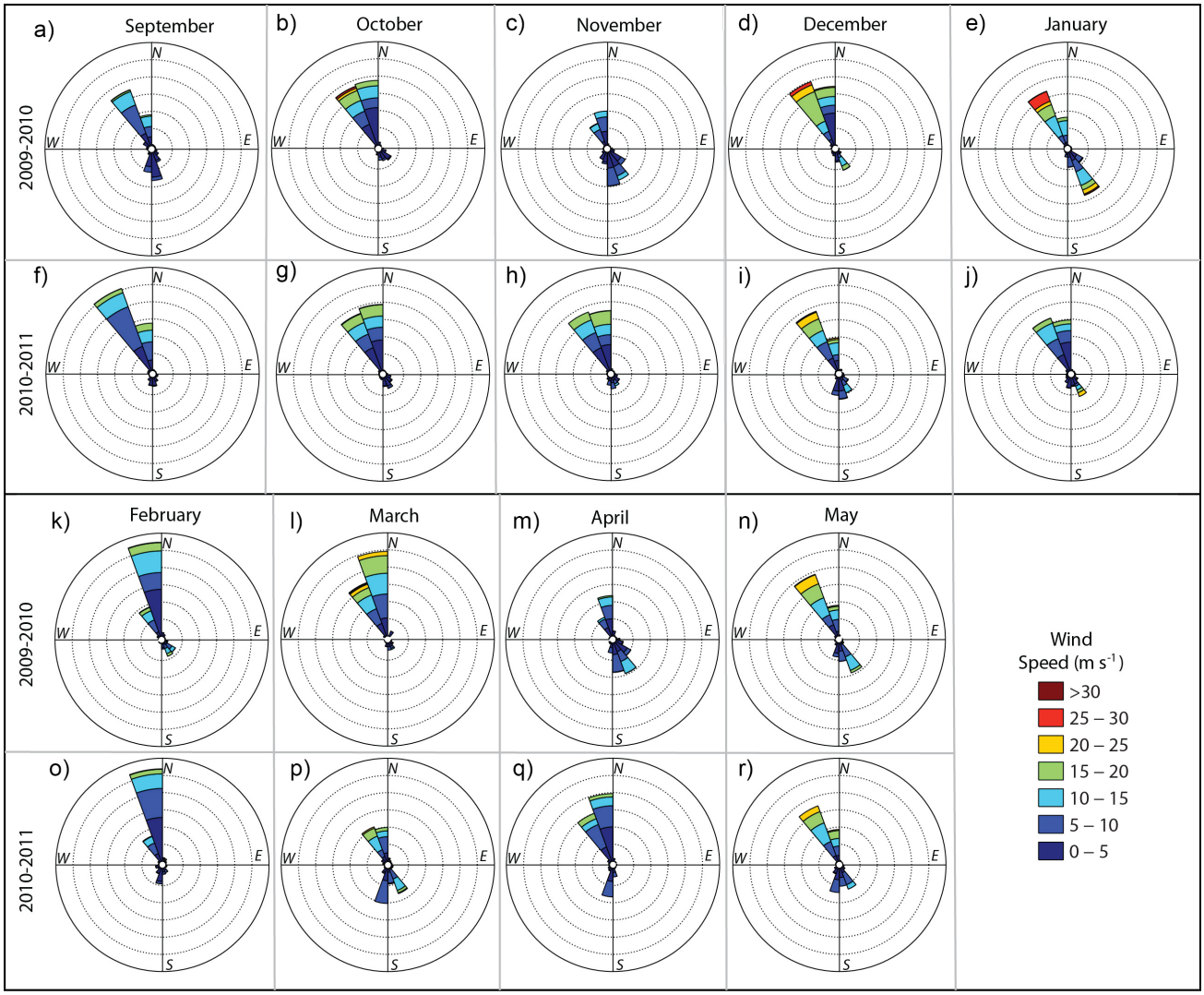

Figure 4.6: Wind roses for the 2009-2010 and 2010-2011 ice seasons from September to May derived from the Hans Island weather station. Dashed circles denote intervals of 5% of the monthly observations.

4.3.3 Atmospheric Temperature

Overall there is a strong annual cycle in surface air temperatures observed at Hans Island, characterized by temperatures < -30°C during winter and near 0°C during early September and late May (Figure 4.7a). As a result, freeze-up typically occurs during September and continues through October as temperatures steadily decline to between -15°C and -20°C by the end of October. Cold air temperatures during winter not only lead to thermodynamic thickening of new

and old ice within Nares Strait but also increase the strength of ice floes, both of which contribute to the consolidation of sea ice into arch formations.

Generally temperatures were relatively similar during September and October between the two ice seasons, with absolute daily differences below 5°C and mean monthly differences of 0.91°C and -1.39°C, respectively (Figure 4.7b), meaning new ice growth likely varied inconsiderably between the two years. During November, December, and January air temperatures were variable, but overall these months during 2009-2010 were colder than 2010-2011 with monthly mean differences of -1.59°C, -3.09°C, and -3.21°C, respectively. During the remaining months of the ice season 2009-2010 was warmer than 2010-2011, with a mean monthly difference of 6.87°C and a peak difference of 12.48°C during April. The temperature difference flipped on January 25, and would only be negative during 16 of the 127 days between January 25 and May 31. Ultimately, between 1 November and 25 January air temperatures were 3.41°C cooler during 2009-2010 than the same period during 2010-2011. Conversely, the period between 25 January and 31 May was on average 6.8°C warmer during 2009-2010 than 2010-2011.

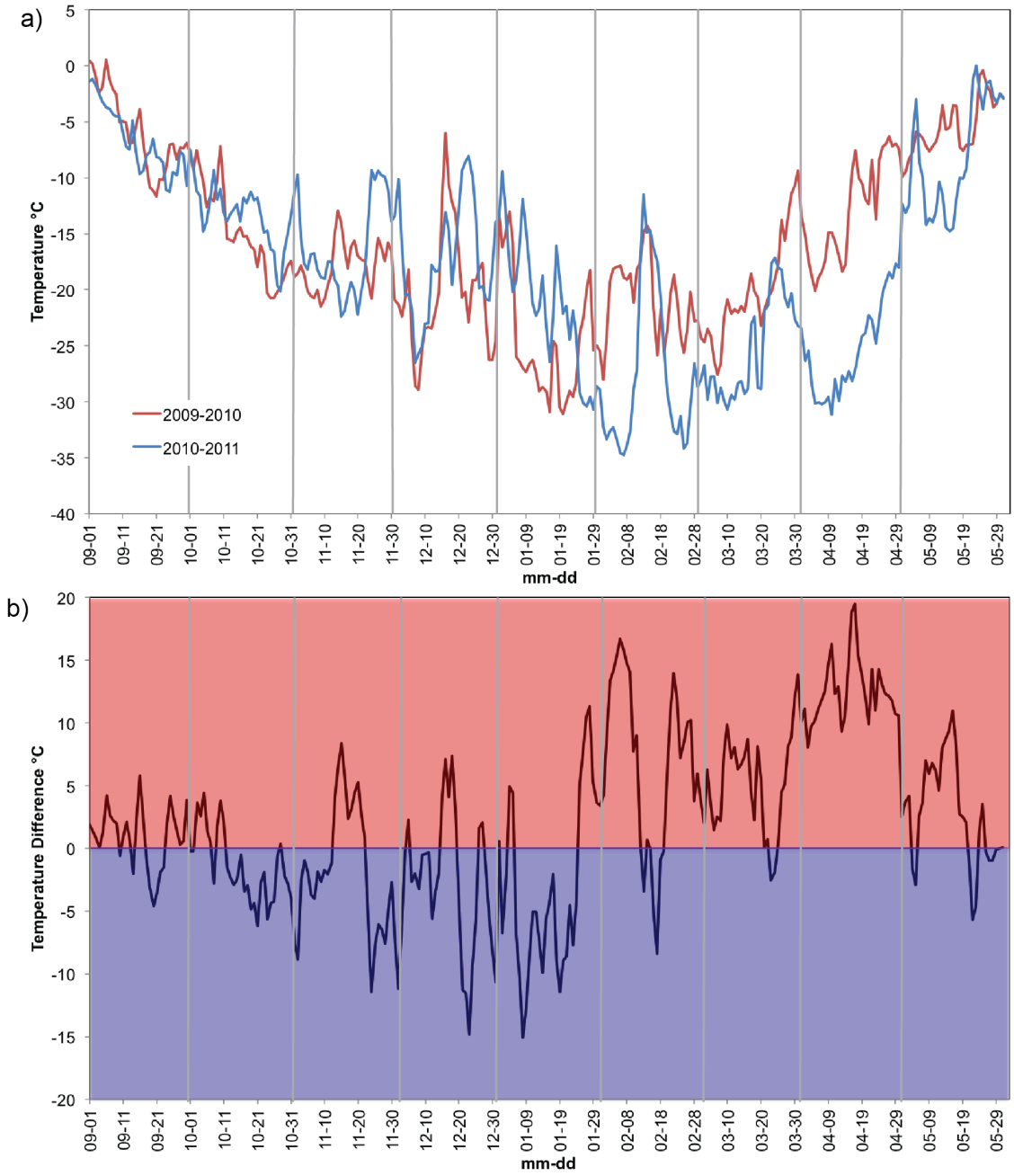

Figure 4.7: a) Atmospheric temperature observed from Hans Island for September to May for 2009-2010 and 2010-2011. b) Temperature differences determined by: 2009-2010 minus 2010-2011. Red indicates positive temperature difference (2009-2010 temperatures were greater) and blue indicates negative temperature difference (2010-2011 temperatures were greater).

4.4 Discussion

It is difficult to determine the degree to which atmospheric temperature affects the consolidation of the ice arch because November 2009 to January 2010 was colder than November 2010 to January 2011 (Figure 4.7b), which would result in greater thermodynamic growth rates, increasing ice thickness and strength. Thicker and stronger ice would be more beneficial for the arch as it would have a greater likelihood to prevent the southward drift of sea ice through Nares Strait. Regardless of potentially thicker ice, the ice arch did not consolidate in 2009-2010 and it is evident other factors influenced the absence.

The large positive temperature difference in April and May between 2009-2010 and 2010-2011 (Figure 4.7b) is of particular interest because the cause could be related to an atmospheric pattern not typically seen until late spring or early summer when warmer temperatures are introduced to the eastern portion of the NOW region via the Greenlandic coast [*Barber et al.,* 2001]. Although this phenomenon did not appear to alter the consolidation of an ice arch, it raises interest in the potential for large-scale weather patterns to influence not only the consolidation of the ice arch, but also it's deterioration. Further investigation into the wind patterns of the Baffin Bay region would assist in understanding possible linkages to overall climate in the region.

MSLP anomalies for 2010-2011 indicate that December 2010 and February 2011 deviate positively from the climatological means (Figure 4.3). The typical high-low pressure gradient from the Arctic Ocean to Baffin Bay in December (Figure 4.2) was stronger in December 2010 (Figure 4.3) and would hypothetically increase wind speeds; however, the northerly and southerly wind fluctuations do not coincide with this finding (Figure 4.8a). The same high-to-low pressure gradient is seen in February (Figure 4.2f) with a similar anomaly (Figure 4.3f) and

wind regime (Figure 4.7a) in February 2010. MSLP anomalies for 2009-2010 (Figure 4.4) do not indicate any extreme deviations from the climatological MLSP over the NOW region (Figure 4.2). November shows -2 kPa anomaly southeast of Greenland, but the region typically exhibits a high-low pressure gradient from the Arctic Ocean to southern Greenland (Figure 4.2) and southerly wind event observed in November 2009 (Figure 4.6a) was not related to the anomaly. The positive anomaly over southern Greenland in February (Figure 4.4f) increased the typically low pressure seen climatologically for this region (Figure 4.2f), which could result in weaker northerly winds; however, this is only partially the result as winds in February 2010 (Figure 4.4a) were both northerly and southerly. Based on the weak linkages between regional SLP and the winds from Hans Island during both a typical and atypical year, we speculate that the atmospheric patterns in the NOW region are highly localized, with the narrow channel of Nares Strait controlling wind speed and direction as documented by *Ingram et al.* [2002].

The examination of winds and temperature at the Hans Island weather station clarified the localized atmospheric regime of Nares Strait during 2009-2010 and 2010-2011. Nares Strait is dominated by a northerly wind regime, created by a high-low pressure gradient from the Arctic Ocean to Baffin Bay, that assists the consolidation of the ice arch and advection of ice needed to open NOW [*Samelson et al.,* 2006]. Of the recorded northerly winds in 2010-2011 35% were >10 m s^{-1} (Figure 4.6), which assisted in the southward drift of sea ice until Smith Sound where the channel narrowed and ice built up. The more frequent and stronger southerly wind events in 2009-2010 potentially disrupted the consolidation of the ice arch. Focusing on two strong southerly wind events from 11 November to 29 November, 2009 (wind speeds > 10 m s-1 4% of the time) and from 1 January to 10 January 2010 (wind speeds >10 m s^{-1} 47% of the time), we speculate that strong southerly winds during these periods, especially the January event,

disrupted consolidation of the ice pack and allowed the ice to be easily exported southwards when northerly winds returned, negating the potential for an ice arch to form. Based on these particular wind events, we speculate that the timing and strength of southerly wind events affects the ice arch consolidation. Timing is key because once the arch has formed it becomes difficult to displace. As an example of this, we highlight the strong southerly wind event between 16 March and 26 March 2011 when wind speeds exceeded 10 m s-1 during 26% of the time. We would anticipate this event could disrupt the ice arch; however, since the arch had formed more than a month earlier it had grown thicker and stronger, and strengthened even more under persistent northerly winds during February 2011 (Figure 4.6o). Given that the ice arch persisted for two months after this wind event we find that the southerly winds during March 2011 had little affect on the ice arch in Nares Strait.

While the results suggest that southerly winds impact the consolidation of the ice arch, atmospheric patterns are not the only factor responsible for the consolidation of the ice arch in Smith Sound. Potential influences include: ocean thermodynamics, sea ice thermodynamics, and the composition of the ice pack. Given that observations of ocean thermodynamics and sea ice thermodynamics were unavailable for this study we focus the remaining discussion on the composition of the ice pack within Nares Strait during our two periods of interest.

Given that the consolidation of the ice arch is dependent upon the now decreasing fluxes of multiyear ice through Nares Strait [*Belchansky et al.,* 2004], there is a greater chance larger portions of young ice could be negatively impacting the consolidation of the arch as thinner ice is not only more susceptible to drift but also results in a weaker ice pack [*Zhang et al.,* 2012]. Using weekly ice charts over the Eastern Canadian Arctic from the Canadian Ice Service we find that there was more old ice present in southern Nares Strait during 2009-2010 compared to 2010-

2011 (Figure 4.9 a and d, respectively). We also note that there was thinner first year ice present in the area during 2009-2010 compared to 2010-2011, which we ascribe to the cooler temperatures observed during October, November, and December 2009 compared to the same months in 2010 (Figure 4.7). Despite a lack of old ice and the presence of thinner first year ice during 2010-2011 (Figure 4.8d and e) the ice arch consolidated in January 2011 (Figure 4.1f). This finding is counterintuitive because increased coverage of old ice and thicker first year ice would theoretically increase the strength and stability of the ice arch. However, as stated previously we surmise that the strong southerly winds in January 2010 (Figure 4.6b) disrupted the consolidation of the ice pack, regardless of a majority of it being old ice, and allowed ice to be exported once northerly winds returned. Based on the evidence of the ice types in Nares Strait in January 2010 and 2011, we have difficulty determining how ice types prevented the ice from consolidating in 2009-2010. However, following previous studies and the logic of ice arches [i.e. *Kubat et al.,* 2006] we still support the notion that the formation of the ice arch across Smith Sound is impacted by the composition of the Nares Strait ice pack and that a shift to younger sea ice within Nares Strait will reduce the likelihood of ice arch formation by reducing the strength and cohesion of the ice pack.

Nares Strait is also a thoroughfare for icebergs and ice islands produced from the glaciers and ice shelves of northwestern Greenland and Ellesmere Island. Under a warming climate calving events have increased [*Meier et al.,* 2007; *van den Broeke et al.,* 2009; *Gardner et al.,* 2011] and are projected to continue to increase in the coming years [*Nick et al.,* 2013] introducing more icebergs and ice islands into Nares Strait. Given that Nares Strait is shallow (< 200 m) these features can run aground [*Pereira et al.,* 1988; *Héquette et al.,* 1995; *Kuijpers et al.,* 2007] and disrupt ice drift, such as the large ice features *Sadler* [1976] observed preventing

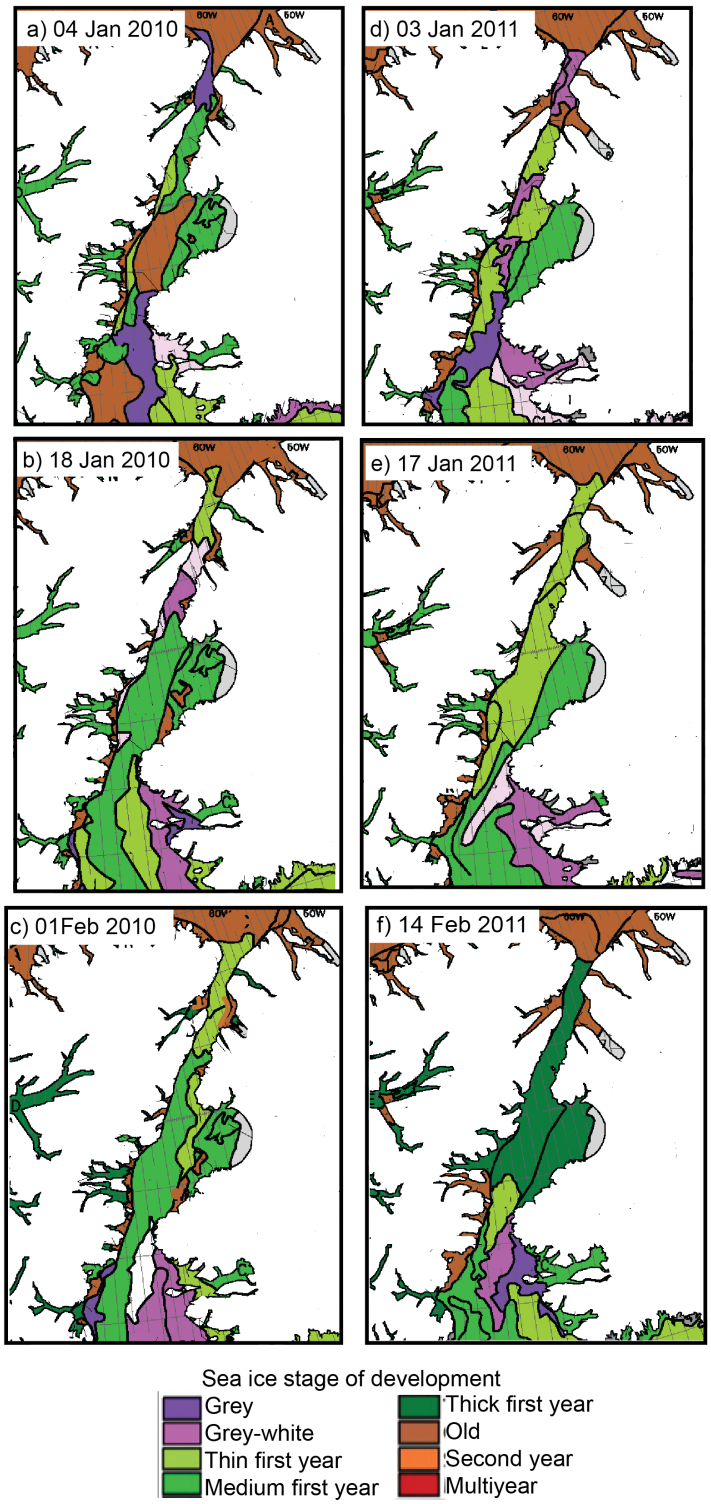

Figure 4.8: Sea ice stage of development from Canadian Ice Service Ice Charts for Nares Strait from January to February 2010 and 2011.

southerly ice drift through Robeson Channel, the northern portion of Nares Strait. The effects of large ice features on the drift of sea ice through Nares Strait have not been investigated and require further investigation that first must develop a technique to identify such features.

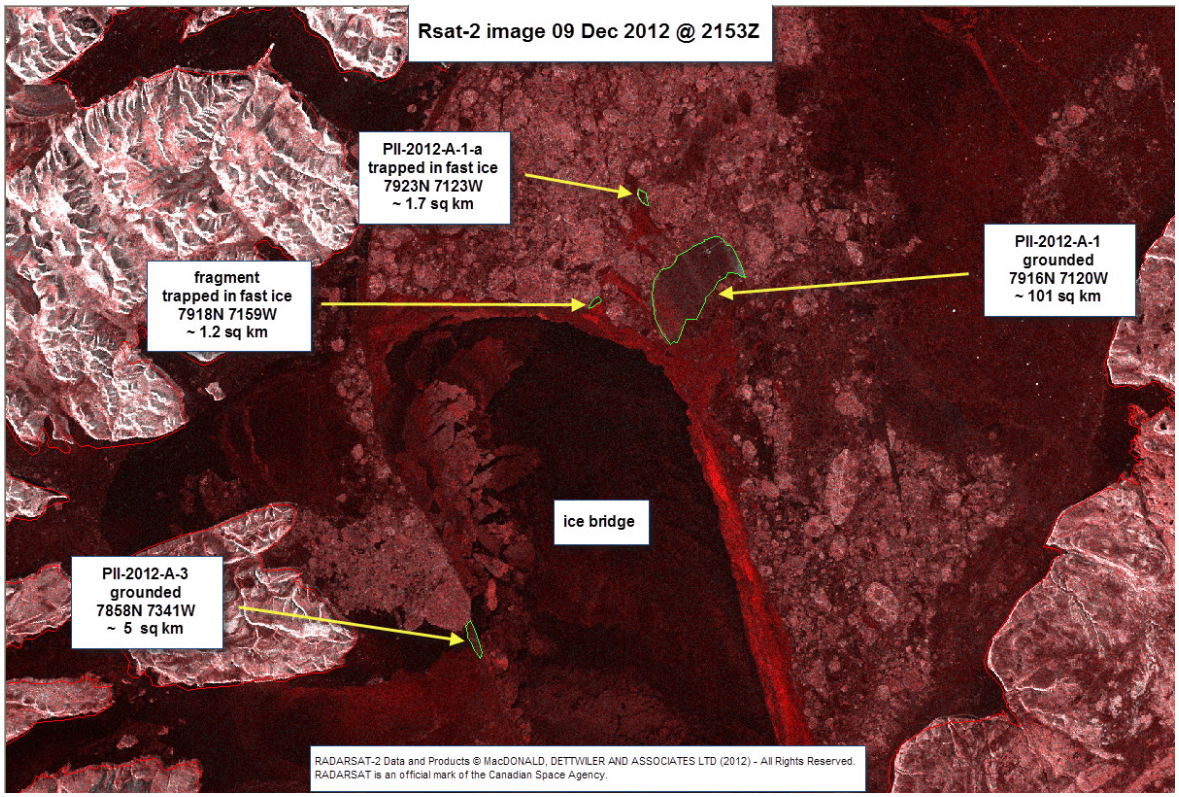

Figure 4.9: RADARSAT image of the Smith Sound ice arch in December 2012. A 100 km^2 ice island (PII-2012-A-1) was grounded just north of the ice arch helping stabilize the arch and open NOW earlier (imagery courtesy of the Canadian Ice Service and the Canadian Space Agency).

As part of its operational mandate the Canadian Ice Service identifies and tracks large ice features within the Canadian Arctic. According to their analysis there were no large ice features documented in Nares Strait during 2009-2010 or 2010-2011, thus such a feature did not likely contribute to ice arch formation during January 2011. However the Canadian Ice Service did identify a grounded ice island was located in Kane Basin during the winter of 2012-2013 when an ice arch did form across Smith Sound (Figure 4.9) [*L. Desjardins,* Canadian Ice Service-retired, personal communication*,* 31 October 2015]. The impact of grounded ice features on the

ice arch are unknown, with potential to affect the southerly drift of the ice pack, increasing the strength of the ice arch as sea ice consolidates around it. Additionally, large ice features could impact the onset of melt in spring – when melt onset commences, large ice features, which have larger sails and keels than sea ice, could speed up dissolution as they are more susceptible to winds and can break the already weakening sea ice. If a greater frequency of large ice features continues, the timing of consolidation and melt could shift, negatively impacting the physical, biological, and geochemical processes associated with NOW. The above is only speculation as this falls outside of the focus of this study and thus should be examined in future studies to investigate the effect of grounded ice islands on the surrounding ice drift and the potential contribution to ice arch formation.

4.5 Conclusion

The overarching objective of this paper was to determine how atmospheric patterns influence the consolidation of the ice arch associated with NOW. We presented a combination of NCEP re-analysis-2 data and *in situ* data from the Hans Island weather station to examine the factors that contributed to the typical NOW formation year of 2010-2011 and the atypical year of 2009-2010.

MSLP from the NCEP data confirmed the dominant high-pressure to low-pressure gradient from the Arctic Ocean to southern Baffin Bay during December, January, and February which assists in the southerly export of sea ice through Nares Strait to the chokepoint of Smith Sound, where the ice arch typically forms. Although the MSLP anomalies for 2009-2010 and 2010-2011 did not indicate any significant deviations from climatological means, wind direction and speed from Hans Island highlighted the importance of consistently strong northerly winds for the consolidation of the ice arch. The fluctuations between strong southerly and northerly winds in

2009-2010 could have influenced the drift of ice through Nares Strait and the consolidation of the ice arch as a wind event in early January 2010 increased wind speeds to a maximum of 31 m s^{-1} potentially displacing the pack in Nares Strait. Although 2010-2011 experienced a strong southerly wind event in March 2011, the arch had already stabilized and did not impact the stability of the arch. It is evident that the timing and strength of southerly wind events affects the consolidation of the ice arch.

The ice pack of Nares Strait, which is heavily influenced by the outflow of sea ice from the Arctic Ocean and the icebergs and ice islands from Ellesmere Island and Greenland, has the potential to influence the consolidation of the ice arch. Although the old ice in Nares Strait in 2009-2010 did not assist in the consolidation of the ice arch and an ice arch consolidated when there was thin first year ice in 2010-2011, we still suggest that the changing ice pack will influence the consolidation of the ice arch. Moreover, the frequency of ice bergs and ice islands can impact the southerly flow of sea ice and thus the consolidation of the ice arch, e.g. the grounded ice island in 2013 in southern Kane Basin. To further this investigation, a greater understanding of the changing ice pack (ice types, associated ice thicknesses) of Nares Strait is necessary to determine the long-term variability of the consolidation of the ice arch and potential impacts on the physical, chemical, and biological processes of NOW.

Literature Cited

Aagaard, K., and E. C. Carmack (1989), The role of sea ice and other fresh water in the Arctic circulation, *J. Geophys. Res.*, *94*(C10), 14,485–14,498, doi:10.1029/JC094iC10p14485.

Babb, D. G., R. J. Galley, M. G. Asplin, J. V. Lukovich, and D. G. Barber (2013), Multiyear sea ice export through the Bering Strait during winter 2011-2012, *J. Geophys. Res. Ocean.*, *118*, 5489–5503, doi:10.1002/jgrc.20383.

Bacle, J., E. Carmack, and R. Ingram (2002), Water column structure and circulation under the North Water during spring transition: April–July 1998, *Deep Sea Res. Part II Top. Stud. Oceanogr.*, *49*, 4907–4925.

Barber, D. G., J. M. Hanesiak, W. Chan, and J. Piwowar (2001), Sea-Ice and Meteorological Conditions in Northern Baffin Bay and the North Water Polynya between 1979 and 1996, *Atmosphere-Ocean*, *39*(3), 342–359.

Barber, D. G., and R. A. Massom (2007), The Role of Sea Ice in Arctic and Antarctic Polynyas, in *Polynyas: Windows to the World*, edited by W. O. Smith and D. G. Barber, pp. 1–54, Elsevier Science, Amsterdam.

Belchansky, G. I., D. C. Douglas, I. V. Alpatsky, and N. G. Platonov (2004), Spatial and temporal multiyear sea ice distributions in the Arctic: A neural network analysis of SSM/I data, 1988-2001, *J. Geophys. Res.*, *109*(C10017), doi:10.1029/2004JC002388.

Boisvert, L. N., T. Markus, C. L. Parkinson, and T. Vihma (2012), Moisture fluxes derived from EOS aqua satellite data for the north water polynya over 2003–2009, *J. Geophys. Res.*, *117*(D06119), doi:10.1029/2011JD016949.

Bourke, R. H. and R. P. Garrett (1987), Sea ice thickness distribution in the Arctic Ocean, *Cold Reg. Sci. and Tech., 113*(3), 259-280.

Canadian Ice Service (2006), *Canadian Ice Service Digital Archive – Regional Charts: History, Accuracy, and Caveats,* Environment Canada, Ottawa, Ont.

Comiso, J. C. (2012), Large Decadal Decline of the Arctic Multiyear Ice Cover, *J. Clim.*, *25*, 1176–1193, doi:10.1175/JCLI-D-11-00113.1.

Dumont, D., Y. Gratton, and T. E. Arbetter (2009), Modeling the dynamics of the North Water Polynya ice bridge, *J. Phys. Oceanogr.*, *39*(6), 1448–1461, doi:10.1175/2008JPO3965.1.

Dunbar, M. (1973), Ice Regime and Ice Transport in Nares Strait, *Arctic*, *26*(4), 282–291.

Dunbar, M., and M. J. Dunbar (1972), The History of the North Water, *Proc. R. Soc. Edinburgh - B*, *72*(21), 231–241.

Gardner, A. S., G. Moholdt, B. Wouters, G. J. Wolken, D. O. Burgess, M. J. Sharp, J. G. Cogley, C. Braun, and C. Labine (2011), Sharply increased mass loss from glaciers and ice caps in the Canadian Arctic Archipelago, *Nature*, *473*(7347), 357–360, doi:10.1038/nature10089.

Haas, C., S. Hendricks, and M. Doble (2006), Comparison of the sea-ice thickness distribution in the Lincoln Sea and adjacent Arctic Ocean in 2004 and 2005, *Ann. Glaciol.*, *44*, 247–252.

Héquette, A., M. Desrosiers, and P. W. Barnes (1995), Sea ice scouring on the inner shelf of the southeastern Canadian Beaufort Sea, *Mar. Geol.*, *128*, 201–219, doi:10.1016/0025-3227(95)00095-G.

Hibler, W.D., J.K. Hutchings and C.F. Ip (2006), Sea-icea arching and multiple flow states of Arctic pack ice, *Annals of Glaciology*, *44*, 339-345.

Howell, S. E. L., T. Wohlleben, M. Dabboor, C. Derksen, A. Komarov, and L. Pizzolato (2013), Recent changes in the exchange of sea ice between the Arctic Ocean and the Canadian Arctic Archipelago, *J. Geophys. Res. Ocean.*, *118*, 3595–3607, doi:10.1002/jgrc.20265.

Ingram, R., J. Bacle, D. Barber, Y. Gratton, and H. Melling (2002), An overview of physical processes in the North Water, *Deep Sea Res. Part II Top. Stud. Oceanogr.*, *49*, 4893–4906, doi:10.1016/S0967-0645(02)00169-8.

Ito, H. (1982), Wind Through a channel: surface wind measurements in Smith Sound and Jones Sound in Northern Baffin Bay, *J. Appl. Meteorol.*, *21*(8), 1053–1062.

Kalnay, E., *et al.,* (1996), The NCEP/NCAR 40-year Reanalysis Project, March 1996, *Bulletin of the American Meteorological Society*, 77(3), 437-471.

Kanamitsu ,M. W. Ebisuzaki, J. Woollen, S-K Yang, J.J. Hnilo, M. Fiorino, and G. L. Potter. (2002), NCEP-DEO AMIP-II Reanalysis (R-2), Nov 2002, *Bulletin of the American Meteorological Society*, 1631-1643.

Kubat, I., M. Sayed, S.B. Savage and T. Carrieres (2006), Flow of ice through converging channels, *Int. Jour. of Offshore and Pol. Eng., 16* (4), 268-273.

Kuijpers, a., F. Dalhoff, M. P. Brandt, P. Hümbs, T. Schott, and A. Zotova (2007), Giant iceberg plow marks at more than 1 km water depth offshore West Greenland, *Mar. Geol.*, *246*, 60–64, doi:10.1016/j.margeo.2007.05.010.

Kwok, R. (2005), Variability of Nares Strait ice flux, *Geophys. Res. Lett.*, *32*(L24502), doi:10.1029/2005GL024768.

Kwok, R. (2009), Outflow of Arctic Ocean sea ice into the Greenland and Barents seas: 1979–2007, *J. Clim., 22*, 2438–2457.

Kwok, R., L. Toudal Pedersen, P. Gudmandsen, and S. S. Pang (2010), Large sea ice outflow into the Nares Strait in 2007, *Geophys. Res. Lett.*, *37*(L03502), doi:10.1029/2009GL041872.

Maslanik, J., J. Stroeve, C. Fowler, and W. Emery (2011), Distribution and trends in Arctic sea ice age through spring 2011, *Geophys. Res. Lett.*, *38*(L13502), doi:10.1029/2011GL047735.

Maxwell, J. B. (1981), Climatic regions of the Canadian Arctic Islands, *Arctic*, *34*(3), 225–240.

Meier, M. F., M. B. Dyurgerov, U. K. Rick, S. O'Neel, W. T. Pfeffer, R. S. Anderson, S. P. Anderson, and A. F. Glazovsky (2007), Glaciers Dominate Eustatic Sea-Level Rise in the 21st Century, *Science*, *317*(5841), 1064–1067, doi:10.1126/science.1143906.

Melling, H., Y. Gratton, and G. Ingram (2001), Ocean circulation within the North Water polynya of Baffin Bay, *Atmosphere-Ocean*, *39*(3), 301–325, doi:10.1080/07055900.2001.9649683.

Miller, L. A., et al. (2002), Carbon distributions and fluxes in the North Water, 1998 and 1999, *Deep. Res. Part II Top. Stud. Oceanogr.*, *49*, 5151–5170, doi:10.1016/s0967-0645(02)00183-2.

Mundy, C. J., and D. G. Barber (2001), On the relationship between spatial patterns of sea-ice type and the mechanisms which create and maintain the North Water (NOW) polynya, *Atmosphere-Ocean*, *39*(3), 327–341, doi:10.1080/07055900.2001.9649684.

Nick, F. M., A. Vieli, M. L. Andersen, I. Joughin, A. Payne, T. L. Edwards, F. Pattyn, and R. S. W. van de Wal (2013), Future sea-level rise from Greenland's main outlet glaciers in a warming climate, *Nature*, *497*(7448), 235–238, doi:10.1038/nature12068.

Newell, J. P. (1993), Exceptionally large icebergs and ice islands in eastern Canadian waters: a review of sightings from 1990 to present, *Arctic*, *46*(3), 205–211.

Pereira, C. P. G., C. M. T. Woodworth-lynas, and J. V. Barrie (1988), Iceberg Scour Investigations and Sedimentology of the Southeast Baffin Island Continental Shelf, *Arctic*, *41*(3), 221–230.

Rignot, E., and P. Kanagaratnam (2006), Changes in the velocity structure of the Greenland Ice Sheet, *Science, 311*, 986–990.

Rigor, I. G., J. M. Wallace, and R. L. Colony (2002), Response of sea ice to the Arctic Oscillation, *J. Clim.*, *15*(18), 2648–2663, doi:10.1175/1520-0442(2002)015<2648:ROSITT>2.0.CO;2.

Sadler, H. E. (1976), Water, heat, and salt transports through Nares Strait, Ellesmere Island, *J. Fish. Res. Board Canada*, *33*, 2286–2295.

Samelson, R. M., T. Agnew, H. Melling, and a Münchow (2006), Evidence for atmospheric control of sea-ice motion through Nares Strait, *Geophys. Res. Lett.*, *33*(2), 2–5, doi:10.1029/2005GL025016.

Samelson, R. M., and P. L. Barbour (2008), Low-level jets, orographic effects, and extreme events in Nares Strait: A model-based mesoscale climatology, *Mon. Weather Rev.*, *136*, 4746–4759, doi:10.1175/2007MWR2326.1.

Smith, S. D., R. D. Muench, and C. H. Pease (1990), Polynyas and leads: an overview of physical processes and environment, *J. Geophys. Res.*, *95*(C6), 9461–9479.

Stark, H. F., L. M. Candlish, and D. G. Barber (2016), Identifying changes in the formation and dissolution of the North Water Polynya, 1979-2012: An index classification approach, *Arctic* (under review).

Steffen, K. (1985), Warm Water Cells in the North Water, Northern Baffin Bay During Winter, *J. Geophys. Res.*, *90*(C5), 9129–9136.

Stirling, I. (1980), The Biological Importance of Polynyas in the Canadian Arctic, *Arctic*, *33*(2), 303–315.

Stirling, I. (1997), The importance of polynyas, ice edges, and leads to marine mammals and birds, *J. Mar. Syst.*, *10*(10), 9–21.

Tremblay, J. E., Y. Gratton, E. C. Carmack, C. D. Payne, and N. M. Price (2002), Impact of the large-scale Arctic circulation and the North Water Polynya on nutrient inventories in Baffin Bay, *J. Geophys. Res.*, *107*(C8), doi:10.1029/2000JC000595.

van den Broeke, M., J. Bamber, J. Ettema, E. Rignot, E. Schrama, W. J. van de Berg, E. van Meijgaard, I. Velicogna, and B. Wouters (2009), Partitioning recent Greenland mass loss., *Science*, *326*(5955), 984–986, doi:10.1126/science.1178176.

Van Wychen, W., D. O. Burgess, L. Gray, L. Copland, M. Sharp, J. A. Dowdeswell, and T. J. Benham (2014), Glacier Velocities and dynamic ice discharge from the Queen Elizabeth Islands, Nunavut, Canada, *Geophys. Res. Lett.*, *41*, 484–490, doi:10.1002/2013GL058558.

Vincent, R. F. (2013), The 2009 North Water anomaly, *Remote Sens. Lett.*, *4*(11), 1057–1066, doi:10.1080/2150704X.2013.837227.

Yao, T., and C. L. Tang (2003), The formation and maintenance of the North Water Polynya, *Atmosphere-Ocean*, *41*(3), 187–201, doi:10.3137/ao.410301.

Zhang, J., R. Lindsay, A. Schweiger, and I. Rigor (2012), Recent changes in the dynamic properties of declining Arctic sea ice: A model study, *Geophys. Res. Lett.*, *39*(L20503), doi:10.1029/2012GL053545.

CHAPTER FIVE: CONCLUSIONS AND RECOMMENDATIONS

5.1 Summary and Conclusions

The overall purpose of this study was to improve our understanding of the formation, maintenance, and dissolution factors that dictate the North Water Polynya (NOW). Specifically this work aims to investigate the spatial and temporal variability of the ice arches associated with NOW. As a result of the shifting Arctic climate and the associated changes in the ice regime, the long-term affects on the formation and dissolution of NOW are unknown. Understanding the response of NOW to changes in the ocean-sea ice-atmosphere interface is important as these changes can impact physical, biological, meteorological, and geochemical characteristics and processes, as well as transportation and local communities around NOW. In chapter one we outlined the three objectives of this thesis as follows:

1) To determine the variability of the formation and dissolution of the North Water Polynya.
2) To investigate the role of atmospheric forcing in the recent variability of the Smith Sound ice arch consolidation.
3) To investigate the role of the timing of ice grounding relative to ice arch formation.

Chapter one provided an introduction to polynyas and rationale for why a better understanding of polynya formation and dissolution is necessary. Chapter two provided essential background and contextual information on growth, motion, and decay of sea ice, passive remote sensing, and the North Water Polynya. Chapter three addressed thesis objective (1), and chapter four addressed thesis objectives (2) and (3).

Results from chapter three show the long-term variability of the formation and dissolution of the North Water Polynya from 1979-2012 using a 25x25 km spatial resolution SSM/I derived sea ice concentration dataset produced by the National Snow and Ice Data Centre. Two regions

of interest were identified: Kane Basin because it showed consistent sea ice conditions when NOW was present and northern Baffin Bay because it exhibited typical polynya behavior with reduced or thinner sea ice concentration. The generation of an index classification algorithm determined the presence or absence of the ice arch at Smith Sound using an 80% sea ice concentration threshold. Results from the algorithm characterized years as typical and atypical, with atypical years exhibiting anomalous behavior that included NOW forming earlier (2003 and 2006), the ice arc not forming in Smith Sound (1983, 1990, 2009), and the ice arch not forming at all (1993, 1995, 2007, 2010). On average, NOW remained open for 81 days, but there was considerable variation in this as it was open for 48 days in 1987 and 144 days in 2006. An investigation of the decadal trends indicated a significant shift in formation and dissolution dates, with formation occurring 18 days earlier and dissolution occurring 17 days earlier. We concluded that the increased variability of NOW was negatively impacted by the changing Arctic system; however, the formation and dissolution of NOW are dynamic processes driven by multiple mechanisms and therefore it is not possible to suggest a single cause for the variability. The results from this paper can be used to compare the variability in formation and dissolution to trends in biological productivity of the region.

The investigation of atmospheric factors that influence the consolidation of the NOW ice arch at Smith Sound during a typical and atypical formation year of the ice arch at Smith Sound is presented in chapter four. During the typical ice season of 2010-2011 an ice arch consolidated, whereas during the atypical ice season of 2009-2010 an ice arch did not consolidate at Smith Sound and Nares Strait remained a thoroughfare for ice export. A combination of NCEP re-analysis-2 and Hans Island *in situ* observations of MSLP, winds, and atmospheric temperature were used to compare and contrast atmospheric regimes during both ice seasons. Climatological

MSLP from 1979 to 2015 confirmed the dominant high-to-low pressure gradient from the Arctic Ocean to Baffin Bay typically seen during the winter months of December, January, and February. The strong northerly winds generated from the pressure gradient assist in the southward advection of ice through Nares Strait and the eventual consolidation of the ice arch, as seen on the ASAR images. MSLP anomalies for 2009-2010 and 2010-2011 did not indicate any significant deviations from climatological means. Atmospheric temperature observations from the Hans Island weather station indicated that November 2009 to January 2010 was 3.4°C colder than the same time period in 2010-2011. Wind direction and wind speed from Hans Island highlighted a significant wind event in January 2010, with wind speeds exceeding 10 m s^{-1} 66% of the time, that could have disrupted the southerly drift of ice, preventing the consolidation of the ice arch. Although we determined that the timing and strength of southerly winds affects the consolidation of the ice arch, the formation of the arch is influenced by many factors, such as the ice pack of Nares Strait, which we included in the discussion section. Despite the presence of old ice in 2009-2010 the ice arch did not consolidate; however, we still suggest that a changing ice pack will influence the consolidation of the ice arch as thinner ice will respond differently atmospheric and oceanic forces. Moreover, the icebergs and ice islands of Nares Strait, which can often ground, disrupt the southerly flow of ice, e.g. the grounded ice island in 2013 that caused the arch to form just south of it, and can also affect the dissolution of the arch. The results and discussion from this paper can be used as a starting point to further investigate the factors that influence the consolidation of the ice arch.

The results presented within this thesis highlight the long-term variability of the formation and dissolution of the North Water Polynya. As a response to the changing Arctic regime, the Smith Sound ice arch and NOW are negatively impacted by atypical atmospheric

patterns and the icescape of Nares Strait. The results also provide insight into the complex system of NOW and the necessity to further investigate the formation mechanisms of the ice arch. This thesis provides analysis that is pertinent to a wide range of the scientific community, especially those who investigate the biological productivity of NOW.

5.2 Recommendations

As the Arctic continues to change at accelerated rates, the dynamics of the ocean-sea ice-atmosphere interface that drive the formation and dissolution of polynyas will also change. The investigation presented in this thesis provides a baseline understanding of the long-term variability of the formation and dissolution of NOW and potential atmospheric and ice related influences; however, there is a need to further investigate the NOW region as the Arctic climate and ice regime continue to change. Based on this, some recommendations for future research include:

- Quantitative analysis of polynya extent and open water area. Specifically the use of synthetic aperture radar to determine trends in the location of the ice arch, open water area, and ice-covered area as a response to a changing Arctic climate. This would assist in determining impacts on geochemical processes and biological productivity of NOW.
- Quantitative analysis of large ice features, similar to the discussion of ice islands in chapter four, present in Nares Strait during fall freeze up. Specifically, the frequency and size of large ice features and their role in the consolidation of the ice arch and the decay of the arch during dissolution should be studied. The transition from a sea ice dominated ice arch to one composed of numerous large ice features will respond differently to the forcing mechanisms in the NOW region.

- Further analysis of the atmospheric regime of the NOW region, specifically the influences of increased atmospheric temperature on thermodynamic ice growth of first year and landfast ice in Nares Strait. Increases in atmospheric temperature, and oceanic temperature as a result, can potentially impact the consolidation of the ice arch and thus the formation of the polynya.

These recommended studies would significantly increase our understanding and ability to determine the factors that influence the formation, maintenance, and dissolution of the North Water Polynya. This work would further our scientific understanding of the variability of NOW and the associated impacts on physical, biological, meteorological, and geochemical processes, as well as commercial transportation and communities relying on NOW.